Doctoral Dissertation (Shinshu University)

Design of metallophthlocyanines for enhancing photo-conversion efficiency in the near-infrared region

March 2017

Satoshi Yamamoto

Declaration

I, *Satoshi Yamamoto*, declare that this thesis, submitted in fulfillment of the requirements for the award of Doctor of Engineering, in the Interdisciplinary Graduate School of Science and Technology, Department of Bioscience and Textile Technology, Shinshu University, is wholly my own work unless otherwise referenced or acknowledged. The document has not been submitted for qualifications at any other academic institution.

Satoshi Yamamoto

March 2017

Publications

1. Satoshi Yamamoto, Angel Zhang, Martin J. Stillman, Nagao Kobayashi, Mutsumi Kimura, "Low-symmetrical Ω-shaped Zinc Phthalocyanine Sensitizers having a Panchromatic Light Harvesting Property for Dye-sensitized Solar Cells", *Chem. Eur. J.,* **2016**, 22, 18760-18768. *Selected as frontispiece
2. Satoshi Yamamoto, Shogo Mori, Pawel Wagner, Attila J. Mozer, Mutsumi Kimura, " A Novel Covalently Linked Zn Phthalocyanine-Zn Porphyrin Dyad for Dye-Sensitized Solar Cells", *Israel Journal of Chemistry*, **2016**, 56, 175-180.
3. Satoshi Yamamoto, Takuro Ikeuchi, Shogo Mori, and Mutsumi Kimura, "Light-Harvesting in the Near-Infrared Region; Dye-Sensitized Solar Cells Sensitized with Asymmetric Ring-Expanded Zinc(II) Phthalocyanines", *Asian Journal of Organic Chemistry*, **2014**, 10, 1083-1088.
4. Satoshi Yamamoto and Mutsumi Kimura, "Extension of Light-harvesting Area of Bulk-heterojunction Solar Cells by Co-sensitization with Ring-expanded Metallophthalocyanines Fused with Fluorene Skeletons", *ACS Applied Materials & Interfaces*, **2013**, 5, 4367-4373.

Conference proceeding

International

1. Satoshi Yamamoto and Mutsumi Kimura, "Low-symmetrical Zinc Phthalocyanine having a Panchromatic Light Harvesting Property for Dye-sensitized Solar Cells", 2nd International Symposium on Center of Excellence for Innovative Material Sciences Based on Supramolecules, Kanazawa, Japan, October 26th-27th, 2016, Poster.
2. Martin J. Stillman, Angel (Qi Wen) Zhang, Satoshi Yamamoto, Lydia Kwan, Nagao Kobayashi, Mutsumi Kimura, "Computational and Spectroscopic Studies in the Design of Novel Porphyrins for Solar Cell Applications", 9th International Conference on Porphyrins and Phthalocyanines (ICPP-9), Nanjing, China, July 3rd-8th, 2016, Poster.
3. Qi Wen Zhang, Satoshi Yamamoto, Lydia Kwan, Nagao Kobayashi, Mutsumi Kimura, Martin J. Stillman, "Computational and Spectroscopic Studies in the Design of Novel Porphyrins for Solar Cell Applications", Phthalocyanines an Close Friends, Elche, Alicante, Spain, January 27th-28th, 2016, Poster.
4. Satoshi Yamamoto and Mutsumi Kimura, "Non-peripheral Substituted Zn Phthalocyanine Sensitizers for Dye-Sensitized Solar Cells", Phthalocyanines an Close Friends, Elche, Alicante, Spain, January 27th-28th, 2016, Poster.
5. Satoshi Yamamoto and Mutsumi Kimura, "Ring-Expanded Phthalocyanine Fused with Fluorene for Light-Harvesting in the Near-IR Region", 227th Electrochemical Society, Chicago, Illinois, USA, May 24th-28th, 2015, Poster.
6. Satoshi Yamamoto, Shogo Mori, Pawel Wagner, Attila J. Mozer, and Mutsumi Kimura, "Phthalocyanine-Porphyrin Dyads for Dye-sensitized Solar Cells", Michinoku International Symposium on Porphyrins, Phthalocyanines and Functional π Molecules, Zao, Japan, 13th-16th, October, 2014, Poster.
7. Satoshi Yamamoto and Mutsumi Kimura, "Organic Solar Cells Co-sensitized near-IR Absorbing Zinc Phthalocyanine", Material Researching Society, Fall

meeting & Exhibit, Boston, U.S.A, 25th-30th, November 2012, Poster.

Domestic

1. Kengo Kuribayashi, Satoshi Yamamoto, Nagao Kobayashi and Mutsumi Kimura, "Selective Synthesis of 1,8,15,22-tetrakis(diphenylamino)phthalocyanine", The 43rd Symposium on Main Group Element Chemistry, Miyagi, December 2016, Poster.
2. Satoshi Yamamoto and Mutsumi Kimura, "Novel Zn Phthalocyanine-based Panchromatic Dye-sensitized Solar Cells", 96th Annual Meeting of Chemical Society of Japan, Aichi, March 2016, Oral.
3. Satoshi Yamamoto and Mutsumi Kimura, "Novel Phthalocyanine-based D-π-A dyes for Dye-sensitized Solar Cells", 95th Annual Meeting of Chemical Society of Japan, Aichi, March 2015, Oral.
4. Satoshi Yamamoto, Shogo Mori, Pawel Wagner, Atilla J. Mozer and Mutsumi Kimura, "Dye-sensitized Solar Cells using Energy Relay Dyes", 94th Annual Meeting of Chemical Society of Japan, Aichi, March 2014, Oral.
5. Satoshi Yamamoto, Shogo Mori, Pawel Wagner, Atilla J. Mozer and Mutsumi Kimura, "Dye-sensitized Solar Cells sensitized by Phthalocyanine – Porphyrin Dyad", The Electrochemical Society of Japan 2013 Fall Meeting, Tokyo, September 2013, Oral.
6. Satoshi Yamamoto and Mutsumi Kimura, "Organic-based Solar Cells doping Ring-expanded Phthalocyanine as Near-IR absorbing Additives", 62th SPSJ Annual Meeting, Kanagawa, May 2013, Oral.
7. Satoshi Yamamoto and Mutsumi Kimura, "Bulkheterojuntion Solar Cells using Zinc Phthalocyanines as Near-IR Absorbing Co-sensitizers", 93th Annual Meeting of Chemical Society of Japan, Shiga, March 2013, Oral.
8. Satoshi Yamamoto and Mutsumi Kimura, "Organic-based Solar Cells containing Ring-expanded Metallophthalocyanine", 61thSPSJ Symposium on

Macromolecules, Aichi, September 2012, Oral.

9. Satoshi Yamamoto and Mutsumi Kimura, "Organic-based Solar Cells Containing Ring-expanded Metallophthalocyanine", 61th SPSJ Annual Meeting, Kanagawa, May 2012, Poster.
10. Satoshi Yamamoto and Mutsumi Kimura, "Syntheses and Characterization of Ring-expanded Metallophthalocyaine Containing Fluorene Unit", 92th Annual Meeting of Chemical Society of Japan, Kanagawa, March 2012, Oral.

Award

1. Best Poster Award, 2nd International Symposium on Center of Excellence for Innovative Material Sciences Based on Supramolecules, Kanazawa, Japan, October 26th-27th, 2016.

Table of contents

Abbreviations

BHJ	Bulk heterojunction
CV	Cyclic voltammetry
DMAE	2-(dimethylamino)ethanol
DPV	Differential pulse voltammetry
DSSCs	Dye-sensitized solar cells
ε	Extinction coefficient
FF	Fill factor
FRET	Förster resonance energy transfer
FTO	Fluorine-doped tin oxide
LUMO	Lowest unoccupied molecular orbital
HOMO	Highest occupied molecular orbital
IPCE	Incident photo-to-current conversion efficiency
IR	Infrared
ITO	Tin-doped indium oxide
J_{SC}	Short circuit current
MALDI	Matrix-assisted laser desprption ionization
MPcs	Metallophthalocyanines
NBS	N-bromosucccinimide
NMP	1-methyl-2-pyrrolidone
NMR	Nuclear magnetic resonance
o-DCB	*o*-Dichlobenzene
OPVs	Organic photovoltaic devices
PCBM	1-(3-methoxycarbonyl)-propyl-1-phenyl-(6,6)C_{61}
PCEs	power conversion efficiencies
Pcs	Phthalocyanines
PEDOT/PSS	poly(3,4-ethylenedioxythiophene)/polystyrenesulfonate
P3HT	poly(3-hexylthiophene)
TBP	4-*tert*-Butyl pyridine
THF	Tetrahydrofuran
V_{OC}	Open-circuit volatage

List of figures

List of tables

Chapter 1

Introduction and literature review

1.1. Introduction

1.1.1. Motivation

Photosynthesis is one of the most important biological processes. It is the process by which plants convert solar energy into biomass thereby generating the biofuel required for sustaining life on the planet.[1] Photosynthetic organisms are capable of harvesting solar energy with near unity quantum efficiency.[2] In natural systems, chlorophyll plays the key role of being the light-harvesting antennae, collecting the maximum number of incoming photons, which are efficiently transferred to the special pair (Figure 1-1a).[3] Chlorophyll is an analog of porphyrin (Figure 1-1b) and has an 18π electron system, absorbing light towards the red end of the spectrum, up to 660 nm.[4] This natural pigment has been extensively studied in order to understand its role in photosynthesis. Moreover, many researchers are interested in porphyrins as artificial antenna systems. To date, many porphyrin models have been proposed for the purpose of understanding natural systems and developing solar energy conversion systems.[5]

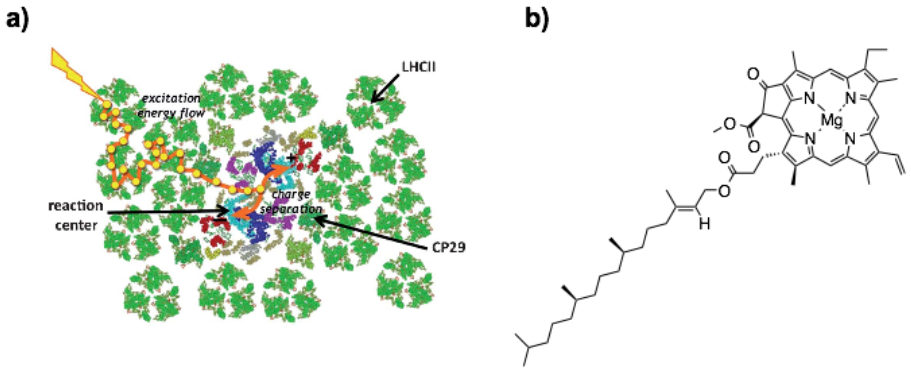

Figure 1-1: a) Light-harvesting in LHC II: the excitation energy migrates from the antennae to the reaction center via a potential trajectory (Figure taken from reference 3); b) chemical structure of chlorophyll a.

Capturing solar energy and converting it to usable forms such as electricity or chemical fuels remains a huge challenge. Recently, photovoltaic devices using organic compounds such as organic photovoltaic (OPV) and dye-sensitized solar cells (DSSCs) have attracted a lot of attention because they are low fabrication cost, lightweight, and scalable solar cells. The solar photon flux incident on the surface of the earth broadens from the visible to near-IR region with about 50 % of the solar radiation incident in the near-IR region.[6] Unfortunately, the light-harvesting range of most organic compounds that are used in solar-to-electricity conversion applications is confined to the visible region. Therefore, one of the key issues for enhancing the performance of organic-based solar cells is the expansion of the light-harvesting wavelength range. To extend the absorption spectrum of the organic compounds used in OPV and DSSCs to longer wavelengths, the energy gap between the highest occupied molecular orbital (HOMO) and lowest unoccupied molecular orbital (LUMO) of these compounds must be reduced. However, organic compounds with narrower HOMO-LUMO gaps cannot perform an efficient photoelectric conversion due to the inevitable loss incurring during photoinduced charge separation. Thus, the design and development of near-IR sensitizing dyes represents a challenging task.

Phthalocyanines and metallophthalocyanines are very attractive dyes for near-IR sensitizing because of their intense absorption around 680 nm (Q band) and tunable properties. Phthalocyanines show similar optical properties to chlorophyll but possess a much higher intrinsic chemical and photophysical stability. This thesis focuses on the development of novel phthalocyanine-based photosensitizers for the expansion of the light-harvesting wavelength range of organic-based solar cells. The author synthesized a series of phthalocyanines with Q bands in the near-IR region, and investigated their optical, electrochemical and photovoltaic properties.

1.2. General introduction and literature review

1.2.1. Near-Infrared region

The range of electromagnetic radiation extends from gamma rays to radiofrequency waves (Figure 1-2). The infrared (IR) region covers electromagnetic wavelengths longer than visible light up to 1000 μm. Depending on the wavelength, the infrared range can be further divided into near-infrared (700 to 3000 nm), mid-infrared (3 to 50 μm), and far-infrared (50 to 1000 μm). Note that these divisions have not been clearly defined, and vary in the litteatures[7]. The definition of each division in this thesis is in accordance with reference 8.

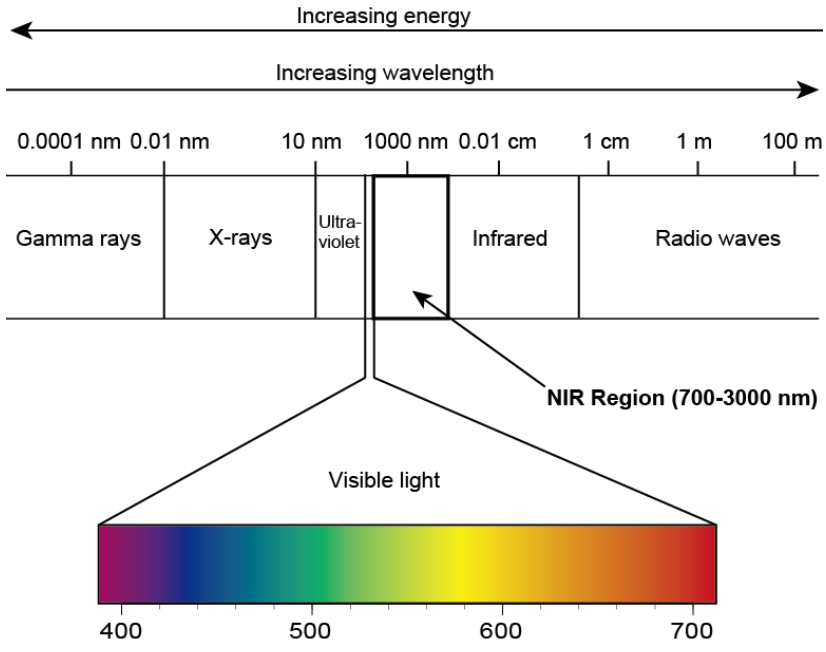

Figure1-2: Electromagnetic radiation.

1.2.2. Porphyrins and phthalocyanines

Porphyrins (por) are an 18π aromatic macrocyclic compound that consisting of four pyrrole units and four bridging carbon atoms. The chemical structure of porphyrin is shown in Figure 1-3. Additional benzene rings can be fused at the β-carbon of the porphyrin core, which is called tetra-benzoporphyrin. Substitution of phenyl groups on the meso position of the porphyrin core results in tetraphenylporphyrin (TPP). The porphyrin structure can often be found in nature, such as in various types of chlorophylls and hems. Porphyrin is a typical functional molecule, playing an important role in diverse areas of scientific research, as a result of its unique electronic and optical properties. Porphyrin research has a long history, covering a wide variety of disciplines of natural science, including artificial photosynthesis, organic photovoltaic cells, photodynamic therapeutic agents, and so on.[9-11]

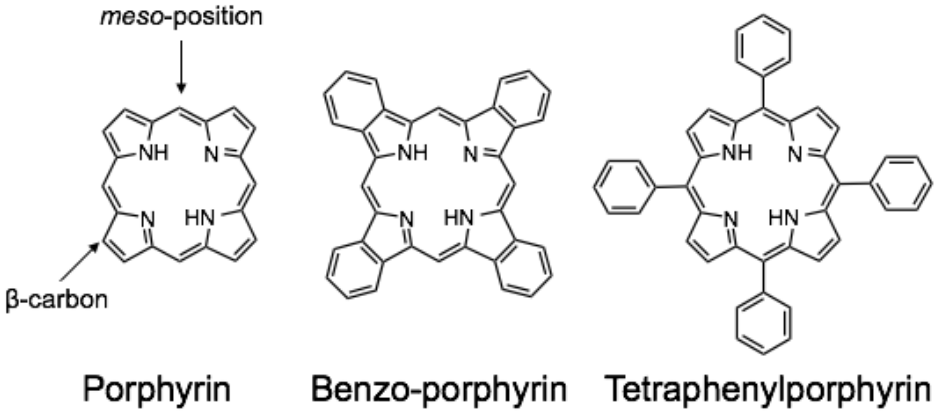

Figure 1-3: The chemical structure of porphyrin, benzo-porphyrin, and tetraphenylporphyrin (TPP).

On the other hand, phthalocyanines (Pcs) are artificial pigments and dyes. They were accidentally discovered as a byproduct in 1907.[12] Linstead characterized the Pc structure in 1934.[13] The structure of Pcs is similar to a porphyrin ring and is an 18π aromatic macrocycle in which meso-carbons of benzo-porphyrin are

replaced with nitrogen atoms. Figure 1-4 shows the structures of metal-free Pc and metallophthalocyanines (MPcs), as well as the numbering scheme traditionally used for their naming convention. The internal and external positions of the fused benzene ring are also commonly known as the α and β positions, respectively. For the last few decades, Pcs and MPcs have been applied in other potential applications as promising materials in numerous fields such as catalysis, organic thin-film transistors, optical discs, sensors, nonlinear optical materials, photovoltaic devices, probes for bio-imaging, and photodynamic therapy.[14-21]

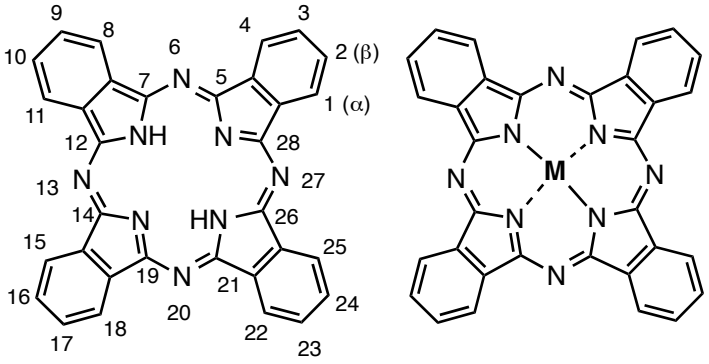

Figure 1-4: Chemical structure of metal-free phthalocyanine (left) and metallophthalocyaine (right)

The electronic structure of porphyrinoids has been explained well by the four-orbital model, which was established by Gouterman *et al.* at around 1960.[22] Gouterman's four-orbital model can reasonably describe most optical properties of Pors and Pcs. Both Pors and Pcs possess two intense π-π* transitions, which are named B (or Soret) and Q bands. In porphyrin molecules, the HOMO and HOMO-1 orbitals are accidentally degenerate. As a result, the B and Q transitions almost completely retain their allowed and forbidden characters, respectively. Thus, UV-Vis absorption spectra of porphyrins show an intense B band around 400-450 nm with even larger extinction coefficients of around 5 x 10^5 $M^{-1}cm^{-1}$ and an extremely weak Q band at 500-650 nm. The UV-Vis spectra of H_2TPP and ZnTPP

are shown in Figure 1-5a. In the case of Pcs, the addition of the aza nitrogen atoms and fused benzenes significantly breaks the degeneracy of the HOMOs due to stabilization of the HOMO-1 orbital. As a result, the Q transition of phthalocyanine gains considerable intensity. Typical MPcs show an intense Q band ($\varepsilon > 10^5$ M^{-1} cm^{-1}) at 650-700 nm because the LUMO and LUMO+1 levels are degenerate. On the other hand, metal free Pc shows a split Q band (Figure 1-5b) because the lower-symmetry of the molecule causes a split of the LUMO energy level into two energy levels. Since the Q band of phthalocyanine can be assigned as a transition from HOMO to LUMO, fine adjustment of the HOMO and LUMO energy levels is critical for controlling the Q band position of phthalocyanine. In the next section 1.2.3, the author describes the control of the Q band position of control of phthalocyanines.

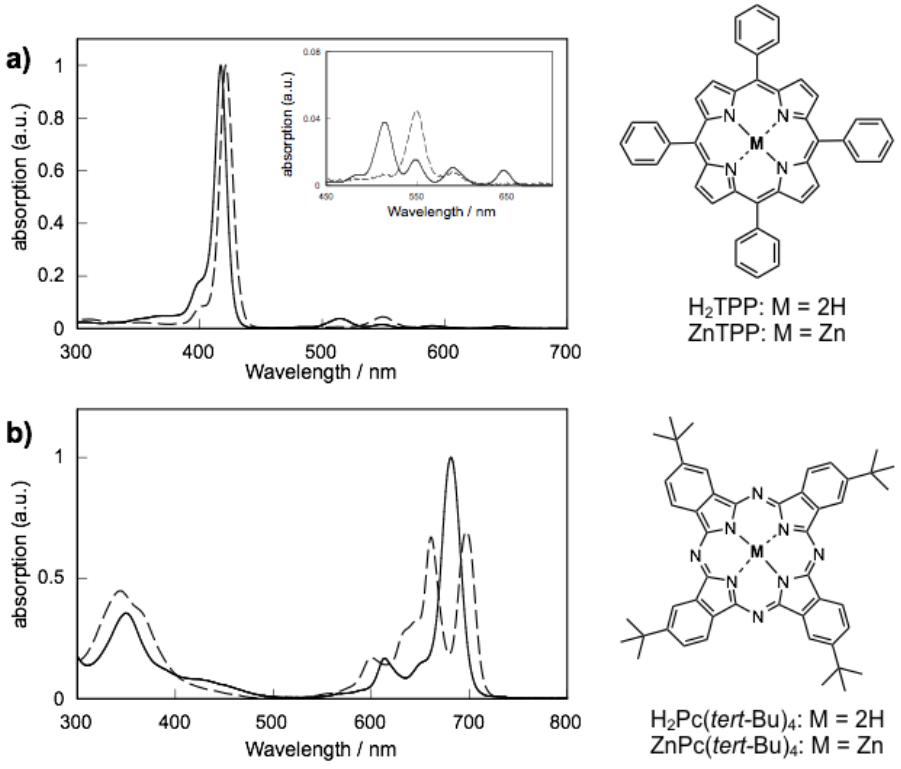

Figure 1-5: a) UV-Vis spectra of metal-free TPP (dashed line), ZnTPP (solid line) (The inset shows the enlarged view of Q band region); b) UV-Vis spectra of metal-free Pc(*tert*-Bu)$_4$ (dashed line) and ZnPc(*tert*-Bu)$_4$ (solid line) in THF

1.2.3. Red-shifting of Q band for metallophthalocyanines

Controlling of the wavelength, bandwidth, and shape of the Q-band of MPcs is one of the most interesting and essential topics in the chemistry of phthalocyanines, and many theoretical and experimental studies of the absorption properties have been reported.[23] Based on the published literature, the approaches for tailoring of Q band can be mainly classified as the following three strategies.[24]

1) Expanding the π conjugation system of the Pc macrocycle

The superphthalocyanine (SPcs), consisting of five isoindole units, is well known as an π-system expanded phthalocyanine (Figure 1-6, **1**).[25] The SPcs show a Q band in the near-IR region beyond λ = 900 nm because their π electron system is larger than the corresponding tetrapyrrolic homologues. In 2012, Luk'yanets and Kobayashi *et al.* reported the π-system expanded phthalocyanine congeners **2** with two central metal ions and four isoindole ring moieties, whose electronic absorption bands extend into the 1200-1500 nm region.[26] The experimental NMR data and theoretical calculations provided evidence for a heteroaromatic 22π electron conjugation system for the ring-expanded Pc system, which satisfies Hückel's (4n+2) π aromaticity. Torres *et al.* synthesized and characterized the new type of π-system expanded phthalocyanine analogue **3** (triazole phthalocyanine) consisting of four subunits of isoindole and two triazole moieties, which is able to coordinate two metal ions within its central binding core.[27] However, the Q-like bands are observed at 604-637 nm, which are blue shifted compared to the Q band of 18π electron phthalocyanine, since the triazole phthalocyanine has a 28π electron system, which does not satisfy Hückel's rule.

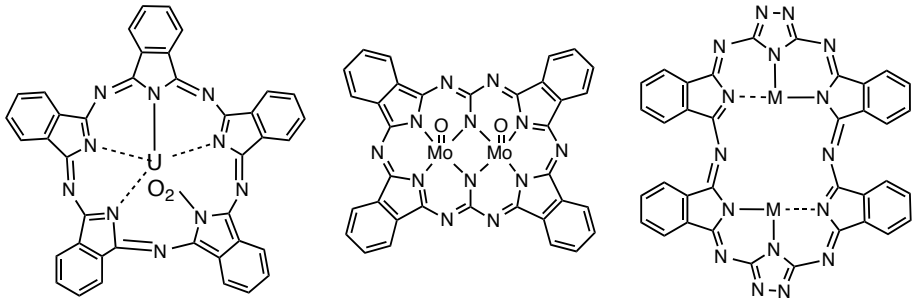

1 **2** **3**

Figure 1-6: Chemical structure of expanded phthalocyanine analogues **1-3**.

2) Changing the size and symmetry of the Pc macrocycle

Naphthalocynines (Ncs), which have a benzene ring fused to the isoindole unit of phthalocyanine, possess a Q band at longer wavelength compared to that of Pcs. Thus, it is known that ring size affects the absorption properties of Pc (Figure 1-7). However, the effect of expanding the size of the ring system has not been systematically reported, because of the lack of a series of compounds possessing corresponding numbers of the same substituents. In 2004, Kobayashi *et al.* synthesized tetraazaporphyrins (TAP), Pcs, Ncs, and anthracocyanines (Acs) with four *tert*-butyl groups and demonstrated that the Q-band shifts to longer wavelength and its intensity increases with expanding molecular size.[28] In 2010, Muranaka *et al.* reported the new ring-expanded Pc, azulenocyanine, having four azulene units fused to a tetraazaporphyrin skeleton. Azulenocyanine exhibits a broad absorption over the visible and near-IR regions beyond 1000 nm.[29] They found that the azulene unit significantly lowers the LUMO level of the macrocycle, while destabilization of the HOMO level is modest, which results in a narrowing of HOMO-LUMO gap.

Lowering the symmetry of the π-conjugated system has a strong effect, such as in splitting the Q bands due to a splitting of the LUMO and LUMO+1 orbitals.

There is typically a pronounced splitting of the Q bands of C_{2v} symmetry mono- and tri-benzo-substituted porphyrazine rings because the perturbation to the structure differs along the x- and y- axes.[30]

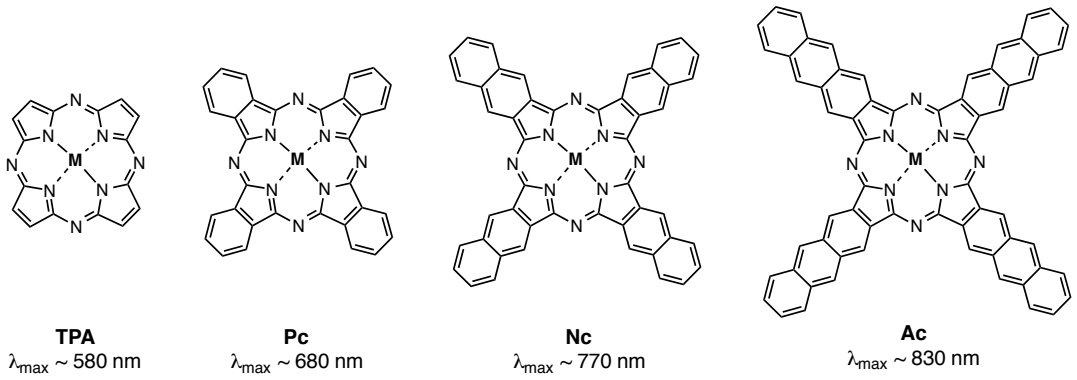

Figure 1-7: Chemical structure of size-expanded phthalocyanine analogues

3) Introducing peripheral substituents of varying type, number and position.

The effects of peripheral substituents on the Pc core have been well studied. It is known that substitution with electron donating and withdrawing substituents at the α and β positions (Figure 1-8) results in different effects on the optical properties.[31] When strongly electron-donating substituents, such as alkoxy and thioalkyl groups, are introduced to the four α-positions, the Q band is red shifted by about 40 nm.[32] Conversely, when the same electron-donating groups are introduced at the β-positions, the Q band is slightly blue shifted. In the case of substitution by strongly electron-withdrawing groups such as nitro- and phenylsulfonyl groups at the α and β positions, the shifts are the opposite of those observed with electron donating groups. These effects can be readily explained by considering the atomic orbital coefficients in MO calculations. The coefficients at the α-carbons in the HOMO level are larger than those at the β-carbons. Therefore, the extent of destabilization of this orbital is larger when electron-donating groups are introduced at the α positions.[33] As a result, the HOMO-LUMO gap becomes

smaller and the Q band shifts to longer wavelength.

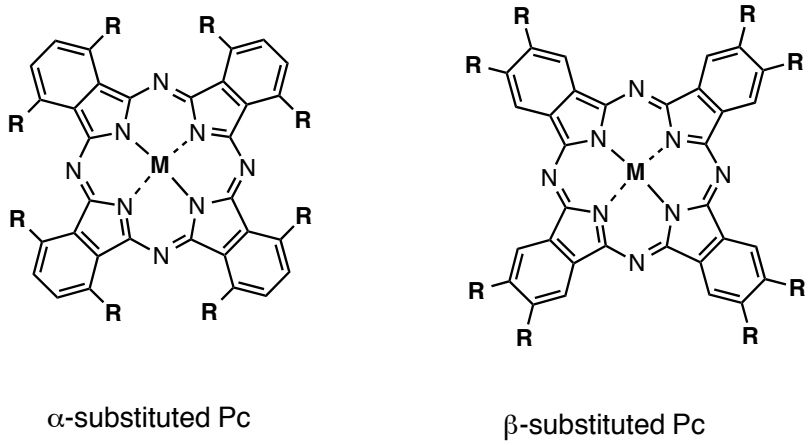

Figure 1-8: Chemical structure of α and β-substituted phthalocyanine analogues

1.2.4. Solar cells

1) Inorganic- and organic-based solar cells

Following the first report of photo-induced elements in 1954 from the Bell lab[34], research on silicon solar cells began worldwide. Silicon-based solar cells are the longest-studied solar cells. A feature of the silicon-based solar cell is its high conversion efficiency and stability. The conversion efficiency of the single crystal silicon solar cell is up to 25 %[35]. However, high-purity silicon is necessary to obtain a high conversion efficiency, and there is a problem of depletion of silicon. Therefore, compound-based solar cells using semiconductors other than silicon have been developed[36]. Compound-based solar cells are based on thin layers of various semiconductor materials such as cadmium telluride (CdTe), copper indium gallium diselenide (CIGS), and gallium arsenide (GaAs). Because compound-based solar cells use thin films of these semiconductors, the amount of semiconductor

required is small, but drawbacks are the use of minor metals such as indium and gallium, and the high toxicity of cadmium and arsenide. These defects would limit future large-scale production. To overcome these limitations, research on alternative organic solar cells such as organic photovoltaics (OPV) and dye-sensitized solar cells (DSSC) using an organic material as an active layer have attracted attention in recent years. In this thesis, the author focuses on organic solar cells and describes their advantages and disadvantages. Figure 1-9 shows the classification of solar cells based on the material used for the active layer. Table 1-1 summarizes the best performances of solar cell type modules.

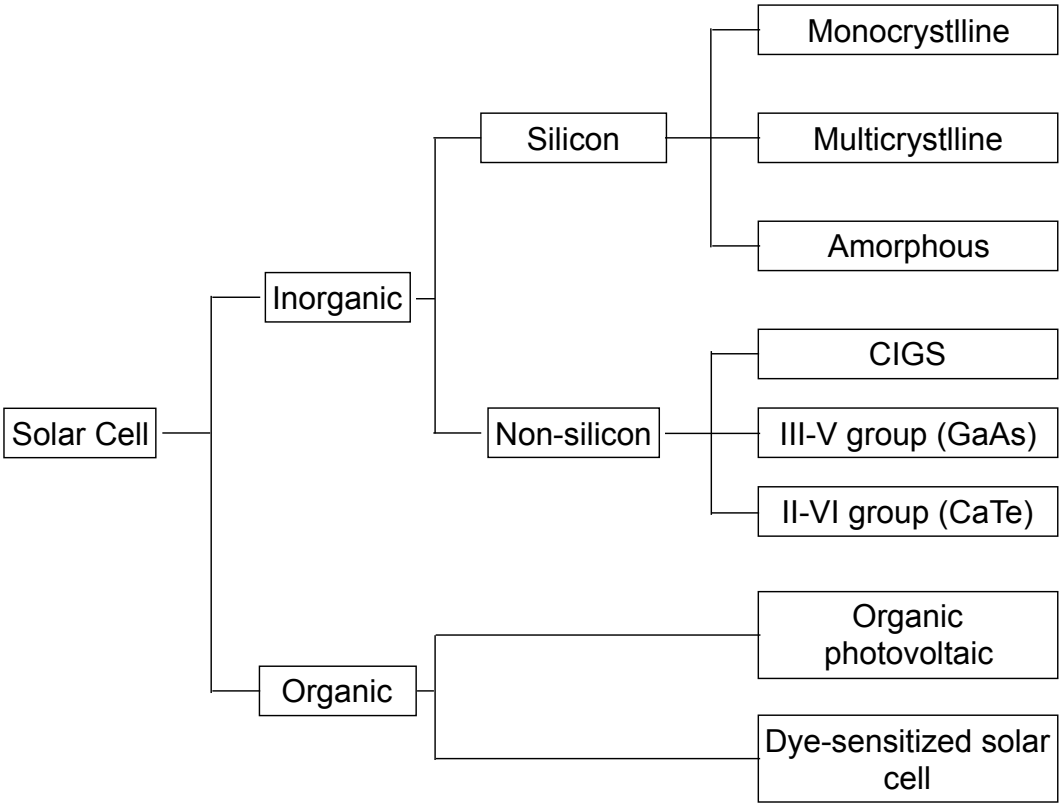

Figure 1-9: Classification of solar cells

Table 1-1: Confirmed terrestrial cell efficiency measured under the global AM1.5 spectrum at 25 °C (Table modified from reference 35)

Classification	Efficiency / %	Area / cm^2	V_{OC} / V	J_{SC} / mA cm^{-2}	FF	Test center [a]
Si (monocrystalline)	25.6 ± 0.5	143.7	0.74	41.8	0.82	AIST
Si (multicrystalline)	20.8 ± 0.6	243.9	0.66	39.0	0.80	FhG-ISE
Si (amorphous)	10.2 ± 0.3	1.001	0.90	16.4	0.70	AIST
GaAs (thin film)	28.8 ± 0.9	0.9927	1.12	29.7	0.86	NREL
CIGS	20.5 ± 0.6	0.9882	0.75	35.3	0.77	NREL
DSSC	11.9 ± 0.4	1.005	0.74	22.5	0.71	AIST
OPV	11.0 ± 0.3	0.993	0.79	19.4	0.71	AIST

[a] AIST = Japanese National Institute of Advanced Industrial Science and Technology, FhG-ISE = Fraunhofer Institut für Solare Energiesysteme, NREL = National Renewable Energy Laboratory.

Organic based solar cells such as OPVs and DSSCs have several inherent advantages compared to silicon-based solar cells. An advantage of organic semiconductors is that they are soluble in common solvents. As a result, this feature allows the fabrication of OPV and DSSC devices by a solution-based process, thereby significantly saving on the manufacturing cost of device. In addition, since the organic compound can efficiently absorb light, the active layer can be thinner (1000 times thinner than a silicon solar cell) [37]. Thus, the cell is flexible and can be printed using a roll-to-roll process. In the case of DSSCs, colorful solar cells derived from a dye can be produced, so that their appearance is excellent. Considering these advantages of organic based solar cells, it is possible to apply them to new market opportunities such as wearable photovoltaic devices.

The main disadvantage of organic based solar cells is low efficiency and short lifetime. There is a fundamental difference in the energy conversion mechanism between conventional inorganic-based solar cells and organic-based exciton solar cells [38]. The main feature of organic based solar cells is that excitons are generated

in organic semiconductors and separated at the hetero interface to produce charge carriers.[39] This is in contrast to conventional solar cells in which carriers are generated in the bulk.[40] Excitons in organic semiconductors are sometimes thought to be bonded electron-hole pairs. However, since it is electrically neutral and strongly coupled with electrons and holes, it is often characterized as a moving excited state [41]. For this reason, the process of charge separation of excitons is slow, and charge transfer extremely is much lower than that of inorganic semiconductors, so that exciton deactivation, charge trapping, and charge recombination occur [42]. Hence, if the details of these physical mechanisms are clarified, it should be possible to enhance the conversion efficiency of organic-based solar cells.

Another significant problem of organic solar cells is the light-harvesting area. The intensity and width of the absorption spectrum of the photoelectric conversion material greatly determine the possibility of harvesting incident solar radiation. Unlike crystalline inorganic semiconductors that absorb continuous spectra of photons with energies larger than the bandgap, organic semiconductors have a rather narrow distinct electronic transition. The solar flux incident on the Earth's surface enters the near infrared region of approximately 50 % from the visible to the near-IR region (Figure 1-10) [6]. However, the optical absorption of most chromophores is confined to the visible region. When the absorption window of the solar cell is expanded to the near-IR region, the efficiency of organic-based solar cells would be substantially improved.

Therefore, attempts to develop new sensitizing dyes in the near-infrared region are essential for enhancing the efficiency of organic-based solar cells, such as that the chromophores investigated in this thesis are likely to meet high demand. In the next section, the research history and working principal of OPVs and DSSCs are summarized.

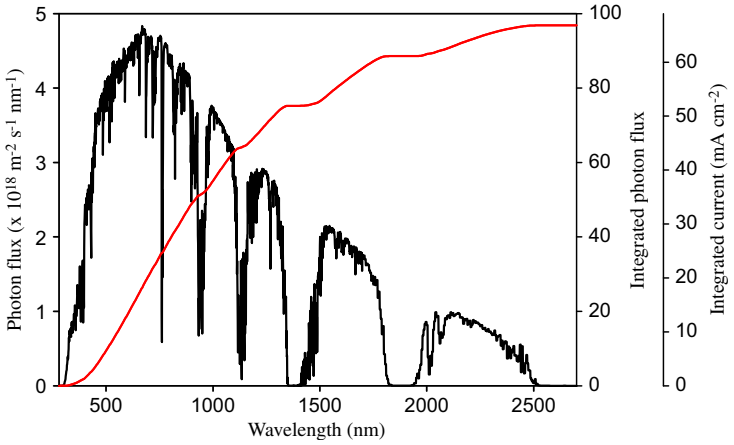

Figure 1-10: Spectral photon flux density at the earth's surface (1000 W m^2, AM1.5G) as a function of wavelength (black line). The cumulative short circuit density integrated over a wavelength range increase as more regions of the spectrum are included (Figure take from reference 6).

2) Organic photovoltaic (OPV)

Historical development of OPV

C. W. Tang of Eastman Kodak Company reported a prototype of an organic thin film solar cell in 1986.[43] This prototype was a heterojunction (p-n junction) solar cell using an organic electron donor and an organic electron acceptor material. A power conversion efficiency of about 1 % was achieved. This prototype is considered the first breakthrough in the organic photovoltaic field. Subsequently, Hiramoto *et al.* reported a p-i-n type device [44], which had an i-layer formed by co-deposition of an electron donor and an electron acceptor between a p-layer and n-layer in 1991. This device exhibited a conversion efficiency of only a little less than 1 %. However, the co-deposition of electron donor and acceptor materials forms the bulk heterojunction structure in the i-layer. Thus, this study was pioneering in the sense that it revealed the usability of bulk heterojunctions in organic thin film solar cells.

In 1995, Heeger *et al.* developed a soluble fullerene derivative and attempted to

form a bulk heterojunction in which a conductive polymer and a fullerene derivative were interblended.[45] The use of a bulk heterojunction layer in which an electron donor and an electron acceptor are interblended made the area of the charge separation interface wider than that of a heterojunction layer and formed a mixed layer with phase separation in the order of tens of nanometers. These advantages made it possible for excitons to reach the charge separation interface effectively. An organic thin film solar cell with a power conversion efficiency of 1.5 % was thus fabricated using the MEH-PPV (2-methoxy-5-(2-ethylhexyloxy)polyphenylenvinylene) and PCBM (phenyl-C_{61}-butyric acid methyl ester) blend. In 2001, a device with a power conversion efficiency of 2.5 % was made by substituted MDMO-PPV for MEH-PPV to optimize the organic thin film morphology that differed depending upon the solvent used.[46] Following this, researchers began examining the use of polythiophene as an alternative electron donor to PPV. In 2002, Brabec *et al.* published the achievement of a PCE of 2.8 % by combining P3HT (poly(3-hexylthiophene)) with PCBM.[47] Since this report, the race to develop P3HT:PCBM organic thin film solar cells has intensified in many countries. Significant power conversion efficiency changes depending upon the treatment after the fabrication of the device, and various post-treatment effects have been reported. In 2003, Sariciftci *et al.* reported the acceleration of polymer crystallization by thermal annealing or application of an external voltage and used this to achieve a PCE of 3.5 %. [48] In 2005, Yang *et al.* obtained a PCE of 4.5 % by annealing at 110 °C for 10 min.[49] In 2006, Bradley investigated the influence of the regioselectivity of polythiophene of the thin film morphology, to produce a device with a PCE of 4.4 %.[50]

Unfortunately, neither the substituted PPV (~560 nm) nor polythiophene (~650 nm) can effectively harvest photons from the solar spectrum. For example, P3HT is only capable of absorbing about ~46 % of the available solar photons. In this

context, many efforts have been devoted to the development of low-bandgap polymers with light absorption extending to longer wavelengths. Leclerc *et al.* developed a new narrow-band gap polymer based on carbazole; poly[N-9'-heptadecanyl-2,7-carbazole-*alt*-5,5-(4',7'-di-2-thienyl-2',1',3'-benzothia diazole)]. Photovoltaic cells based on this polymer blended with PCBM exhibited a PCE of 3.6 %.[51] In 2010, Li and Yu *et al.* synthesized thieno[3,4-*b*]-thiophene/benzodithiophene (PTB7) and found that the stabilization of the quinoidal structure from thieno[3,4-*b*]-thiophene results in a low bandgap of the polymer of about 1.6 eV (~700 nm).[52] A PCE of about 7.4 % has been achieved from a PTB7/$PC_{71}BM$ solar cell device, which is the first polymer solar cell showing a PCE of over 7 %.

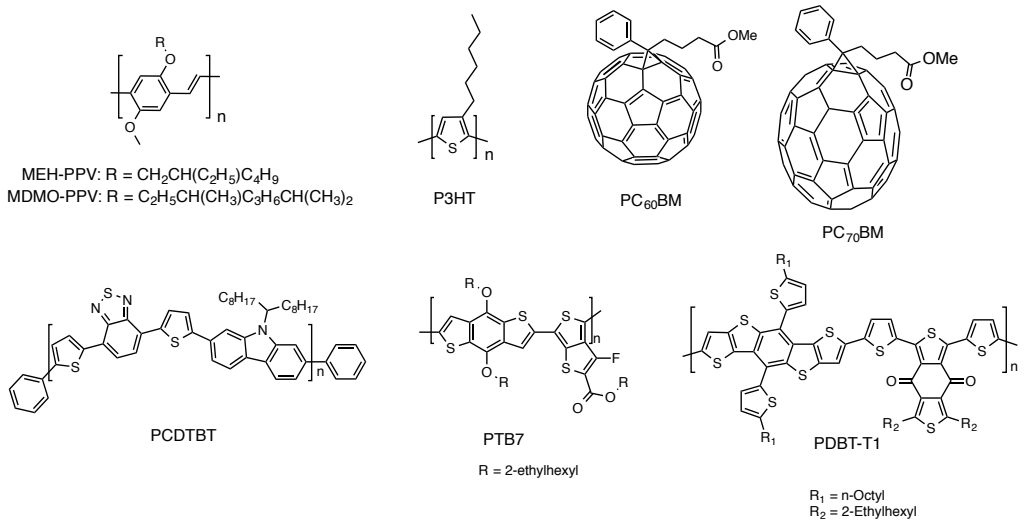

Figure 1-11: The chemical structure of MEH-PPV, MDMO-PPV, P3HT, $PC_{60}BM$, $PC_{70}BM$, PCDTBT, PTB7, and PDBT-T1.

Mechanism of photoelectric conversion in organic solar cells

Figure 1-12a shows the photoelectric conversion mechanism in organic solar cells. Incident light reaching an organic thin film solar cell is absorbed mainly by electron donor molecules, which are excited and produce excitons. These excitons

diffuse to the interface between the electron donor and electron acceptor, where electrons flow from the electron donor to the electron acceptor to form a charge separation state. In other words, the electron donor turns into cations (holes) by providing electrons for the electron acceptor, whereas the electron acceptor becomes anions by receiving those electrons. The holes flow towards the transparent electrode substrate, while the electrons flow towards the counter electrode, and thus, the solar cell provides a current to an external circuit.

The mechanism for this photoelectric conversion can also be described by using an energy diagram as shown in Figure 1-12b. An electron donor molecule is excited to induce an electron present in the HOMO to rise to the LUMO. The electron flows smoothly downwards in the energy diagram smoothly without encountering any barrier. Since the LUMO of the electron acceptor can accommodate an electron more stably, the raised electron transfers from the LUMO of the electron donor to the LUMO of the electron acceptor, to form a charge separation state. In this state, the HOMO of the electron donor has a vacancy, which means that a hole is present, and the LUMO of the electron acceptor is occupied by an electron. The former is a radical cation, and the latter is a radical anion. A hole moves smoothly upwards in the energy diagram smoothly without encountering any barrier, flowing from an electron donor molecule to the ITO electrode, while an electron is collected by the aluminum electrode. Light induces electrons to flow within the solar cell from the ITO electrode with a high work function to the aluminum electrode with a low work function, enabling the solar cell to produce a current to an external circuit.

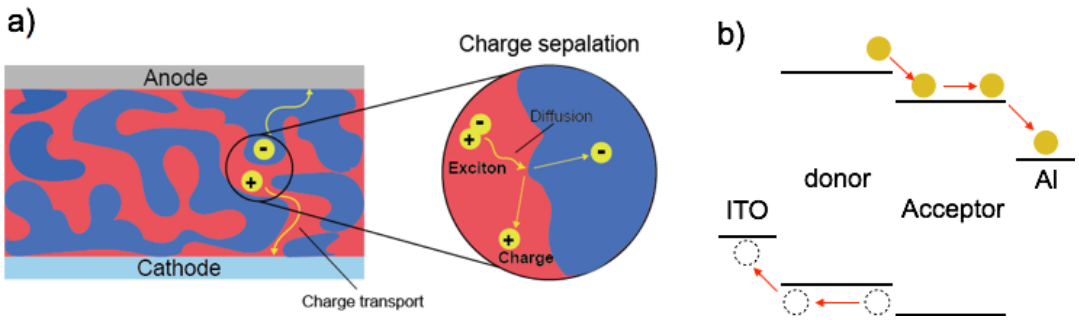

Figure 1-12: a) Mechanism for photoelectric conversion in organic thin film solar cells; b) Energy diagram of organic thin film solar cells

3) Dye-sensitized solar cells (DSSCs)

History of DSSCs

An alternative solar cell technology is the dye-sensitized solar cells (DSSCs). DSSCs consist of a dye-sensitized semiconductor material, where sensitizing dye molecules attached to the semiconductor act as light absorbers. Honda and Fujishima discovered the photocatalytic properties titanium dioxide (TiO_2) in 1967, and published in 1972.[53] However, the large band gap of TiO_2 yielded low conversion efficiencies because the light-harvesting area of TiO_2 is limited to only the ultraviolet region. In 1976, Tsubomura *et al.* demonstrated a working dye-sensitized porous zinc oxide photocell using a platinum counter electrode and an iodide/triiodide redox couple.[54] Desilvestro *et al.* used a rough TiO_2 electrode sensitized with a ruthenium complex yielding enhanced photoconversion efficiency in 1985.[55] The breakthrough for DSSCs occurred in 1991, when Grätzel and O'Regan managed to attain a high PCE of 7.1 % using photovoltaic device based on a dye-sensitized 10 μm thick porous TiO_2 electrode.[56] The sensitizing dye is responsible for the capture of sunlight, which plays an important role in DSSCs. Thus, many efforts have been made to synthesize and investigate novel dyes. Sensitizing dyes can be classified into three categories, which include ruthenium complexes, organic dyes, porphyrins, and phthalocyanines.

Ruthenium complexes

Ruthenium (Ru) complexes have shown good photovoltaic properties because of a broad absorption spectrum, suitable excited and ground state energy levels, relatively long excited-state lifetime, and good chemical stability. In 1993, Grätzel *et al.* reported a mononuclear Ru complex (N3), which exhibited a broad visible light absorption spectrum and a photon-to- electric energy conversion efficiency spectrum extending to 800 nm, and sufficiently long excited state lifetime.[57] As a result, a solar-to-electric energy conversion efficiency of 10 % was achieved. Nazeerudidin *et al.* investigated the effect of deprotonation of the carboxylic acid groups in the N3 dye, which resulted in a shift of the oxidation and reduction potentials to more negative values.[58] Grätzel *et al.* designed the N749 dye, in which the Ru center has three thiocyanato ligands and one terpyridine ligand substituted with three carboxyl groups. They found that a red shift of the MLCT band occurred, as a result of a decrease in the π* level of the terpyridine ligand. As a result, N749-based cells showed a wide range of response up to the near-IR region in IPCE measurement and provided a PCE of 10.4 %.[59] Although these dyes exhibit photon-to-electron conversion in the near-IR region, the drawback is that the absorption coefficient in the near-IR is lower. Therefore, many dyes are required in order to sufficiently absorb near infrared light.

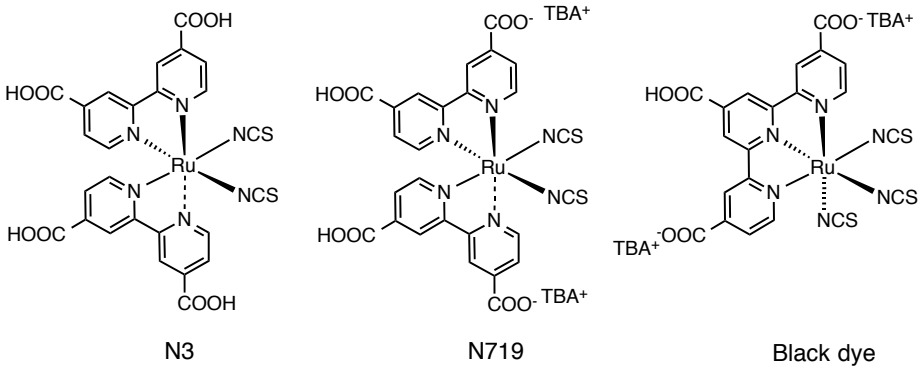

N3 N719 Black dye

Figure1-13: The chemical structure of N3, N719, and N749 (Black dye).

Organic dyes

Metal-free organic dyes have attracted attention over recent decades, because of the ease of design and synthesis, high molar extinction coefficients, and low cost. The most common design for an organic dye is based on a D-π-A structure, in which D is an electron-donor group, π is a conjugated spacer, and A is an electron-withdrawing group. This structure yields an intramolecular charge separation upon excitation, which is desired for DSSCs. Many different structures have been utilized as organic sensitizers such as triphenylamine, coumarine and carbazole. The conjugated spacer can be a chain of methine units or aromatic compounds such as thiophene. The most commonly used acceptor is 2-cyanoarcylic acid. The structures of three well investigated organic dyes are shown in Figure 1-14.

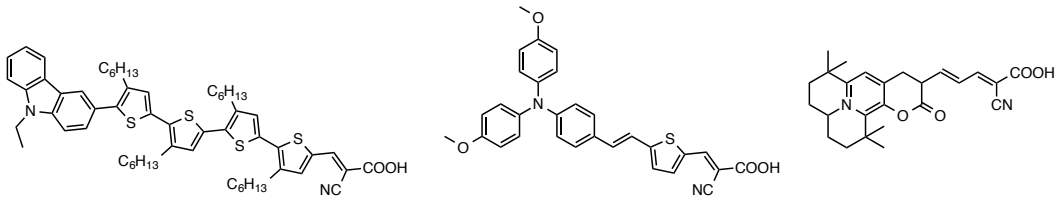

Figure1-14: The chemical structure of MK2[60], D9[61], NKX-2311[62].

Porphyrins and phthalocyanines

Porphyrins and phthalocyanines have strong absorption in the far-red/near-IR, and hence, are good potential candidates for the sensitizing dye. Recent advances in optimizing the device performance of a zinc porphyrin sensitizer co-sensitized with an organic dye and using a cobalt-based electrolyte to enhance the photovoltaic performance of the device, obtained an unprecedented power conversion efficiency of 12.3 %.[63] In 2014, Mathew *et al.* developed a new porphyrin dye (SM315) which functionalized the porphyrin core with the bulky

bis(2',4'-bis(hexyloxy)-[1,1'-biphyl]-4-yl)amine and a benzothiadiazole unit. The SM315-based DSSCs exhibited a PCE of 13.0 %.[64]

MPcs are attractive sensitizers for DSSCs due to their extremely intense red absorbance and excellent photochemical and electrochemical stabilities, but the efficiencies of MPcs-based DSSCs have not been dominant. The main reason is their strong tendency to aggregate on the surface of TiO_2 and lack of directionality of electron transfer in the excited state. Control of the formation of molecular aggregates on the semiconductor nanoparticles has been the key to achieving currently good efficiencies in DSSCs employing MPcs.[65] In 2014, Kimura *et al*. designed and synthesized a highly efficient phthalocyanine dye (PcS20) which provides a PCE of 6.4 %.[66]

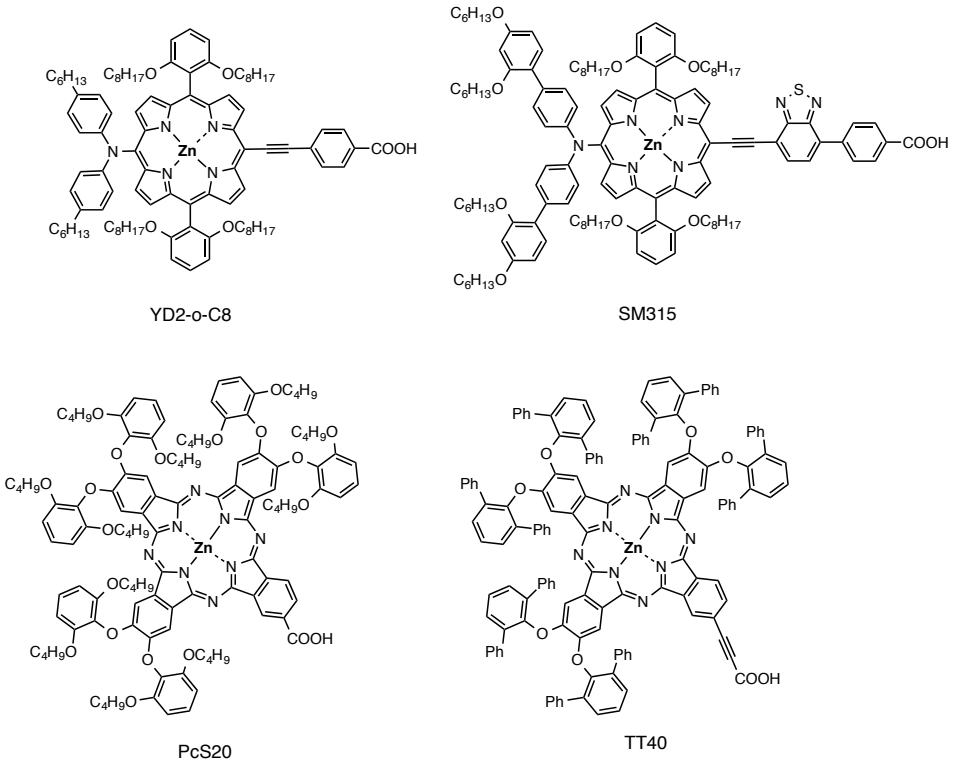

Figure1-15: The chemical structure of YD2-o-C8, SM315, PcS20, and TT40.

Working principal of DSSCs

The working principal of DSSCs involves some critical processes; light absorption, charge separation and charge collection (Figure 1-16). Under sunlight illumination, the dyes will absorb photons and become photoexcited. The adsorbed dye molecules will inject electrons into the TiO_2 working electrode and thus become oxidized. Charge separation is attained across the semiconductor interface where an electron will then percolate through the porous network of TiO_2 and eventually reach the back contact of the working electrode where charge collection and charge extraction occurs. The extracted charge can subsequently perform electrical work in the external circuit and eventually return to the counter electrode, where reduction of the redox mediator takes place. The liquid redox electrode will complete the circuit by reduction the oxidized dye.

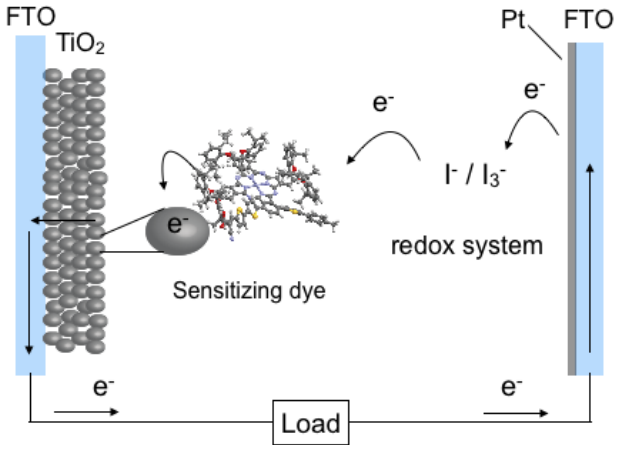

Figure 1-16: Schematic illustrations of the electron flow in an operating DSSC. [1] Dye excitation, [2] electron injection from photoexcited dye into TiO_2, [3] charge collection at working electrode, [4] reduction of triiodide at counter electrode and [5] regeneration (reduction) of the oxidized dye.

1.3. Thesis Objectives

The aim of this thesis is the design and synthesis of photosensitizers to increase the conversion efficiency of sunlight into energy in the near infrared region. The solar flux incident on the surface of the Earth spreads from the visible region to the near-infrared region. This suggests, therefore, that a panchromatic chromophore is ideal. However, since the absorption wavelength region of general organic semiconductors is limited to the visible region, light in the near-infrared region cannot be sufficiently utilized for photoelectric conversion. Hence, synthetic chemists are interested in the design and development of molecules that can efficiently photon-to-electron convert efficiently in the near-IR region. This thesis focuses on the development of metallophthalocyanines due to their strong absorption in the near infrared region (Q band), adjustable optical and electrochemical properties, and excellent chemical and thermal stability. As mentioned above, the advantage of metallophthalocyanines as a near-IR sensitizing dye is that their HOMO-LUMO energy bandgap can be finely tuned using several approaches. In this thesis, the author focuses on shifting the Q band of the metallophthalocyanine to longer wavelength, by changing the size and symmetry of the Pc macrocycle (**Chapters 3** and **4**), forming a dyad system (**Chapter 5**), and the introduction of peripheral substitutes (**Chapter 6**). These studies are summarized in the relevant sections as follows:

Chapter 3 describes the design, syntheses, and characterization of novel ring-expanded phthalocyanines. The effects of fusing fluorene rings with the porphyrazine core were investigated. The photovoltaic properties of synthesized ring-expanded phthalocyanines **1-3** were also examined by using them as

co-sensitizing dyes in P3HT/PCBM BHJ solar cells.

Chapter 4 describes the potential of the novel ring-expanded phthalocyanines as photosensitizers in DSSCs because of their suitable HOMO/LUMO levels and the red-shifted Q band. The optical and electrochemical properties of asymmetrical **FcS1** are described. The author investigated the performance of solar cells of DSSCs using **FcS1** as a photosensitizer.

In **Chapter 5**, a novel covalently linked zinc phthalocyanine - zinc porphyrin dyad is reported. The phthalocyanines and porphyrins are considered to be important molecular components in molecular arrays due to their complementary absorption regions in visible light. Moreover, intramolecular energy transfer from the porphyrin to phthalocyanine occurs very efficiently in most phthalocyanine-porphyrin dyads because the Q band absorption of phthalocyanine almost overlaps the fluorescence wavelength of porphyrin. Thus, a new phthalocyanine – porphyrin dyad was designed and synthesized to use as the photosensitizer of DSSCs. The optical and electrochemical properties of this novel Pc-Por dyad were investigated in this chapter, as well as its photovoltaic properties.

Chapter 6 describes the optical effect of the substitution of thiophene at the α or β position. As a result, α-substituted ZnPc showed a larger red shift of the Q band compared with that of β-substituted ZnPc. Thus, two new hybrid chromophoric systems (**αPcS1** and **αPcS2**) were designed and synthesized, in which a π-conjugated side chain with an adsorption site was introduced at an α position of the MPc to act as the photosensitizer in DSSCs.

References

[1] D. A. Bryant and N.-U. Frigaard, *Trends in Microbilogy*, **2006**, 14, 488-496.

[2] J. Barber, *Chem. Soc. Rev*., **2009**, 38, 185-196.

[3] G. R. Fleming, G. S. Schlau-Cohen, K. Amarnath, and J. Zaks, *Faraday Discuss*., **2012**, 155, 27-41

[4] L. L. Shipman, T. M. Cotton, J. R. Norries, J. J. Katz, *J. Am. Chem. Soc*., **1976**, 98, 8222-8230.

[5] a) M. R. Wasielewski, *Acc. Chem. Res*., **2009**, 43, 1910-1921; b) D. Gust, T. A. Moore and A. L. Moore, *Acc. Chem. Res*., **2009**, 42, 1890–1898; c) S. Fukuzumi, *Pure Appl. Chem.*, **2007**, 79, 981–991; d) J. L. Sessler, C. M. Lawrence and J. Jayawickramarajah, *Chem. Soc. Rev.*, **2007**, 36, 314–325; e) A. K. Burrell, D. L. Officer, P. G. Plieger and D. C. W. Reid, *Chem. Rev*., **2001**, 101, 2751–2796.

[6] G. P. Smestad, F. C. Krebs, C. M. Lampert, C. G. Granqvist, K. L. Chopra, X. Mathew, H. Takakura, *Sol. Energy Mater. Sol. Cells*, **2008**, 92, 371.

[7] a) D. A. McQuarrie and J. D. Simon, *Physical Chemistry A Molecular Approach*, University Science Books, Sausalito, California, **1997**, pp.496; b) N. J. Turro, V. Ramamrthy, J. C. Scaiano, *Modern Morecular Photochemistry of Organic Molecules*, University Science Books, Sausalito, California, **2010**, pp.29; c) D. W. Ball, *Physical Chemistry*, Thomson Learning Inc., California, **2003**, pp.464; d) P. Atkins and J. de Paula, *Atkins' Physical chemistry 7th Edition*, Oxford university press, New York, **2002**, pp484; e) W. Kaim, *Coord. Chem. Rev.*, **2011**, 255, 2503-2513; f) J. Fabilan, *Chem. Rev*, **1992**, 92, 1197-1226.

[8] James K. Drennen and Robert A. Lodder, "Pharmaceutical applications of near-infrared spectrometry", *In Advances in Near-Infrared Measurements*, edited by G. Patonay, JAI, **1993**, pp. 93-112

[9] M. R. Wasielewski, *Chem. Rev*. **1992**, 435-461.

[10] H. Imahori and S. Fukuzumi, *Adv. Funct. Mater*. **2004**, 14, 526.

[11] M. Ethirajan, Y. Chen, P. Joshi, R. K. Pandey, *Chem. Soc. Rev*. **2011**, 40,

340-362.

[12] A. Braun and J. Tchernicac, *Ber. Deut. Chem. Ges.*, **1907**, 40, 2709-2714

[13] R. P. Linstead, *J. Chem. Soc*., **1934**, 1016-1017.

[14] A. B. Sorokin, *Chem. Rev*. **2013**, 113, 8152-8191

[15] O. A. Melville, B. H. Lessard, T. P. Bender, *ACS Appl. Mater. Interfaces*, **2015**, 7, 13105-13118

[16] D. Gu, Q. Chen, X. Tang, F. Gan, S. Shen, K. Liu, H. Xu, *Optics Communications*, **1995**, 121, 125-129.

[17] F. I. Bohrer, C. N. Colesniuc, J. Park, M. E. Ruidiaz, I. K. Schuller, A. C. Kummel, W. C. Trogler, *J. Am. Chem. Soc.* **2009**, 131, 478-485.

[18] C. M. Allen, W. M. Sharman, J. E. Vanlier, *J. Porphyrins Phthalocyanines*, **2001**, 5, 161-169.

[19] G. de la Torre, C. G. Classens, T. Torres, *Chem. Commun*., **2007**, 2000-2015.

[20] S. J. Mathews, S. C. Kumar, L. Giribabu, S. V. Rao, *Materials Letters*, **2007**, 61, 4426-4431.

[21] L. Martín-Gomis, F. Fernández-Lázaro, Á. Sastre-Santos, *J. Mater. Chem. A,* **2014**, 2, 15672-15682.

[22] a) Martin Gouterman, *Chem. Phys.*, **1959**, 30, 1139-1161; b) Martin Gouterman, J. Mol. *Spectrosc*, **1961**, 6, 138-163; c) Martin Gouterman, G. H. Wagnière, and L. C. Snyder, *J. Mol. Spectrosc.*, **1963**, 1, 108-127; d) L. Edwards and M. Gouterman, *J. Mol. Spectrosc*, **1970**, 33, 292-319.

[23] a) P.-C. Lo, X. Leng, and D. K. P. Ng, *Coord. Chem. Rev.*, **2007**, 251, 2334-2353; b) S. Tannert, E. A. Ermilov, J. O. Vogel, M. T, M. Choim, D. K. P. Ng, and B. Röder, *J. Phys. Chem. B,* **2007**, 111, 8053-8062.

[24] a) N. Kobayashi, H. Konami, In Phthalocyanines: Properties and Applications (Eds.: C. C. Leznoff and A. B. P. Lever), Vol. 4, Wiley-VCH, Weinheim, Germany, 1996, Chapter9, pp 343-404; b) K. Ishii and N. Kobayashi, in The Porphyrin Handbook (Eds.: K. M. Kadish, K. M. Smith, R. Guilard),

Academic Press, New York, 2002, Chapter 102, pp. 1-40; c) T. Fukuda and N. Kobayashi, In Handbook of Porphyrin Science (Eds.: K. M. Kadish, K. M. Smith, R. Guilard), World Scientific,Singapore, Chapter 42, pp. 2-602.

[25] J. E. Bloor, J. Schlabitz, C. C. Walden, *Can. J. Chem.* **1964**, 42, 2201-2208.

[26] O. Matsushita, V. M. Derkacheva, A. Muranaka, S. Shimizu, M. Uchiyama, E. A. Luk'yanets, and N. Kobayashi, *J. Am. Chem. Soc*. **2012**, 134, 3411-3418

[27] M. S. Rodríguez-Morgade, B. Cabezón, S. Esperanza, and T. Torres, *Chem. Eur. J.* **2001**, 7, 2407-2413.

[28] N. Kobayashi, S. Nakajima, H. Ogata, and T. Fukuda, *Chem. Eur. J*. **2004**, 10, 6294-6312.

[29] A. Muranaka, M. Yonehara, M. Uchiyama, *J. Am. Chem. Soc*. **2010**, 132, 7844-7845

[30] H. Miwa, K. Ishii, N. Kobayashi, *Chem. Eur. J*. **2004**, 10, 4422.

[31] N. Kobayashi, N. Sasaki, Y. Higashi and T. Osa, *Inorg. Chem*. **1995**, 34, 1636-1637.

[32] N. Kobayshi, H. Ogata, N. Nonaka, and E. A. Luk'yanets, *Chem. Eur. J*. **2003**, 9, 5123-5134.

[33] J. Mack, N. Kobayshi, *Chem. Rev.* **2011**,111, 281-321.

[34] D. M. Chapin, C. S. Fuller and G. L. Pearson, *J. Appl. Phys*. **1954**, 25, 676

[35] M. A. Green et al. *Prog. Photovolt: Res. Appl.* **2015**, 23, 1-9

[36] M. Afzaal and P. O'Brien, *J. Mater. Chem*. **2006**, 16, 1597-1602.

[37] G. Dennler, M.C. Scharber and C.J. Brabec, *Adv. Mater.* **2009**, 21, 1323.

[38] B. A. Gregg, *J. Phys. Chem. B* **2003**, 107, 4688-4698.

[39] B. A. Gregg, M. A. Fox, A. J. Bard, *J. Phys. Chem.* **1990**, 94, 1586-1598.

[40] A. L. Fahrenbruch, R. H. Bube, *Fundamentals of Solar Cells. PhotoVoltaic Solar Energy ConVersion*, Academic Press, New York, **1983**.

[41] B. A. Gregg, M. C. Hanna, *J. Appl. Phys.* **2003**, 93, 3605- 3614.

[42] B. A. Gregg, J. Sprague, M. Peterson, *J. Phys. Chem. B* **1997**, 101,

5362-5369.

[43] C.W. Tang, *Appl. Phys. Lett.* **1986**, 48, 183.

[44] M. Hiramoto, H. Fujiwara, M. Yokoyama, *Appl. Phys. Lett.* **1991**, 58, 1062.

[45] G. Yu, J. Gao, J. C. Hummelen, F. Wudl, A. J. Heeger, *Science*, **1995**, 270, 1789.

[46] C. J. Brabec, G. Zerza, G. Cerullo, S. De Silenstri, S. Luzzatti, J.C. Humelen, N. S. Sariciftci, *Chem. Phys. Lett*. **2001**, 340, 232.

[47] J. C. Hurmmelen, B. W. Knight, F. LePeq, F. Wudl, J. Yao, C. L. Wilkins, *J. Org. Chem.*, **1995**, 60, 532,

[48] F. Padinger, F. R. S. Rittberger, N. S. Sariviftci, *Adv. Funct. Mater.*, **2003**, 13, 85.

[49] G. Li, V. Shrotriya, J. Huang, Y. Yao, T. Moriarty, K. Emery, Y. Yan, *Nat. Mater.* **2005**, 4, 864.

[50] Y. Kim, S. Cook, S. M. Tuladhar, S. A. Choulis, J. Nelson, J. R. Durrant, D. D. C. Bradley, M. Giles, I. McCulloch, C.-S. Ha, M. Ree, *Nat. Mater.* **2006**, 5, 197..

[51] N. Blouin, A. Michaud, and M. Leclerc, *Adv. Mater.* **2007**, 19, 2295-2300.

[52] Y. Liang, Z. Xu, J. Xia, S.-T. Tsai, Y. Wu, G. Li, C. Ray, and L. Yu, *Adv. Mater*. **2010**, 22, E135-E138.

[53] A. Fujishima, K. Honda, *Nature,* **1972**, 238, 37-38

[54] H. Tsubomura, M. Matsumura, Y. Nomura, T. Amamiya, *Nature*, **1976**, 261, 402-403.

[55] J. Desilvestro, M. Gratzel, L. Kavan, J. Moser, J. Augustynski, *J. Am. Chem. Soc*. **1985**, 107, 2988-2990.

[56] B. O'Regan, M. Grätzel, *Nature*, **1991**, 353, 737-740.

[57] M. K. Nazeeruddin, A. Kay, I. Rodicio, R. Humphry-Baker, E. Müller, P. Liska, N. Vlachopoulos, and M. Grätzel *J. Am. Chem. Soc*. **1993**, 115, 6382-6390.

[58] M. K. Nazeeruddin, S. M. Zakeeruddin, R. Humphyr-Baker, J. P. Liska, N. Vlachopoulos, V. Shklover, C.-H. Fischer, and M. Grätzel, *Inorg. Chem.* **1999**, 38, 6298-6305.

[59] M. K. Nazeeruddin, P. Péchy and M. Grätzel, *Chem. Commun*., **1997**, 17050-1706.

[60] Z.-S. Wang, N. Koumura, Y. Cui, M. Takahashi, H. Sekiguchi, A. Mori, T. Kubo, A. Furube, and K. Hara, *Chem. Mater*., **2008**, 3993-4003.

[61] D. P. Hagberg, J.-H. Yum, H. Lee, F. De Angelis, T. Marinado, K. M. Karlsson, R. Humphry-Baker, L. Sun, A. Hagfeldt, M. Grätzel, and M. K. Nazeeruddin, *J. Am. Chem. Soc*. **2008**, 130, 6259-6266.

[62] K. Hara, T. Sato, R. Katoh, A. Furube, Y, Ohga, A. Shinpo, S. Suga, K. Sayama, H. Sugihara, and H. Arakawa, *J. Phys. Chem. B* **2003**,107, 597-606.

[63] A. Yella, H.-W. Lee, H. N. Tsao, C. Yi, A. K Chandiran, M. K. Nazeeruddin, E. W.-G. Diau, C.-Y. Yeh, S. M. Zakeeruddin, and M. Gräzel, *Science*, **2011**, 334, 629.

[64] S. Mathew, A. Yella, P. Gao, R. Humphry-Baker, B. F. E. Curchod, N. Ashari-Astani, I. Tavernelli, U. Rothlisbeger, M. K. Nazeeruddin, M. Gräzel, *Nat. Chem*., **2014**, 6, 242-247.

[65] a) S. Mori, M. Nagata, Y. Nakahata, K. Yasuta, R. Goto, M. Kimura, M. Taya, *J. Am. Chem. Soc.* **2010**, 132, 4054-4055; b) M. Kimura, H. Nomoto, N. Masaki, and S. Mori, *Angew. Chem. Int. Ed*. **2012**, 51, 4371-4374; c) M. Kimura, H. Nomoto, H. Suzuki, T. Ikeuchi, H. Matsuzaki, T. N. Murakami, A. Furube, N. Masaki, M. J. Griffith, and S. Mori, *Chem. Eur. J.* **2013**, 19, 7496-7502.

[66] T. Ikeuchi, H. Notomo, N. Masaki, M. J. Griffith, S. Mori, and M. Kimura, *Chem. Commun*., **2014**, 50, 1941-1943.

Chapter 2

General experimental

2.1. Syntheses and characterizations

2.1.1. Materials and syntheses

All chemicals were purchased from commercial suppliers used without further purification. Column chromatography was performed with activated alumina (Wako, 200mesh). Recycling preparative gel permeation chromatography was carried out by a Japan analytical industry Co., Ltd. (JAI) recycling preparative HPLC using $CHCl_3$ as an eluent. Analytical thin layer chromatography was performed with commercial Merck plates coated with aluminum oxide 60 F_{254}.

2.1.2. Characterization of compounds

NMR spectra were recorded on a Bruker AVANCE 400 FT NMR spectrum at 399.65 and 100.62 MHz for ^{1}H and ^{13}C in $CDCl_3$ solution. NMR data are reported as follows: Chemical shift in ppm, multiplicity (s = singlet, d = doublet, t = triplet, m = multiplet). Chemical shifts are reported relative to internal TMS. IR spectra were obtained on a SHIMADZU IR Presige-21 with DuraSamole IR II. MALDI-TOF mass spectra were obtained on a Bruker autoflex spectrometer with dithranol as matrix. High resolution mass spectra with electrospray ionization were obtained on a Bruker Daltonics micrOTOF Ⅱ.

2.1.3. UV-Vis absorption and fluorescence spectroscopy

The absorption coefficients (ε) were calculated from absorption measurements:

$$Abs = log(\frac{I}{I_0}) = c\,\varepsilon\,L$$

where Abs is the measured absorbance, I is the transmitted intensity, I_0 is the intensity of the incident light at a given wavelength, L is the pass length through the sample. UV-Vis spectra and fluorescence spectra were measured on a JASCO V-650 and a JASCO FP-750, respectively.

2.1.4. Magnetic circular dichroism (MCD) spectroscopy

MCD spectroscopy gives many key insights into the optical spectroscopy and electronic structure of molecules. MCD spectroscopy measures with a magnet attached to a circular dichroism (CD) spectrometer. Unlike CD measurement, MCD signal can be measured even if it is not an optically active molecule. In particular, it is effective tool for analysis of electronic structure of highly symmetrical molecules such as porphyrin and phthalocyanine. The MCD spectra were measured with JASCO J-820 using a 1.38 T magnet.

2.1.5. Electrochemistry

Electrochemistry provides information about the dye ground state oxidation potentials in solution and when adsorbed onto TiO_2. Cyclic voltammetry (CV) and Differential pulse voltammetry (DPV) was performed with 0.1 M tetrabutylammonium hexafluorophosphate ($TBAPF_6$) as supporting electrolyte. A platinum working electrode platinum counter electrode and a Ag/Ag+ reference electrode were normally used. The system was internally calibrated with ferrocene/ferrocenium (Fc/Fc^+). CV and DPV data were recorded with an ALS 720C potentiostat, and electrochemical experiments were performed under purified

nitrogen gas.

2.1.6. Computational chemistry

Molecular electronic structure calculation was carried out using density functional theory (DFT) and time-dependent density functional theory (TD-DFT). The DFT method and the TD-DFT method provide a modern and diverse means for investigating molecular structure and solid-state structure, reaction path, thermal chemistry, dipole moment, spectroscopic response, and many other properties. DFT calculation was performed using Becke's three parameter exchange function (B3) and Lee-Yang-Parr (LYP) correlation function. The B3LYP hybrid function is selected as it provides a fairly accurate description of metal interactions. B3LYP correctly reproduces thermochemical reactions of many compounds including transition metal atoms. In this thesis, the geometric optimization of the dye was calculated using B3LYP/6-31g (d) level. The excited state electronic structure and UV-Vis electron absorption were calculated using the hybrid function CAM-B3LYP/6-31g (d).

2.2. Fabrication of devices

2.2.1. OPV solar cells

Indium tin oxide (ITO) patterned glass substrates were cleaning with sonication in neutral detergent, distilled water, acetone, and 2-propanole. The substrates were dried and apply UV-O_3 treatment for 30 min. Electron blocking layer were prepared by spin-coated the PEDOT/PSS (H. C. Starck) with a thickness of 40 nm.

A solution containing a mixture of P3HT, PCBM, and ZnFcs (1:1:0.11 wt. ration) in chlorobenzene were spin-coated onto the PEDOT/PSS layer and apply thermal annealing treatment at 150 °C for 10 min in the argon filled globe box. Titanium oxide solution was spin-coated onto the active layer then place in air for 30 min. The counter electrode of aluminum was prepared by thermal deposition with a thickness of 100 nm.

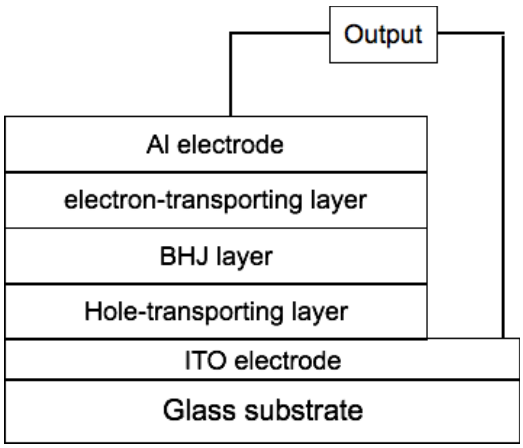

Figure 2-1: The basic structure of BHJ solar cells

2.2.2. Dye-sensitized Solar Cells (DSSCs)

Double layered nanoporous TiO_2 electrodes were prepared by applying pastes of TiO_2 nanoparticles having two different diameters of 15-20 and 400 nm onto transparent conducting glass substrates (SnO_2:F, on 1.8 mm thick glass substrate, Asahi Glass) with the screen printing technique. The electrodes were sintered at 550 °C for 30 min in air. $TiCl_4$ treatment was applied to obtain higher efficiency. The apparent surface area of the TiO_2 electrode was 0.25 cm^2 (0.5 x 0.5 cm). A black mask (0.16 cm^2) was applied on the cell to reduce diffusive light. The adsorption of dye to nanocrystalline TiO_2 films was achieved by immersion of metal oxide electrodes in 0.05 mM toluene solutions of the dyes for 24 h at 25 °C.

The dye-adsorbed TiO_2 electrodes were washed with toluene to remove the physically adsorbed dye completely before measurements. Working and Pt counter electrodes were separated by a 50 mm thick hot melt ring (Surlyn, DuPont) and sealed by heating. Redox electrolytes (0.1 M LiI, 0.6 M DMPImI, 0.5 M tBP, and 0.05 M I_2 in dehydrated acetonitrile) were introduced into the space between the dye-adsorbed TiO_2 electrode and the counter electrode.

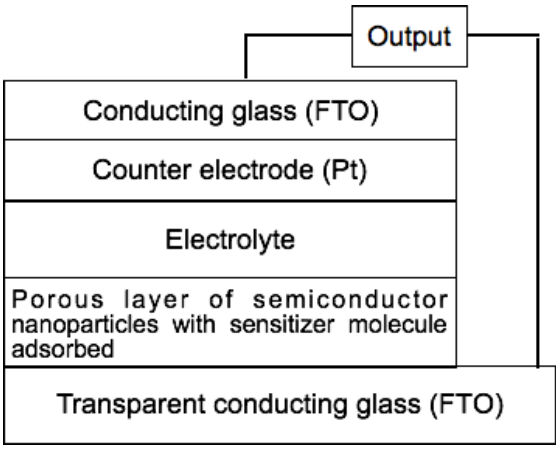

Figure 2-2: The basic structure of DSSCs.

2.2.3. Evaluation methodology for solar cells

Solar cells are generally evaluated with parameters such as power conversion efficiency (PCE) and incident photon-to-current efficiency (IPCE). The efficiency of the BHJ solar cells and DSSCs is related to a large number of parameters. The current density-voltage curves were measured using a Keithley 2400 Source Measuer Unit.

PCE is determined from the *J-V* characteristic of the solar cells under light irradiation. Schematic *J-V* characteristics of the cell in the dark and under irradiation are depicted in Figure 2-3. When the light is irradiated, photocurrent is

generated and the curve is shifted to downward. The current obtained at zero voltage is called short circuit current, J_{SC} and the voltage obtained at zero current is called open circuit voltage, V_{OC}. The maximum output is the area where is the product of V_{max} and J_{max}, shown in Figure 2-3. The ratio of the maximum output and the product of V_{OC} and J_{SC} is called fill factor (FF).

$$FF = \frac{J_{max} \times V_{max}}{J_{SC} \times \mathrm{V_{OC}}}$$

PCE is then defined as the ratio of the maximum output of the energy of the irradiated light (P_{in}).

$$PCE = \frac{J_{max} \times V_{max}}{P_{in}} \times \frac{FF \times J_{SC} \times V_{OC}}{P_{in}} \times 100$$

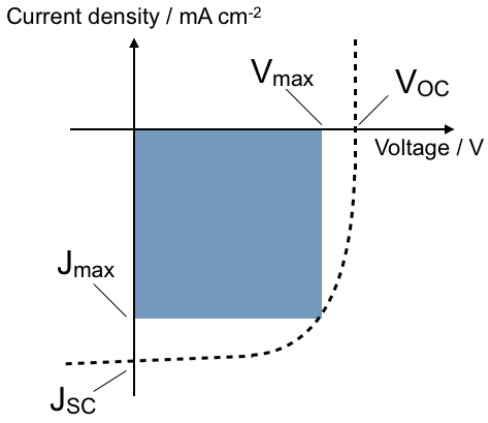

Figure 2-3: Schematic *J-V* characteristics under the light irradiation.

In this thesis, PCE was evaluated under global sunlight (AM 1.5 G) irradiation with a simulated air mass of 1.5, which is an international standard. Outside the atmosphere, sunlight is a spectrum as shown in Figure 2-4a, but it scatters by molecules in the air and changes due to absorption of oxygen or moisture until

reaching the surface of the earth. Therefore, AM 0, AM 1, and AM 1.5 are defined for space, equatorial region, and subtropical regions, respectively, as reference sunlight for solar cell measurement (Figure 2-4b). It is standardized to measure with reference sunlight of AM 1.5 G, irradiance of 1000 W/m^2, temperature 25 °C in Japan.

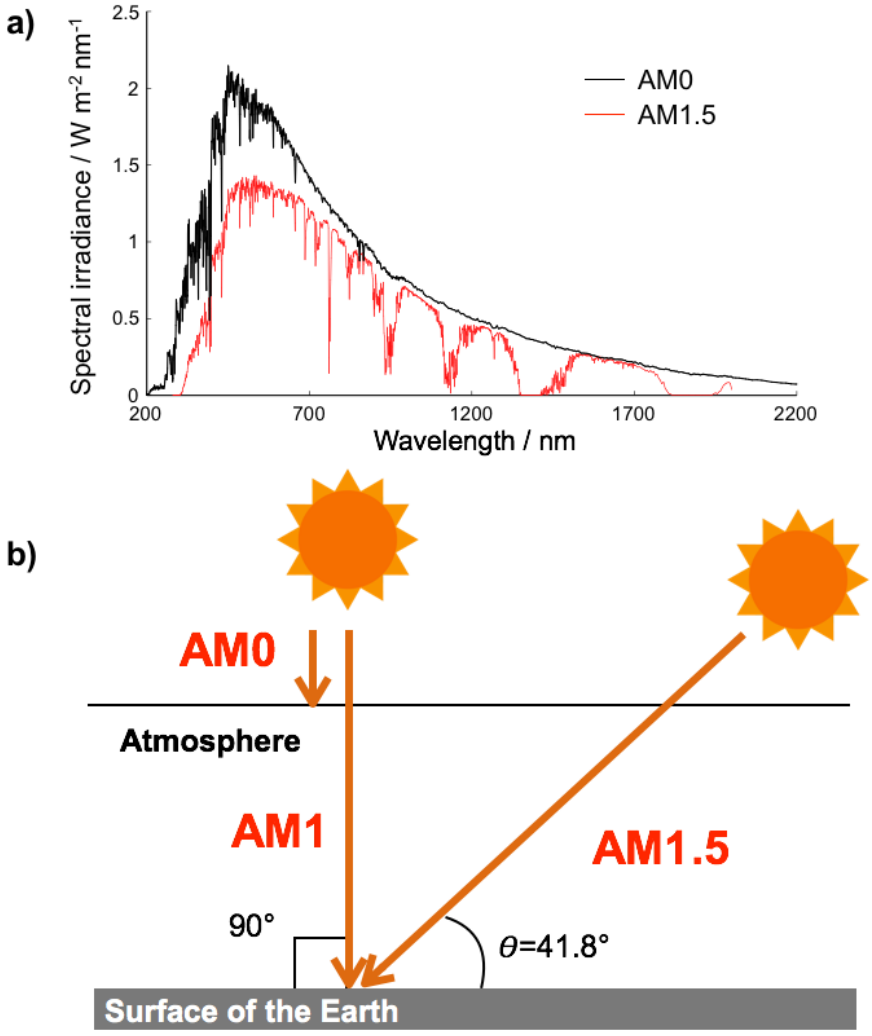

Figure 2-4: a) Standard solar spectra of AM0 and AM1.5G; b) Schematic image of AM0, AM1, and AM1.5

IPCE is defined as the ratio of number of electrons extracted ($n_{electron}$) from the solar cell and number of photons irradiated (n_{photon}). IPCE is evaluated under

monochromeatic light irradiation, which directly measures how efficiently the incident photons are converted to electrons.

$$IPCE\ (\%)\ = \frac{number\ of\ collected\ electrons}{number\ of\ incident\ photons} \times 100$$

$$= \frac{1240 \times J_{SC}}{\lambda \times \Phi_{in}} \times 100$$

J_{SC} is the short circuit current density, λ is the wavelength of the incident light and Φ_{in} is the intensity of the incident light.

Chapter 3

Extension of light-harvesting area of bluk-heterojunction solar cells by co-sensitization with ring-expanded metallophthalocyanines fused with fluoren skeletons

Summary: Near-IR absorbing zinc fluorenocyanine complexes **1-3** were designed and synthesized as a co-sensitizer for bulk-heterojunction solar cells. Fusing fluorene rings with the porphyrazine rings resulted in narrower band gap and stabilization of both the HOMO and LUMO energy levels compared with a zinc phthalocyanine complex. The synthesized fluorenocyanines **1-3** were incorporated in to bulk-heterojunction solar cells based on regioregular poly(3-hexylthiophene) and 1-(3-methocyacarbonyl)-propyl-1-phenyl-(6,6)C_{61}. The addition of **3** decorated with eight alkyl chains resulted in improved device performance with a 16 % enhancement of the short circuit current compared with that of the reference cell without **3**.

3.1. Introduction

Organic photovoltaic devices (OPVs) based on thin films of organic semiconductors have been intensely investigated as a promising candidate for low-cost, light weight, and scalable solar cells.[1-3] The performance of OPVs was greatly improved by producing an interpenetrating nanostructured interface between electron donor and acceptor materials to overcome the limited diffusion length of excitons in organic semiconductors. A bulk heterojuntion (BHJ) architecture, which is constructed donor and acceptor materials, provides a suitable nanostructure for high conversion efficiencies of OPVs, as well as printable fabrication processes.[4] Controlling BHJ structure in the active layers allows a high interfacial area that optimizes the exciton dissociation and the efficient transport of the generated charges to the electrodes.[5,6] BHJ solar cells based on a blend of regioregular poly(3-hexylthiophene) (P3HT) and 1-(3-methoxycarbonyl)-propyl-1-phenyl-(6,6)C_{61} (PCBM) are a benchmark active layer with average power conversion efficiencies (PCEs) of 2-4 % under a standard global AM 1.5 illumination (100mW/cm^{-2}).[7-12] Since the light-harvesting area of P3HT/PCBM active layer can not convert the energy of red light into electricity. To further enhance the performance of BHJ solar cells, several efforts have been devoted to the development of tandem architectures, novel active layer materials based on low band gap polymers, and additional co-sensitizers.[3] Adding co-sensitizers with energy levels that are intermediate of those of conjugated polymers and PCBM into the blended active layers is a simple and versatile approach, and several near-IR absorbing molecules have been used as a co-sensitizer in BHJ solar cells to expand the light-harvesting region.[13-17]

Phthalocyanines (Pcs) and their metal complexes have been widely investigated

as near-IR absorbing dye because of their high stability, the presence of an intense absorption band in the near-IR region, and tunable redox activety.[18] Regarding BHJ solar cells, several groups have reported the enhancement of PCE values through the expansion of the light harvesting region of the cells by the addition of silicon phthalocyanine derivatives (SiPc), liquid crystalline Pcs, and fullerene-functionalized ZnPcs.[19-23] Ohkita et al. discussed the location of SiPc at the interface of P3HT and PCBM domains in the active layer of BHJ solar cells.[23] They found that the selective doping of SiPc at the disordered P3HT domains improved device performance. However, ZnPc lacking axial substituents did not exhibit the PCE improvement in the P3HT/PCBM-based BHJ solar cells. In this study, we developed near-IR absorbing co-sensitizers based on ring-expanded ZnPcs for the BHJ solar cells.

The electronic structure and properties of MPcs can be tailored by modifying the macrocyclic ligands and changing the central metals.[24] Substitutions to the macrocycles by electron-donating and electron-accepting groups were found to change the significant red shift of the Q band beyond 1000 nm in phosphorus phthalocyanines by the introduction of electron-donating groups at the α positions and deformation of the planarity of the Pc plane.[25] The other approach to tuning the electronic properties of MPcs is to modify the extension of the π-conjugation system. Considerable studies were concerned with expanded MPcs that fuse additional aromatic rings attached to the Pc ring. Muranaka et al. succeeded in shifting the Q band and stabilizing the LUMO level by fusing an electron-accepting azulene skelton with the prophyrazine ring.[26] While fluorene rings have been used as molecular components for various organic devices,[27] a prohyrazine derivative fused with fluorene rings has not been reported. Fusing fluorene rings with the porphyrazine rings may change the electronic structure. Here, the author described the synthesis and characterization of zinc fluorenocaninse (ZnFcs) **1**-**3**, in which

four fluorene rings were connected with the porphyriazine ring (Figure 3-1). The author also discusses solar cell performance improved by the addition of ZnFcs in the blended films of P3HT and PCBM.

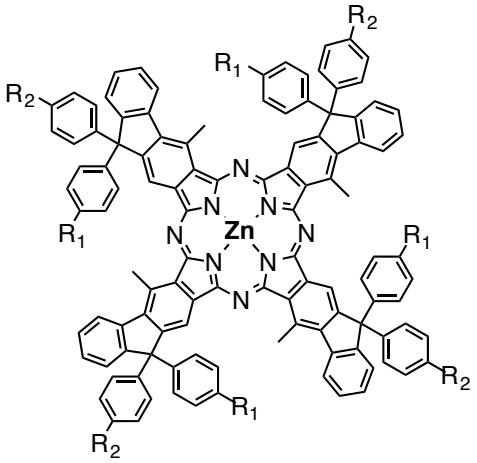

1: $R_1 = R_2 = -CH_3$
2: $R_1 = -CH_3$; $R_2 = -(CH_2)_5CH_3$
3: $R_1 = R_2 = -(CH_2)_5CH_3$

Figure 3-1: Structure of zinc fluorenocyanines (ZnFcs) **1-3**. ZnFcs **1-3** are composed of a mixture of structural isomers.

3.2. Experimental section

Synthesis of ZnFcs 1-3

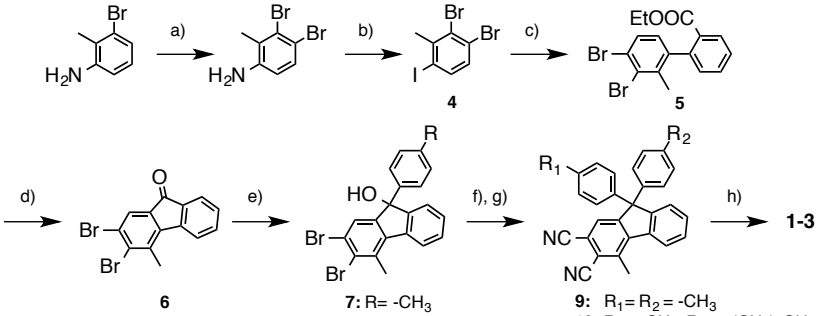

Scheme 3-1: a) TBA Br_3, CH_2Cl_2, MeOH; b)HBF_4, NaNO, KI; c) 2-(ethoxycarnonyl)phenylboronic acid pinacol ester, $Pd(PPh_3)_4$, toluene/THF/$NaCO_3$ aq.;d) H_2SO_4; e) ArMgBr, Et_2O; f) ArH, CF_3SO_3H; g) CuCN, NMP; h) $Zn(AcO)_2$, DMAE

3,4-dibromo-2methylaniline: A solution of tetrabutylammonium tribromide (12.5 g, 26.0 mmol) in CH_2Cl_2 (35 ml) was added to 3-bromoaniline (4.8 g, 28.0 mmol) in CH_2Cl_2 (30 ml). The mixture was stirred at room temperature for 30 min. After evaporation of solvent, the residue was suspended in 2M aqueous NaOH (100 ml). The aqueous mixture was extracted with Et_2O and the organic layers were washed with water. After the organic layer was dried over Na_2SO_4, the solvent was removed under reduced pressure. Crystallization from cyclohexane afforded 3,4-dibromo-2methylaniline as white solid (4.8 g, yield 70 %). ^{1}H-NMR($CDCl_3$, 400.13MHz): δ (ppm) 7.26 (t, *J* = 8.0 Hz, 1H, ArH), 6.52 (d, *J* = 8.0 Hz, 1H, ArH), 3.71 (s, 2H, -NH_2), 2.35 (s, 3H, -CH_3); ^{13}C-NMR ($CDCl_3$, 100.61 MHz): δ (ppm) 144.4, 130.9, 127.5, 124.3, 115.2, 113.4, 18.8.

4: A solution of $NaNO_2$ (0.63 g, 9.1 mmol) in water (10 mL) was added dropwise to a suspension of 3,4- dibromo-2-methylaniline (2 g, 7.6 mmol) in a mixture of water (60 mL) and 48% aqueous tetrafluoroboric acid (3.0 mL, 18.9 mmol) at 0 °C. The mixture was stirred at 0 °C for 1 h. After 1 h, the solution of potassium iodide (2.5 g, 0.015 mmol) in water (10 mL) was added to the mixture, and the reaction mixture was stirred at 0 °C for 1 h. The reaction mixture was poured into water, and the aqueous layer was extracted with 3 × 50 mL of Et_2O. The collected organic layer was washed with $Na_2S_2O_3$ and water. After the mixture was dried over Na_2SO_4, the solvent was evaporated and the residue was purified by column chromatography on silica gel by eluting with CH_2Cl_2 followed by recrystallization from methanol afforded **4** as white solid (1.9 g, yield 67%). ^{1}H NMR (400.13 MHz, CDCl3): δ (ppm) 7.63 (d, *J* = 8.4 Hz, 1H, ArH), 7.15 (d, *J* = 8.4 Hz, 1H, ArH), 2.77 (s, 3H, −CH_3). ^{13}C NMR ($CDCl_3$, 100.61 Hz): δ (ppm) 142.9, 138.8, 132.2, 126.4, 126.2, 98.9, 31.6.

5: A solution of 4 (0.82 g, 2.2 mmol), 2-ethoxycarbonylphenylbor- onic acid pinacol ester (0.5 g, 1.8 mmol), and $Pd(PPh_3)_4$ (41.6 mg, 36 μmol) in toluene (6.6 mL), THF (8.3 mL), and 2 M K_2CO_3 aqueous solution (5 mL) was stirred at 70 °C for 48 h under nitrogen. After cooling to room temperature, the reaction mixture was poured into water, extracted with Et_2O. The organic layer was dried over Na_2SO_4 and solvent was evaporated. The residue was purified by column chromatography on silica using hexane/CH_2Cl_2 (10/1 v/v) and then (1/10 v/v) followed by recycling preparative HPLC to give 5 (0.74 g, yield 52%). ^{1}H NMR (400.13 MHz, $CDCl_3$): δ (ppm) 8.01 (d, *J* = 6.0 Hz, 1H, ArH), 7.55 (t, *J* = 8.0 Hz, 1H, ArH), 7.44−7.49 (m, 2H, ArH), 7.17 (d, *J* = 8.0 Hz, 1H, ArH), 6.91 (d, *J* = 8.4 Hz, 1H, ArH), 4.04−4.12 (m, 2H, −$COOCH_2$-), 2.21 (s, 3H, −CH3), 1.03 (t, *J* = 7.2 Hz, 3H, −CH_3). ^{13}C NMR ($CDCl_3$, 100.61 Hz): δ (ppm) 166.9, 142.2, 141.6, 138.5, 131.8, 130.6, 130.4, 130.3, 130.1, 128.5, 127.8, 127.3, 124.3, 60.9, 22.6, 13.7. IR (ATR): ν 1714 (−COO−) cm^{-1}.

6: A solution of **5** (0.74 g, 1.86 mmol) in concentrates sulfuric acid (22.3 mL) was stirred at room temperature for 12 h. The reaction mixture was poured into ice water, and it was stirred for a further 15 min. The aqueous layer was extracted with 3 × 50 mL of CH_2Cl_2. The solvent was evaporated, and the residue was purified by column chromatography on silica gel using CH_2Cl_2 to give **6** as yellow solid (0.63 g, 97%). ^{1}H NMR (400.13 MHz, $CDCl_3$): δ (ppm) 7.75 (s, 1H, ArH), 7.73 (d, *J* = 6.8 Hz, 2H,ArH), 7.53 (t, *J* = 7.6 Hz, 1H, ArH) 7.35 (t, *J* = 7.2 Hz, 1H, ArH), 2.80 (s, 3H, −CH3). ^{13}C NMR ($CDCl_3$, 100.61 Hz): δ (ppm) 192.2, 144.6, 141.8, 136.5, 135.6, 135.4, 134.6, 134.3, 129.7, 126.8, 126.7, 125.1, 124.2, 21.9. IR (ATR): ν 1705 (−C=O) cm^{-1}.

7: The Grignard reagents were prepared from magnesium powders (100 mg, 4.1 mmol) in dry Et_2O (1 mL) and *p*-bromotoluene (8.2 mmol). Compound **6** (0.15 g,

0.43 mmol) was added into the Grignard solution and the resulted reaction mixture was refluxed for 12 h. The reaction mixture was hydrolyzed with saturated NH_4Cl solution followed by extracted with Et_2O.The organic layer was washed with water. The mixture was dried over $MgSO_4$ and the solvent was evaporated. The residue was purified by column chromatography on silica gel using CH_2Cl_2/hexane (1/10) and then (10/1) followed by recycling preparative HPLC to give **7** (0.16 g, 87%). 1H NMR (400.13 MHz, $CDCl_3$): δ (ppm) 7.85 (d, *J* = 8.0 Hz, 1H, ArH), 7.45 (s, 1H, ArH), 7.40 (t, *J* = 6.8 Hz, 1H, ArH), 7.28−7.35 (m, 2H, ArH), 7.22 (d, *J* = 8.4 Hz, 2H, ArH), 7.09 (d, *J* = 8.4 Hz, 2H, ArH), 2.92 (s, 3H, −CH3), 2.39 (s, 1H, −OH), 2.31 (s, 3H, −CH3). ^{13}C NMR ($CDCl_3$, 100.61 Hz): δ (ppm) 151.5, 151.3, 142.9, 139.9, 139.6, 138.2, 135.8, 129.7, 129.1, 128.8, 127.9, 125.6, 125.5, 124.0, 83.1, 21.8. IR (ATR): ν 3306 (−OH) cm^{-1}.

8: Compound **8** was synthesized from **6** and *p*-hexylphenyMgBr according to the same procedure of **7**. Yield: 69%. ^1H NMR (400.13 MHz, $CDCl_3$): δ (ppm) 7.85 (d, *J* = 7.6 Hz, 1H, ArH), 7.46 (s, 1H, ArH), 7.40 (t, *J* = 7.6 Hz, 1H, ArH), 7.29−7.37 (m, 2H, ArH), 7.23 (d, *J* = 8.4 Hz, 2H, ArH), 7.08 (d, *J* = 8.4 Hz, 2H, ArH), 2.92 (s, 3H, $-CH_3$), 2.40 (s, 1H, -OH), 1.53−1.61 (m, 2H, Ar-CH_2-), 1.24−1.35 (m, 8H, $-CH_2-$), 0.87 (t, *J* = 6.8 Hz, 3H, $-CH_3$). ^{13}C NMR ($CDCl_3$, 100.61 Hz): δ (ppm) 151.5, 151.3, 142.9, 139.9, 139.6, 138.2, 135.8, 129.7, 129.1, 128.8, 127.9, 125.6, 125.5, 124.0, 83.1, 36.0, 32.1, 31.7, 29.5, 23.0, 22.4, 14.5. IR (ATR): ν 3393 (−OH) cm^{-1}.

9: Compound **7** (0.41g, 0.92 mmol) was dissolved in dry toluene, and 0.16 mL CF_3SO_3H was added to this solution. The reaction mixture was heated at 50 °C with stirring for 10 min. The mixture was poured into an ice-cold $NaHCO_3$ aqueous solution. The product was extracted with Et_2O and the collected organic layer was dried over Na_2SO_4. After evaporation, the residue was purified by column

chromatography on silica gel using CH_2Cl_2/hexane (1/1) to give diaryl compound as white solid (0.24 g, 50%). ^{1}H NMR (400.13 MHz, $CDCl_3$): δ (ppm) 7.93 (d, *J* = 7.6 Hz, 1H, ArH), 7.51 (s, 1H, ArH), 7.35−7.39 (m, 2H, ArH), 7.29 (t, *J* = 7.6 Hz, 1H, ArH), 7.03 (s, 8H, ArH), 2.96 (s, 3H, −CH_3), 2.29 (s, 6H, −CH_3).

A CuCN (290 mg, 3.3 mmol) was added to a solution of diaryl compound (240 mg, 0.41 mmol) in NMP (10 mL). After stirred at 180 °C for 24 h, the mixture was cooled down to room temperature, and 30% aqueous ammonia (30 mL) was added. The product was extracted with Et_2O and the collected organic layer was dried over Na_2SO_4. After evaporation, the residue was purified by column chromatography on silica gel using CH_2Cl_2/hexane (1/1) to give **9** as white solid (100 mg, 60%). ^{1}H NMR (400.13 MHz, $CDCl_3$): δ (ppm) 8.00 (d, *J* = 9.2 Hz, 1H, ArH), 7.66 (s, 1H, ArH), 7.48−7.40 (m, 3H, ArH), 7.06 (d, *J* = 8.0 Hz, 4H, ArH), 6.99 (d, *J* = 8.0 Hz, 4H, ArH), 3.02 (s, 3H, −CH_3), 2.30 (s, 6H, −CH_3). ^{13}C NMR (CDCl3, 100.61 MHz): δ 156.8, 152.9, 145.5, 143.5, 140.4, 138.6, 137.7, 137.41, 130.0, 129.4, 128.8, 128.2, 127.8, 126.6, 124.7, 116.4, 115.9, 115.3, 114.0, 65.1, 21.3, 20.9, 19.6. IR (ATR): ν 2337.72 (−CN) cm^{-1}.

10: Compound **10** was synthesized according to same procedure of **9**. Yield: 47% (for two steps). ^{1}H NMR (400.13 MHz, $CDCl_3$): δ (ppm) 8.00 (d, *J* = 9.6 Hz, 1H, ArH), 7.66 (s, 1H, ArH), 7.41−7.48 (m, 3H, ArH), 7.03 (d, *J* = 6.0 Hz, 4H, ArH), 6.98 (d, *J* = 6.0 Hz, 4H, ArH), 3.02 (s, 3H, −CH_3), 2.55 (t, *J* = 7.6 Hz, 2H, $ArCH_2$-), 2.31 (s, 3H, −CH_3), 1.26−1.34 (m, 8H, −CH_2−), 0.87 (t, *J* = 6.8 Hz, 3H, −CH_3). ^{13}C NMR ($CDCl_3$, 100.61 MHz): δ 156.9, 152.9, 143.5, 142.4, 140.5, 138.5, 137.6, 137.4, 134.3, 130.0, 129.4, 128.9, 128.7,128.2, 127.8, 127.7, 126.6, 124.7, 116.4, 115.9, 115.3, 114.0, 65.1, 35.5, 31.7, 31.3, 29.0, 22.6, 20.9, 19.5, 14.1. IR (ATR): ν 2225.85 (−CN) cm^{-1}.

11: Compound **11** was synthesized from **8** with hexylbenzene and CH_3SO_3H.

Yield: 12% (for two steps). ^{1}H NMR (400.13 MHz, $CDCl_3$): δ (ppm) 7.93 (d, *J* = 9.6 Hz, 1H, ArH), 7.66 (s, 1H, ArH), 7.44−7.49 (m, 3H, ArH), 7.06 (d, *J* = 8.0 Hz, 4H, ArH), 7.00 (d, *J* = 8.0 Hz, 4H, ArH), 3.02 (s, 3H, $-CH_3$), 2.55 (t, *J* = 8.0 Hz, 4H, Ar CH_2-), 1.26−1.33 (m, 16H, $-CH_2-$), 0.87 (t, *J* = 8.0 Hz, 6H, $-CH_3$). ^{13}C NMR ($CDCl_3$, 100.61 MHz): δ 157.3, 153.4, 143.9, 142.9, 141.0, 138.9, 138.1, 130.3, 129.3, 129.1, 128.6, 128.2, 127.1, 125.1, 116.85, 116.3, 115.7, 114.4, 65.5, 35.9, 32.1, 31.7, 29.5, 23.0, 20.0, 14.4. IR (ATR): ν 2223.92 (−CN) cm^{-1}.

Zinc Fluorecyanines 1−3. **1**: A mixture of **9** (200 mg, 296 μmol) and $Zn(AcO)_2$ (43 mg, 197 μmol) in 4 mL of DMAE was heated at 150 °C with stirring for 24 h. After the mixture was cooled, the solvent was removed and washed with methanol several time to remove excess Zn ion. The residue was purified by column chromatography on activated alumina by eluting with CH_2Cl_2 and recycling preparative HPLC to give **1**. Yield: 36 mg, 35%. ^{1}H NMR ($CDCl_3$, 400.13 MHz): δ (ppm) 9.28−9.36 (m, 4H, ArH), 8.53−8.56 (m, 4H, ArH), 7.58−7.67 (m, 8H, ArH), 7.41−7.58 (m, 20H, ArH), 7.13−7.18 (m, 16H, ArH), 4.43−4.54 (m, 12H, $-CH_3$), 2.34 (s, 24H, $-CH_3$). MALDI-TOF Ms (dithranol): m/z 1705 (M + H). Calcd for $C_{120}H_{88}N_8Zn$: m/z 1705.6.

ZnFcs **2** and **3** were synthesized by the same procedure of **1**.

2. Yield: 26%. ^{1}H NMR ($CDCl_3$, 400.13 MHz): δ (ppm) 9.34−9.36 (m, 4H, ArH), 8.55−8.57 (m, 4H, ArH), 7.58−7.69 (m, 8H, ArH), 7.42−7.51 (m, 20H, ArH), 7.15−7.19 (m, 16H, ArH), 4.44−4.56 (m, 12H, −CH3), 2.57 (br, 8H, ArCH2-), 2.34 (s, 24H, $-CH_3$), 1.60 (br, 8H,$-CH_2-$), 1.25−1.31 (m, 24H, $-CH_2$), 0.82 (t, 12H, $-CH_3$). MALDI-TOF Ms (dithranol): m/z 1987 (M + H). Calcd for $C_{140}H_{128}N_8Zn$: m/z 1985.9.

3. Yield: 49%. ^{1}H NMR ($CDCl_3$, 400.13 MHz): δ (ppm) 9.36−9.40 (m, 4H, ArH),

8.54−8.56 (m, 4H, ArH), 7.57−7.68 (m, 8H, ArH), 7.41−7.49 (m, 20H, ArH), 7.14−7.18 (m, 16H, ArH), 4.43−4.55 (m, 12H, $-CH_3$), 2.57 (br, 16H, $ArCH_2-$), 1.59 (br, 16H, $-CH_2-$), 1.24−1.30 (m, 48H, $-CH_2$), 0.83 (t, 24H, $-CH_3$). MALDI-TOF Ms (dithranol): m/z 2265 (M + H). Calcd for $C_{160}H_{168}N_8Zn$: m/z 2265.2.

3.3. Results and Discussion

3.3.1. Synthesis of Zinc Fluorenocyanine 1-3

Scheme 1 illustrates the synthetic route of ZnFcs **1-3**. Precursors **9-11** were synthesized from 4-bromo-2-methylninine as a starting material through seven steps. The reaction of aniline with tetrabutylammonium tribromoide in a CH_2Cl_2 methanol readily gave 3,4-dibromo-2-methylaniline.[28] After the conversion of amine to iodide,[29] a palladium-catalyzed coupling reaction between **4** and 2-(ethoxycarbonyl)phenylboronic acid pinacol ester gave **5**. The fluorenone derivative **6** was obtained in a good yield by treating **5** with concentrated sulfuric acid.[30] Two aryl Grigard reagents, *p*-TolMgBr and *p*-hexylphenyMgBr, were reacted with **6** in diethyl ether at reflux temperature.[31] the corresponding alcohol derivatives **7** and **8** were isolated in good yields. The Friedel-Crafts reactions of **7** and **8** with touluene or hexylbenzene were carried out in the presence of an excess amount of CF_3SO_3H to give three 9,9-diarylfluorenes. In the final step, the bromides were transformed into dinitrile **9-11** by treatment with CuCN in 1-methyl-2-pyrrolidone (NMP). The target ZnFcs **1-3** were prepared by tetracyclization of **12-15** by refluxing in 2-(dimethylamino)ethanol (DMAE) in the presence of $Zn(AcO)_2$. All final ZnFcs and their corresponding intermediates were fully characterized by using spectroscopic techniques. ZnFcs **1-3** were obtained as a mixture of structural isomers depending on the direction of the fluorene rings.

3.2.2. Optical and electrochemical properties

The extended planar shape of non-substituted MPcs resulted in poor solubilities in any solvents owing to their strong tendency to from dense stacking through the intermolecular π-π interaction. According to the molecular models of **1-3** (Figure 3-2a), aryl substituents at the C9 position of the fluorene in **1-3**, which lie out of the plane of the macrocycles, act as a steric hindrance to avoid the stacking among the macrocycles. Thus, ZnFcs **1-3** exhibited a good solubility in common organic solvents, such as toluene, $CHCl_3$, and THF. Figure 3-2b shows the UV-Vis absorbing and fluorescence spectra of **3** in THF. **ZnFc3** exhibited a sharp peak at λ_{max} = 711 nm and a relatively weak peak at λ_{max} = 386 nm as the Q band and the B band, respectively.[32] The position of the Q band shifted to 33 nm compared with that of zinc (II) tetra(tert-butyl)phthalocyanine (Zn(tBu)Pc, λ_{max} = 678 nm). Since the Q band can be assigned to a transition between the HOMO and the LUMO or LUMO+1, the HOMO-LUMO band gap of **3** was slightly smaller than that of Zn(tBu)Pc. When **3** was excited at the Q band of the ZnFcs core in a degassed THF solution, tit exhibited a strong fluorescence at 718 nm. The optical HOMO-LUMO band gaps (E_g) for **1-3** were determined to be 1.7 eV form the cross point of the normalized absorption and fluorescence spectra. Figure 3-2c shows the UV-Vis absorbing spectra of spin-coated films of **1-3** on quartz plates. The Q band of the spin-coated films of **1** was broadened relative to tat in THF, which implies the formation of aggregated in the solid films. In contrast, **3** possessing eight hexyl chains displayed a sharp Q band and the half width of the Q band in the solid film was almost the same as that in the solution. This indicates that the introduction of alkyl chains prevents the formation of aggregation in the solid films.

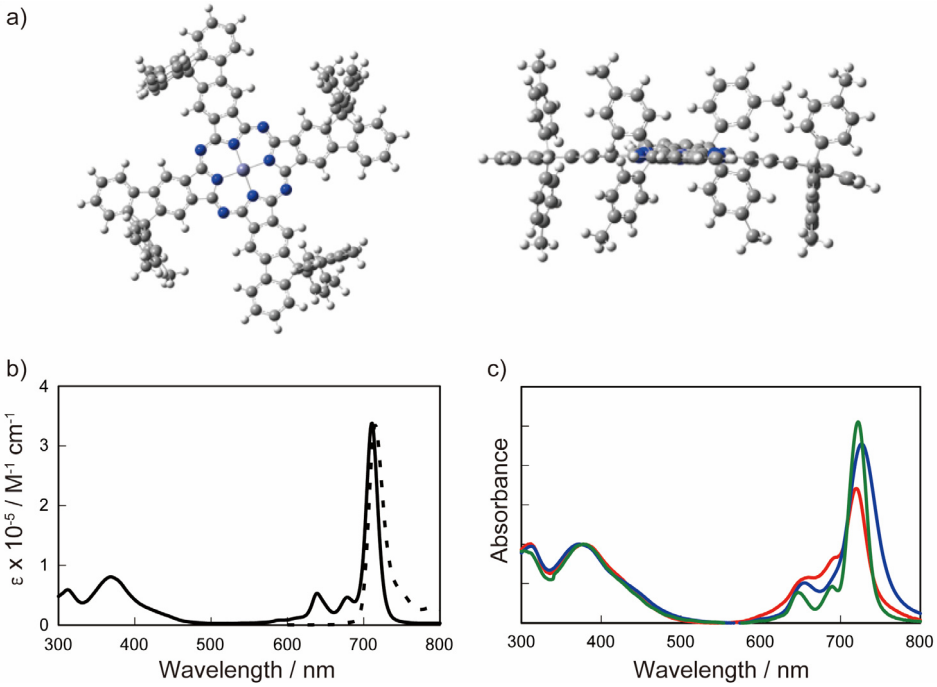

Figure 3-2: a) Computer-simulated molecular structure of **1** optimized by Gaussian 09 (Right: top view, Left: side view); b) UV-Vis absorbing and fluorescence spectra of **3** in THF; c) UV-Vis spectra of spin-coated thin films of **1-3** on quartz substrates (**1**: red line, **2**: blue line, **3**: green line).

The onset potentials (E_{ox}) for the first oxidation of **1-3** appeared at +0.53 V versus ferrocene/ferrocenium redox couple (Fc/Fc+) determined by cyclic voltammetry measurement in dry CH_2Cl_2 containg 0.1 M tetrabutylammonium perchlorate (TBAP) as a supporting electrolyte (Figure 3-3a).[33] The HOMO energy levels of **1-3** were estimated to be -5.3 eV from the Eox values calibrated by the Fc/Fc+ redox couple versus vacuum.[34] The lumo energy levels for **1-3**, estimated from the HOMO energy levels and E_g, were evaluated to be -3.6 eV. The ring expansion from phthalocyanine to naphthalocyanine (Nc) resulted in a decraseing HOMO-LUMO gap because of the destabilizeation of the HOMO energy level.[25, 26] In contrast, the HOMO and LUMO enrgy levels of **1-3** were lower than those of Zn(tBu)Pc (HOMO = -5.0 eV, LUMO = -3.1 eV), indicating that the fusing of fluorene rings with the porphyrazine ring leads to the stabilization of HOMO and

LUMO energy levels. The UV-Vis absorbing spectra of spin-coated films of **1-3** remaind unaltered after being stored in air under ambient light for one month, revealing good satbilities of **1-3** under ambient conditions because of the stabilization of HOMO energy levels. The Stability under ambient conditions is one of the most important factors for using molecules as optoelectronic materials in organic-based devices.

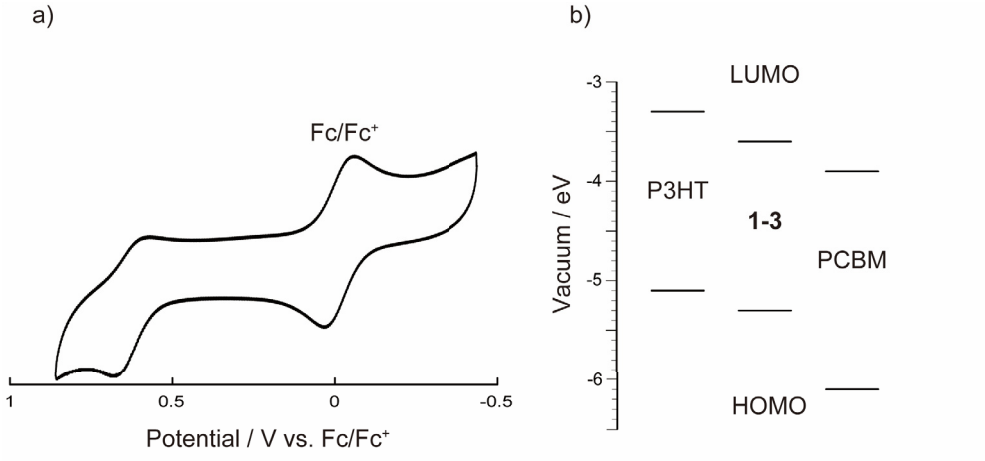

Figure 3-3: a) Cyclic voltammetry data for **1** containing ferrocene as an internal standard. Cyclic voltammogram was acquired from **1** mg/mL solution of **1** in dry CH_2Cl_2 containing 0.1 M TBAP as a supporting electrolyte; b) Energy level diagram for P3HT, **1-3**, and PCBM.

Energy levels of ZnFcs **1-3** are located at the intermediate between those of P3HT (HOMO = -5.1 eV, LUMO = -3.3 eV) and PCBM (HOMO = -6.1 eV, LUMO = -3.9 eV) (Figure 3-3b).[4, 9-23] If ZnFcs are located at the interface between P3HT and PCBM, ZnFcs can work as co-sensitizers in the BHJ solar cells based on the P3HT/PCBM blended active layer. The cascaded energy levels of P3HT, ZnFcs, and PCBM at the BHJ interface ma enable electrons and holes generated from ZnFc excitons to be injected into PCBM and P3HT, respectively. Figure 3-4 shows the UV-Vis absorbing spectra of spin-coated films of P3HT/PCBM/**3** (in a 1:1:0.11 wt. ratio) before and after thermal annealing at 145 °C for 30 min. The as-cast film

displayed a mixed absorption spectrum of P3HT and **3**, and the position of the Q band agreed with that of **3** in the solution. After annealing, the absorbance of the P3HT band increased, and vibronic absorption shoulders appeared at a longer wavelength (500-620 nm), indicating the formation of an ordered stacking of P3HT backbones.[35] The thermal annealing of as-cast films leads to a formation of BHJ crystalline nanostructure by the phase separation of the blends, and the increased crystallinity enhances the carrier mobility and absorption co-efferent of the P3HT/PCBM blended films.[36-38] The Q band of **3** remained unaltered after the thermal annealing. ZnFc **3** was incorporated within the P3HT/PCBM blended film without the formation of aggregates. The other ZnFcs **1** and **2** in the blended films showed broad Q bands relative to **3**, suggesting the aggregation of ZnFcs.

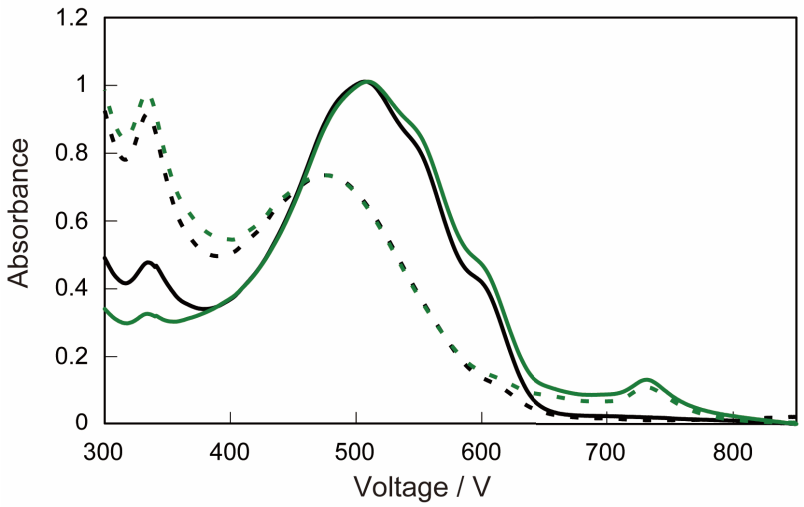

Figure 3-4: UV-Vis spectra of spin-coated films of P3HT/PCBM (black line) and P3HT/PCBM doped with **3** (green line) before (dotted line) and after annealing (solid line)

3.2.3. Device performance

BHJ solar cells were fabricated by using P3HT as the electron donor materials

and fullerene derivatives as the electron acceptor materials in the presence of ZnFcs **1-3** through the convectional spin-coating process. The cleaned tin-doped indium oxide (ITO)-coated glass anode was modified by spin-coating on poly(3,4-ethylenedioxythiophene)/polystyrenesulfonate (PEDOT/PSS) as a hole-extraction/electron-blocking layer with a 40 nm thickness. The active layer was deposited from the mixed chlorobenzene solutions onto the PEDOT/PSS-modified ITO anodes in an argon-filled glove box ($[O_2] < 0.1$ ppm and $[H_2O] < 0.1$ ppm), and the thickness was typically 180 nm. After spincoating, the resulting active layer was annealed at 145°C for 10 min. TiO_x on the active layer has been used as an electron collection layer in the BHJ solar cells.[39] Finally, an aluminum cathode was deposited through a shadow mask by thermal evaporation under vacuum. Figure 3-5a shows the *J-V* curves of BHJ solar cells fabricated from the mixed solution with a P3HT/PCBM /ZnFc composition with a weight ratio of 1:1:0.11 under a standard global AM 1.5 solar condition, and the device parameters (the short-circuit current density (J_{SC}), open-circuit voltage (V_{OC}), fill factor (FF), and overall power conversion efficiency (PCE)) of these cells are summarized in Table 1. The PCE of the cell with **3** was higher than that of the control P3HT/PCBM cell, which was mainly due to the increase in J_{SC}. The addition of **3** increased J_{SC} by 1.5 mA cm^{-2} from 9.2 to 10.7 mA cm^{-2}. The PCE values were increased by increasing the dye concentration up to 5.4 wt % of **3** showed a drop PCE value. In contrast, the introduction of **1** and **2** decreased the PCR values, which can be ascribed to the formation of aggregates in the blended films. In particular, FF and the device series resistance (R_{SA}) strongly depended on the number of alkyl chains in ZnFcs.

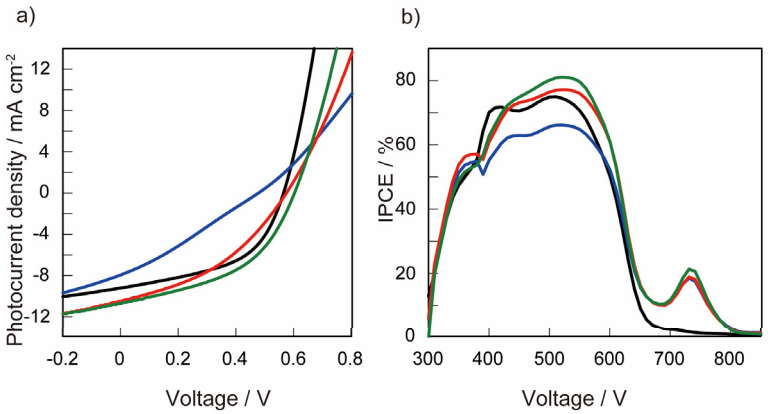

Figure3-5: a) *J-V* curves of P3HT/PCBM blended films doped with **1** (blue line), **2** (red line), **3** (green line) under a standard global AM 1.5 solar condition. The black line is the curve of the reference P3HT/PCBM cell without ZnFcs; b) Incident photon-to-current conversion efficiency spectra for P3HT/PCBM blended films doped with **1** (blue line), **2** (red line), **3** (green line). The estimated J_{SC} values from the integration of IPCE spectra were almost agreed with the J_{SC} values obtained form *J-V* curves (The differences were less than 10 %).

The incident-photo to current conversion efficiency (IPCE) spectra of P3HT/PCBM cell, as shown in Figure 3-5b. The IPCE spectra of BHJ solar cells with **1-3** exhibited an additional photocurrent at the ZnFcs absorption range, revealing that ZnFcs incorporated within P3HT/PCBM blended films effectively absorbed the incident light in the near-IR region and contributed to the photocurrent generation. While the IPCEs at 400-600 nm corresponding to the P3HT absorption were diminished by the addition of **1**, the cells with **2** and **3** exhibited improved IPCEs at this wavelength region. The dye contribution efficiency in the ternary blended BHJ solar cells with 5.2 wt% **3** is estimated to be 54 % at 715 nm from the ration of the IPCE value to the absorption efficiency.[20] These results indicated that a majority of ZnFcs were located at the interface between P3HT and PCBM domains and acted as the mediator of charge transfer by the formation of energetic cascades, this observation agreed with the results of ternary blended BHJ solar cells co-sensitized with MPcs.[19-23]

Table 3-1: Summary of device performance for P3HT/PCBM solar cells doped with **1-3**

Active layer	J_{SC} /mA cm^{-2}	V_{OC} / V	FF	PCE / %	R_{SA} / Ω cm^2
P3HT/PCBM	-9.2	0.56	0.51	2.6	4.2
P3HT/PCBM/**1**	-7.9	0.49	0.28	1.1	28.8
P3HT/PCBM/**2**	-10.5	0.58	0.39	2.4	12.8
P3HT/PCBM/**3**	-10.7	0.60	0.46	3.0	7.1

All parameters are averaged values for at least 8 devices

The surface morphologies of active layers with **1-3** were examined by taping mode atomic force microscopy (AFM) to discuss the relationship between the solar cell performance and the film morphology (Figure 3-6). The samples were prepared by spin coating of a mixed solution on a quartz substrate, and the resulting thin films were annealed at 145 °C or 30 min. The P3HT/PCBM bended film exhibited a smooth surface composed of almost uniform sized island domains with a root-mean-square (rms) roughens of 2.3 nm. Although the blended film with **3** showed a similar domain size, the films with **1** or **2** contained larger sized domains as shown in Figure 3-5b and c. The author found that the number of alky chains in the co-sensitizers affected the phase-separation process of P3HT and PCBM, and **3** decorated with eight alkyl chains could disperse within the P3HT/PCBM blend films through van der Waals interaction among the alkyl chains. The AFM results are consistent with the corresponding solar cell performance. ZnPc **3** maintained the large interface area of the P3HT/PCBM active layer, and the morphology of nanoscale phase separation resulted in a better FF in the BHJ solar cell.

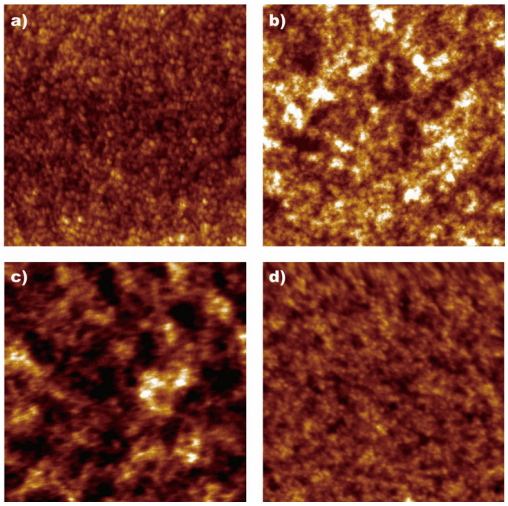

Figure 3-6: AFM images (5 x 5 μm) of P3HT/PCBM blended films without ZnFcs (a), doped with **1** (b), **2** (c), **3** (d).

Photoinduced charge carrier mobility in the BHJ solar cells was measured by photoinduced charge career extraction in a linearly increasing voltage (Photo-CELIV) technique.40 The photo-CELIV current transient showed a single extraction peak at 2.5 μs caused by an applied offset bias at +0.15 V. The carrier mobility (μ) was estimated to be 1.8 x 10^{-4} cm^2 V^{-1} s^{-1}, calculated by the equation reported by Mozer et al.41 The obtained carrier mobility of our P3HT/PCBM cell was almost the same as the reported value.40 In constrast, the charge carrier mobility of the cell doped with **3** (1.0 x 10^{-4} cm^2 V^{-1} s^{-1}) was slightly low relative to that of the reference P3HT/PCBM cell. The low mobility may affect the FF value of device performance.

3.4. Conclusion

In summary the author designed and synthesized new ring-expanded ZnFcs **1-3**

fused with fluorene skeletons. Fusing fluorene rings with the porphyrazine rings resulted in a narrower band gap and stabilization of both the HOMO ad LUMO energy levels compared with ZnPcs. The author also demonstrated the expansion of the light-harvesting area in P3HT/PCBM BHJ solar cells by co-sensitizing with ZnFcs. ZnFc **3** decorated with eight alkyl chains could disperse at the interface between P3HT and PCBM without unfavorable aggregation and contribute to the photocurrent generation by photoexcitation and enhancement of charge transfer between P3HT and PCBM. The incorporation of **3** at the interface of the BHJ structure of P3HT and PCBM lead to a higher device efficiency with 6 % enhancement of J_{SC} as compared with that of the reference P3HT/PCBM BHJ solar cell. The systematic exploration of ring-expanded metallophthalocyanines may enhance the polymer-based BHJ solar cell performance by the expansion of the light harvesting area and the control of the phase-separation process.

References

[1] S. Günes; H. Neugebauer, N. S. Sariciftci, *Chem. Rev.* **2007**, 107, 1324-1338.

[2] Y.-J. Cheng, S.-H. Yang, C.-S. Hsu, *Chem. Rev*. **2009**, 109, 5868-5923.

[3] C. J. Brabec, S. Gowrisanker, J. J. M. Halls, D. Laird, S. Jia, S. P. Willams, *Adv. Mater*. **2010**, 22, 3839-3856.

[4] S. E. Shaheen, C. J. Brabec, N. S. Sariciftci, F. Padingger, T. Dromherz, J. C. Hummelen, *Appl. Phys. Lett*. **2001**, 78, 841.

[5] T. M. Clarke, J. R. Durrant, *Chem. Rev.* **2010**, 110, 6736-6767.

[6] J. Rivnay, S. C. B. Mannsfeld, C. E. Miller, A. Salleo, M. F. Toney, *Chem. Rev*. **2012**, 112, 5488-5519.

[7] P. Schilinsky, C. Waldauf, C. J. Brabec, *Appl. Phys. Lett.* **2002**, 81, 3885.

[8] M. Reyes-Reyes, K. Kim, D. L. Carroll, *Appl. Phys. Lett*. **2005**, 87, No. 083506.

[9] G. Li, V. Shrotriya, J. Huang, Y. Yao, T. Moriarty, K. Emery, Y. Yan, *Nat. Mater*., **2006**, 5, 197-203.

[10] C. N. Hoth, S. A. Choulis, P. Schilinsky, C. J. Brabec, *Adv. Mater.*, **2007**, 19, 3973-3978.

[11] J. M. Lobez, T. L. Andrew, V. Bulović, T. M. Swager, *ACS Nano*, **2012**, 6, 3044-3056.

[12] H. Neugebauer, M. A. Loi, C. Winder, N. S. Sariciftci, G. Cerullo, A. Gouloumis, P Vázquez, T. Torres, *Sol. Energy Mater. Sol. Cells,* **2004**, 83, 201-209.

[13] E. M. J. Johonsson, A. yartsev, H. Resmo, V. Sundström, *J. Phys. Chem. C*, **2009**, 113, 3014-3020.

[14] J. Peet, A. B. Tamayo, X.-D. Dang, J. H. Seo, T.-O. Nguyen, *Appl. Phys. Lett.*, **2008**, 93, 163306.

[15] P. Suresh, P. Balraju, G. D. Sharma, J. A. Milroyannidis, M. M. Stylianakis, *ACS Appl. Mater. Interface*, **2009**, 1, 1370-1374.

[16] S. S. Sharma, G. D. Sharma, J. A. Mikroyannidis, *Sol. Energy Mater. Sol. Cells* **2011**, 95, 1219-1223.

[17] G. de la Torre, C. G. Claessensm T. Torres, *Chem. Commun.*, **2007**, 2000-2015.

[18] S. Honda, T. Nogami, H. Ohkita, H. Benten, S. Ito, *ACS Appl. Mater. Interface*, **2009**, 1, 804-810.

[19] S. Honda, H. Ohkita, H. Benten, S. Ito, *Chem. Commun*., **2010**, 46, 6596-6598.

[20] S. Honda, H. Ohkita, H. Benten, S. Ito, *Adv. Energy Mater*., **2011**, 1, 588-598.

[21] T. Hori, T. Masuda, N. Fukuoka, T. Hayashi, Y. Miyake, T. Kamikado, H. Yoshida, A. Fujii, Y. Shimizu, M. Ozaki, *Org. Electron*., **2012**, 13, 335-340.

[22] J. U. Lee, Y. D. Kim, J. W. Jo, J. P. Kim, W. H. Jo, *J. Mater. Chem*., **2011**, 21, 17209-17218.

[23] J. Mack, N. Kobayashi, *Chem. Rev.*, **2011**, 111, 281-321.

[24] N. Kobayashi, T. Furuyama, K. Satoh, *J. Am. Chem. Soc.*, **2011**, 133, 19642-19645.

[25] A. Muranaka, M. Yonehara, M. Uchiyama, *J. Am. Chem. Soc.*, **2010**, 132, 7844−7845.

[26] C. Li, M. Liu, N. G. Pschierer, M. Baumgarten, K. Müllen, *Chem. Rev*., **2010**, 110, 6817−6855.

[27] S. Kajigaeshi, T. Kakinami, H. Tokiyama, T. Hirakawa, T. Okamoto, *Chem. Lett*., **1987**, 627−630.

[28] V. Diemer, F. R. Leroux, F. Colobert, *Eur. J. Org. Chem.*, **2011**, 327−340.

[29] I. Hussain, M. A. Yawer, M. Lau, T. Pundt, C. Fischer, L. P. Görls, *Eur. J. Org. Chem.*, **2008**, 503−518.

[30] K.-T. Wong, Z.-J. Wang, Y.-Y. Chien, C.-L. Wang, *Org. Lett.,* **2001**, 3, 2285−2288.

[31] M. J. Stillman, T. Nyokong, *Phthalocyanines Properties and Applications*, Vol. 1; Leznoff, C. C., Lever, A. B. P., Eds.; VCH: New York, **1989**; Chapter 3, pp 139−247.

[32] A. B. P. Lever, E.R. Milaeva, G. Speier, *Phthalocyanines Properties and Applications*, Vol. 3; Leznoff, C. C., Lever, A. B. P., Eds.; VCH: New York, **1993**; Chapter 1, pp 1−70.

[33] R. Grisorio, G. Allegretta, G. P. Suranna, P. Mastrorilli, A. Loiudice, A. Rizzo, M. Mazzeo, G. Gigli, *J. Mater. Chem.,* **2012**, 22, 19752−19760.

[34] S. Samitsu, T. Shimomura, S. Heike, T. Hashizume, K. Ito, *Macromolecules,* **2008**, 41, 8000−8010.

[35] F. Padinger, R. S. Rittberger, N. S. Sariciftci, *Adv. Funct. Mater.*, **2003**, 13, 85−88.

[36] A. J. Moulé, S. Allard, N. M. Kronenberg, A. Tsami, U. Scherf, K. Meerholz, *J. Phys. Chem. C,* **2008**, 112, 12583−12589.

[37] W. Ma, C. Yang, X. Gong, K. Lee, A. Heeger, *J. Adv. Funct. Mater.*, **2005**, 15, 1617−1622.

[38] A. Hayakawa, O. Yoshiokawa, T. Fujieda, K. Uehara, S. Yoshikawa, *Appl. Phys. Lett.*, **2007**, 90, No. 163517.

[39] A. J. Mozer, N. S. Sariciftci, L. Lutsen, D. Vanderzande, R. Österbacka, M. Westerling, G. Juška, *Appl. Phys. Lett.*, **2005**, 86, No.112104.

[40] B. T. De Villers, C. J. Tassone, S. H. Tolbert, B. J. Schwartz, *J. Phys. Chem. C,* **2009**, 113, 18978−18982.

Chapter 4

Light-harvesting in the near-infrared region: dye-sensitized solar cells with asymmetric ring-expanded zinc(II) phthalocyanines

Summary: A near-IR absorbing dye (**FcS1**), in which three fluorene rings were fused with a porphyrazine ring, has been designed and synthesized as a photosensitizer for dye-sensitized solar cells (DSSCs). The fusion of the fluorene rings led to tailoring of the HOMO and LUMO energy levels as well as an expansion of the π-system. The absorption spectrum of **FcS1** adsorbed onto a nanocrystalline TiO_2 film suggested the formation of J-aggregates with tilted orientation of the macrocyclic ligands. While the power conversion efficiency of DSSCs sensitized with **FcS1** was modest 3.2 % under simulated air mass 1.5 global sunlight, FcS1 can convert the red and near-IR light regions between 500 and 860 nm into electricity.

4.1. Introduction

Since the development of dye-sensitized solar cells (DSSCs) with high power conversion efficiency by Grätzel and O'Regan,[1] DSSCs have been regarded as one of the most promising candidates among alternative photovoltaic devices.[2] After extensive optimization of porous TiO_2 layers, redox electrolytes, photosensitizers, and device structures, conversion efficiencies above 13 % have been achieved.[3] In order to further improve the performance of DSSCs, harvesting the photons in the red and near infrared spectral regions is essential. However, a few sensitizers for energy conversion in these regions have been developed.[4] Metallophthalocyanines (MPcs) have been widely studied as red absorbing dyes due to their strong Q band in the red region, suitable electro- and photochemical properties, and remarkable chemical and thermal stability.[5] The performance of MPc-sensitized DSSCs has significantly improved by electronic push-pull structure, steric suppression of aggregation, and optimization of adsorption sites.[6] Recently, we reported an overall efficiency of 6.4 % in DSSCs employing zinc Pc **PcS20** substituted with short alkyl chains under one-sun conditions.[7] Although the **PcS20** cell exhibited over 80 % of incident photon-to-current efficiency (IPCE) at 600-720 nm, the IPCE value steeply decreased in the far red and infrared regions.

The Q band position of MPcs can be shifted to the near-IR region by extension of the π system of macrocyclic ligands.[8] The expansion of π-conjugation results in the narrowing of HOMO-LUMO energy-gaps between the HOMO and LUMO energies, and the narrowing of the gap leads to the red-shifting of Q bands. Several groups have tested low energy-gap naphthalocyanines (Ncs) as sensitizers of DSSCs to convert in near-IR region.[9] Macor et al. reported the production of

photocurrent in DSSCs sensitized by an axially anchored silicon Nc dye.[9b] Recently, Lim *et al.* evaluated a solar cell performance of DSSCs sensitized by an asymmetrical silicon Nc dye **LBG1** having two axial siloxane side chains.[9c] However, these Nc-sensitized DSSCs have exhibited power-conversion efficiencies less than 1 %, presumably due to unfavorable energy levels for photoinduced electron transfer reactions in DSSCs. Here, the author describes the synthesis and characterization of a novel ring-expanded near-IR absorbing sensitizer **FcS1**, in which three fluorene rings were fused with the porphyrazine ring. While the DSSC cells sensitized by **FcS1** showed a modest efficiency of 3.2 % under simulated air mass 1.5 global sunlight, **FcS1** could convert the red and near-IR light regions between 600 and 860 nm.

4.2. Experimental

Synthesis of FcS1

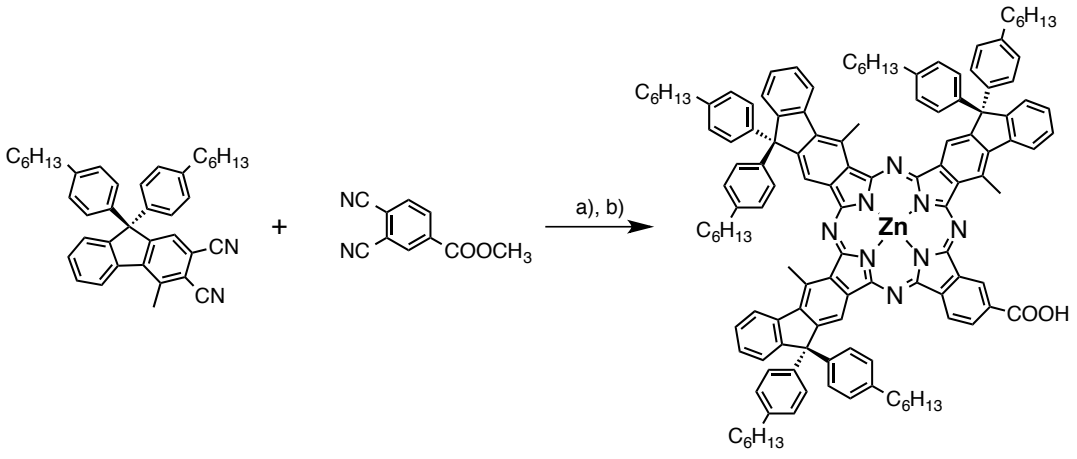

Scheme 4-1: a) $Zn(AcO)_2$, DMAE; b) NaOH, H_2O/THF

2,3-Dicyano-4-methyl-9,9-di(4-hexylphenyl)fluorene **1** was synthesized according to a method as **Chapter 1**. Phthalonitrile **2** was synthesized by the literature method.[11]

4: A mixture of **1** (80.0 mg, 1.45 x 10^{-4} mol), **2** (9.0 mg, 4.8 x 10^{-5} mol), $Zn(CH_3COO)_2$ (5.3 mg, 2.4 x 10^{-5} mol) in dimethylaminoethanol (1 mL) was heated at 150 °C with stirring for 6 h. After the mixture was cooled, the solvent was removed and washed with methanol several times to remove excess Zn ion. The residue was purified by column chromatography on activated alumina (eluent: CH_2Cl_2) and recycling preparative HPLC to give **3**. The structure of **3** was confirmed by FT-IR and MALDI-TOF mass. Yield: 25 mg, 26.9 %. IR (ATR): ν = 1770 (-COOR) cm^{-1}. MALDI-TOF Ms (dithranol): *m/z* 1958.8 (M+H, 100%), Calcd for $C_{133}H_{139}N_9O_2Zn$: *m/z* 1958.03.

An aqueous solution of NaOH (3.0 M, 43 mL) was added to the solution of **3** (25 mg, 1.3 x 10^{-5} mol) in THF (1 mL). The mixture was stirred at 70 °C for 8 h. The solvent was removed in vacuo and the residue was dissolved in water (10 ml). The aqueous solution was refluxed for 1 h. The resulting green solution was filtered and neutralized with acetic acid. The precipitate was collected by filtration and dried in vacuo. Yield: 19.2 mg, 78.4 %. ^1H NMR ($CDCl_3$, 400.13MHz): δ (ppm) = 9.35-9.46 (m, 3H, Ar*H*), 8.52-8.59 (m, 3H, Ar*H*), 7.56-7.67 (m, 6H, Ar*H*), 7.41-7.55 (m, 15H, Ar*H*), 7.02-7.24 (m, 12H, Ar*H*), 4.46-4.55 (m, 12H, -C*H*$_3$), 2.58 (br, 12H, ArC*H2*-), 1.60 (br, 12H, -C*H*$_2$-), 1.23-1.29 (m, 36H, -C*H*$_2$-), 0.83 (br, 18H, -C*H*$_3$). IR (ATR): u = 1692 (-COOH) cm^{-1}. MALDI-TOF Ms (dithranol): *m/z* 1887.1 (M+H), Calcd for $C_{129}H_{130}N_8O_2Zn$: *m/z* 1886.96. UV-Vis (THF): λ_{max} (log ε) = 704 (5.26), 632 (4.54), 365 (4.75).

1: A solution of **2** (38 mg, 37 mmol), **3** (29 mg, 37 mmol) and $Pd(PPh_3)_4$ (1.7 mg,

1.5 mmol) in 4 ml dimethoxyethane (DME) and 2 ml 1.0 M K_2CO_3 aqueous solution was stirred at 70 ^oC for 12 h under a nitrogen atmosphere. After cooling to room temperature, the reaction mixture was poured into water. The organic layer was dried over with Na_2SO_4 and the solvent was evaporated. The residue was purified by column chromatography on silica gel using CH_2Cl_2 and recycling preparative HPLC to give **FcS1** (13 mg, 20 %). MALDI-TOF Ms: *m/z* 1776.77 (M+H, 100%), Calcd for $C_{110}H_{77}BrN_{12}Zn_2$: *m/z* 1777.42. A solution of **FcS1** (10 mg, 5.6 mmol), 4-ethoxyphenylboronic acid (5 mg, 5.6 mmol) and $Pd(PPh_3)_4$ (1 mg, 0.87 mmol) in 2 ml DME and 1 ml 1.0 M K_2CO_3 aqueous solution was stirred at 70 °C for 12 h under a nitrogen atmosphere. After cooling to room temperature, the reaction mixture was poured into water. The organic layer was dried over with Na_2SO_4 and the solvent was evaporated. The residue was purified by column chromatography on silica gel using CH_2Cl_2 and recycling preparative HPLC to give ester-terminated dyad (10 mg, 97 %). MALDI-TOF Ms: *m/z* 1847.56 (M+H, 100%), Calcd for $C_{119}H_{86}N_{12}O_2Zn_2$: *m/z* 1845.56. Aqueous solution of 30 µl 3.0 M NaOH was added to the solution of ester-terminated dyad (10 mg, 5.4 µl) in 3 ml THF. The mixture was stirred at 70 °C for 24 h. The solvent was removed in vacuo and the residue was washed with water several times. The residue was dissolved in THF and neutralized with acetic acid. After evaporation and washing with water, the solid was collected by filtration and dried in vacuo. (8 mg, 82 %). ^1H NMR (400.13 MHz, $CDCl_3$): δ (ppm) = 9.02-8.93 (m, 4H, Pc*H*), 8.76-8.73 (m, 4H, Por*H*), 8.61-8.41 (m, 8H, Pc*H*+Por*H*), 8.29-7.98 (m, 12H, Pc*H*+Ar*H*), 7.82-7.68 (m, 12H, Ar*H*), 7.51-7.39 (m, 6H, Ar*H*), 7.20-7.13 (m, 8H, Ar*H*), 2.31 (s, 12H, -CH_3), 1.29 (s, 9H, -CH_3), 1.10 (s, 6H, -CH_3); MALDI-TOF Ms: *m/z* 1818.47 (M+H, 100%), Calcd for $C_{117}H_{82}N_{12}O_2Zn_2$: *m/z* 1817.53; UV-Vis (THF): λ_{max} (log ε) = 698 (5.03), 632 (4.34), 559 (4.23), 426 (5.59), 361 (4.49).

4.3. Results and Discussion

4.3.1. Synthesis of ZnFc4

The synthesis and characterization of zinc fluorenocyanine complexes (ZnFcs) from 9,9-diarylfluorene precursors are reported in **Chapter 3**. Furthermore, the authour demonstrated the ZnFcs could enhance the short circuit current in the bulk-heterojunction solar cell based on poly(3-hexylthiophene) and fullerene derivative through the additional light-harvesting of near-IR absorbing ZnFcs.[10] The author also found that fusing of fluorene rings with the porphyrazine ring stabilized the HOMO energy levels. In the case of Ncs, the ring-expansion of Pc rings resulted in the destabilization of HOMO level. The destabilized HOMO energy levels in Nc dyes are insufficient for the efficient regeneration of oxidized dyes by the I^-/I_3^- redox shuttle.[9] In this study, the author expected a tailoring of the HOMO energy levels by the fusion of fluorene rings with porphyrazine ring for the efficient DSSC operation as well as the red-shifting of the Q band through the expansion of π-conjugation.

Asymmetrical **FcS1**, containing three fused fluorene rings and one carboxylic acid, was synthesized using the statistical condensation of 2,3-dicyano-4-methyl-9,9-di(4-hexylphenyl)fluorene **1** and methyl 3,4-dicyanobenzoate **2** in a 3:1 molecular ratio in the presence of $Zn(AcO)_2$ (Scheme 4-1). Precursor **1** bearing two hexylphenyl units at the C9 position of fluorene was synthesized according to a previously reported procedure,[10] and the other phthalonitrile **2** was prepared by the method reported by Pozzi *et al.*[11] The target ZnFc **3** containing one carboxylic ester was separated by column

chromatography as a second fraction, and the ester in **3** was hydrolyzed by alkaline aqueous solution. Density functional theory (DFT) calculations at the B3LYP/6-31G* level (Gaussian 09) were conducted for **FcS1** to gain insight into optimized geometry and electronic structure for the frontier orbitals. Six hexylphenyl units attached at the C9 position of fluorenes in **FcS1** lie out of the plane of macrocyclic ligand (Figure 4-1a). The steric hindrance of hexylphenyl units would affect the intermolecular interaction among sensitizers adsorbed onto the TiO_2 surface. Figure 1b shows the spatial distributions of the frontier orbitals for the HOMO and LUMO of **FcS1**. The HOMO is symmetrically distributed over the porphyrazine ring and the fused benzene rings within the macrocyclic ligand. The LUMO and LUMO+1 are distributed along the x and y axis of the macrocyclic ligand with sufficient electron densities on the carboxylic acid moiety, suggesting an electronically good connection between π-conjugated macrocylic ligand and TiO_2 by linking of carboxylic acid in **FcS1** with the TiO_2 surface.

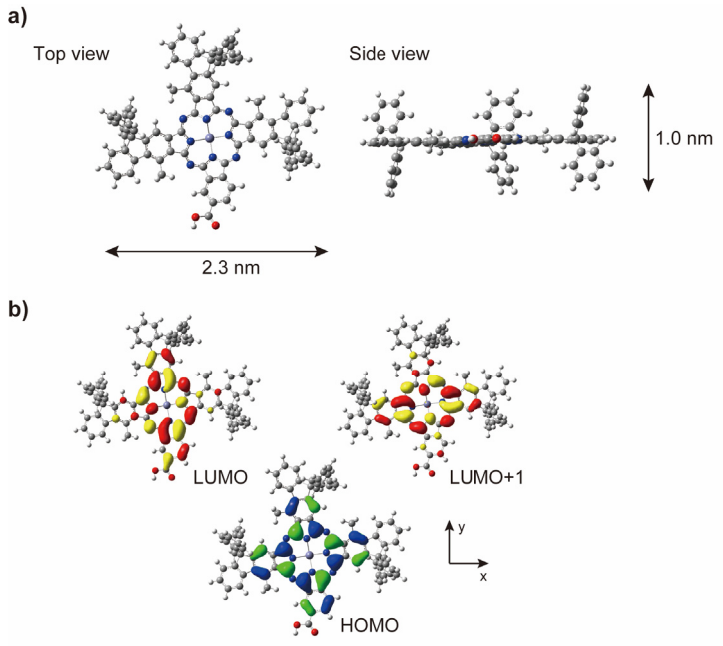

Figure 4-1: a) Computer-simulated molecular structure of **FcS1** optimized by Gaussian 09; b) Relevant electronic transitions at the TD-DFT B3LYP 6-31G* level for **FcS1**.

4.3.2. Optical and electrochemical properties

Figure 4-2a shows the absorption and fluorescence spectra of **FcS1** in THF. Asymmetrical compound **FcS1** containing three fluorene and one carboxylic acid groups exhibited a sharp intense peak at λ_{max} = 704 nm as the Q band.[12] The shape and position of the Q band are known to be an indicator for determining the aggregation behavior of MPcs.[12] The Q band of **FcS1** in THF indicates a low tendency toward aggregation, suggesting that the aggregation of planar macrocyclic ligands in **FcS1** is diminished by the bulky hexylphenyl units attached at the C9 position of fluorene rings. The absorption maximum of the Q band for **FcS1** shifts to 11 nm compared with the symmetrical ZnFc, in which four fluorene rings were connected with the porphyrazine core (λ_{max} = 715 nm).[10] This blue-shift of the Q band in **FcS1** is ascribed to the reduction of π-system by fusing with one benzene ring with the porphyrazine core. "Push-pull" ZnPc sensitizers having split Q bands have displayed high efficiencies in ZnPc-sensitized DSSCs through the enhancement of charge-transfer directionality.[5f, 5h, 6] The narrow Q band of **FcS1** reveals a poor push-pull character as compared with efficient ZnPc sensitizers. When **FcS1** was excited at the B band in a degassed THF solution, it exhibited a strong fluorescence at 718 nm. The optical HOMO-LUMO band-gap (E_g) of **FcS1** was determined to be 1.70 eV from the cross point of the normalized absorption and fluorescence spectra. The E_g of **4** was slightly smaller than that of ZnPcs.[6a, 7]

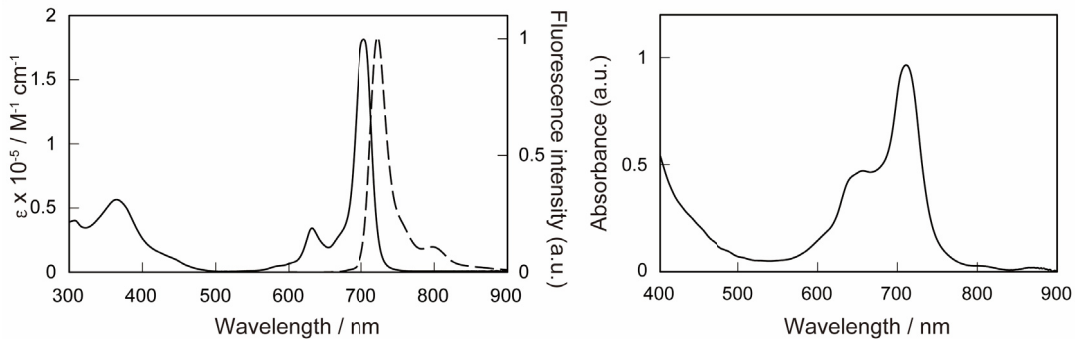

Figure 4-2: UV-Vis absorbing and fluorescence spectra of **FcS1** in THF; b) UV-Vis absorbing spectrum of **FcS1** adsorbed on TiO_2 film.

The oxidation potential of **FcS1** was determined by differential pulse voltammetry (DPV) in THF containing 0.1 M of teterabutylammonium hexafluorophosphate ($TBAPF_6$) as the supporting electrolyte. The first oxidation potential (E_{ox}) of **FcS1** appeared at +0.91 V *vs.* normal standard electrode (NHE), which is attributed to the phthalocyanine ring-based oxidation process.[8,14] The ring expansion from phthalocyanine to naphthalocyanine resulted in a decreasing of HOMO-LUMO gap owing to the destabilization of the HOMO energy level.[8] In contrast, the E_{ox} value of **FcS1** is similar to that of the ZnPc sensitizer **PcS20**, indicating that the ring expansion of porphyrazine ring with fluorenes does not lift the HOMO energy level. The E_{ox} value of **FcS1** is more positive than the potential of the I^-/I_3^- redox couple (+0.41 V *vs.* NHE). The LUMO energy level of **FcS1** is -0.80 V *vs.* NHE calculated from E_{ox} and E_g values. While the LUMO level of **FcS1** is slightly stabilized relative to **PcS20**, the LUMO level of **FcS1** is sufficiently negative of the conduction-band-edge energy of TiO_2 (ca. -0.50 V *vs.* NHE). The HOMO and LUMO energy levels of **FcS1** are adequate for the electron injection from the excited dye to TiO_2 and the regeneration of oxidized dyes by the I^-/I_3^- redox shuttle in the DSSCs. Thus, the fusion of fluorene rings with the porphyrazine core enables the turning of the HOMO and LUMO energy levels as well as the red-shifting of Q bands.

Figure 4-2b shows the absorption spectrum of **FcS1** adsorbed onto a nanocrystalline transparent TiO_2 film. Compared to the dilute solution spectrum of **FcS1** in THF, the Q band of **FcS1** on TiO_2 film was broadened, and the absorption maximum was red shifted to 7 nm. Controlling dye-aggregation has been one of key issues to improve DSSC performance.[15] MPc-based sensitizers without bulky substituents required the mixing of co-adsorbant such as 3a,7a-dihydroxy-5b-cholanic acid (CDCA) to suppress the formation of *H*-aggregates.[6a,b] The formation of *H*-aggregates on the TiO_2 surface leads to the intermolecular quenching among the adsorbed dyes. In contrast, the red-shift of Q band and the tailing of absorption in the near-IR region for **FcS1** implies the formation of *J*-aggregates among macrocyclic ligands on the TiO_2 surface.[16] When the carboxylic acid in **FcS1** grafts onto the TiO_2 surface, the bulky hexylphenyl units can control the intermolecular stacking morphology within the monolayer of dyes adsorbed on the TiO_2. The onset of the absorption was extended to 850 nm by the formation of *J*-aggregates. The absorption extension toward the near-IR region could increase the photocurrent in DSSCs due to the expansion of light-harvesting area.

The adsorption density of **FcS1** was determined from the absorbance of **FcS1** released from **FcS1**-stained TiO_2 film.[17] The adsorption density of **FcS1** on a 4 μm TiO_2 film was determined to be 3.9×10^{-5} mol/cm^3. The occupied area per one molecule of **FcS1** on the TiO_2 surface was ca. 5.4 nm^2/molecule estimated from the adsorption density and the surface area of TiO_2. The adsorption density of **FcS1** was much lower than that of **PcS20** (1.9×10^{-4} mol/cm^3), indicating the poor adsorption density on TiO_2.[6] When the carboxylic acid in **FcS1** linked to the TiO_2 surface, the macrocyclic ligands are vertically oriented with respect to the TiO_2 surface. Assuming the molecular dimension of **FcS1** from the optimized molecular model as shown in Figure 4-1a, the occupied area per molecule for the vertical

orientation is calculated to be 2.3 nm^2 (width 2.3 nm x thickness 1.0 nm). The large difference between the calculated and experimental occupied areas suggests the tilted orientation of dyes to the TiO_2 surface.[16,17] These results of absorption spectrum and adsorption density analysis confirm the formation of *J*-aggregates with the tilted orientation to the TiO_2 surface when **FcS1** was adsorbed onto the TiO_2 surface.

4.2.3. Device performance

FcS1-sensitized DSSCs were fabricated by using screen-printed triple-layer TiO_2 films consisting of a 7 mm transparent layer, a 6 mm scattering layer, and a 7 mm reflection layer. Figure 3a shows a photocurrent density-voltage curve of the **FcS1**-sensitized DSSC with electrolytes containing 0.6 M 1,2-dimethyl-3-propylimidazolium iodide (DMPImI), 0.1 M LiI, 0.05 M I_2, 0.5 M 4-*tert*-buthylpyridine (tBP) in acetonitrile under a standard AM 1.5 solar condition. **FcS1** achieves a short-circuit photocurrent (J_{sc}) of 8.1 mA/cm^2, an open circuit voltage (V_{oc}) of 554 mV, and a fill factor (*FF*) of 0.71 for an overall cell efficiency (PCE) of 3.2%. In previously reported Nc-sensitized DSSCs, an electrolyte with a higher concentration of Li^+ ion was used for optimal performance of the devices.[9c] The higher concentration of Li^+ ion enhanced the electron injection efficiency by increasing the driving force between LUMO level of Ncs and the titania conduction band.[18] Although the Nc-sensitized cell displayed a high photocurrent by using electrolyte containing 1.0 M LiI without tBP, the V_{oc} and *FF* values of cells were low. In contrast, the tuning of HOMO and LUMO energy levels by the fusion of fluorene rings with the porphyrazine core results in the improvements of V_{oc} and *FF* values in DSSCs with the conventional electrolyte (ELA1). **FcS1** cell exhibits a broad IPCE between 650 and 860 nm (Figure 3b), and the estimated J_{sc} value from the overlap integral of IPCE with the solar spectrum was almost agreed with the

experimental value of **FcS1** cell. The onset of IPCE spectrum is 860 nm, but a maximum IPCE value is limited to 40-45% between 640-730 nm. The IPCE spectrum of **FcS1** cell is wider than that of **PcS20** cell, which is attributable to the red-shifting of Q band by the expansion of π system and the formation of *J* aggregates on the TiO_2. **FcS1** sensitizer showed low IPCE values compared to that of push-pull ZnPc sensitizers,[6,7] mainly because of the lacking of electron transfer directionality in the excited state.

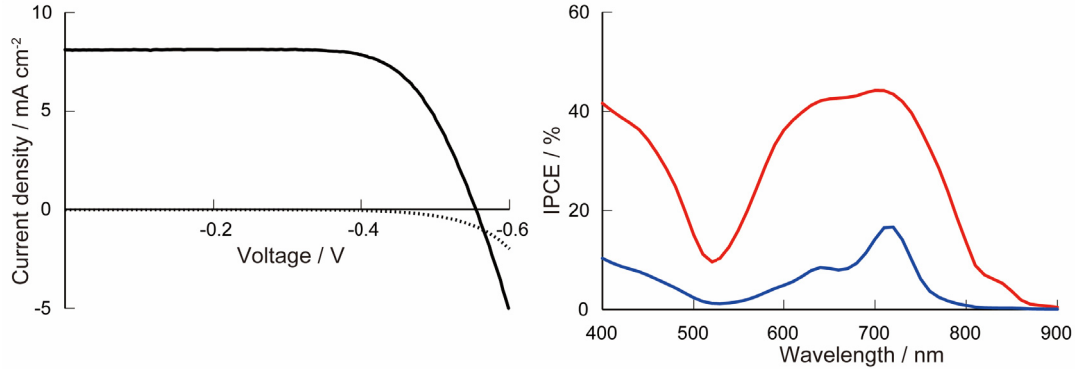

Figure 4-3: a) Photocurrent voltage curves obtained with DSSCs based on **FcS1** under a standard global AM 1.5 solar conditions (solid line) and dark current (dotted line); b) IPCE spectra of DSSCs based on **FcS1** (red) and **FcS1+CDCA** (blue).

The co-adsorption of CDCA suppresses dye aggregation/interaction on TiO_2 surface and affects photovoltaic performance.[6a-c] The TiO_2 electrode was stained with **FcS1** solution ([**FcS1**] = 0.05 mM) with 0.5 mM CDCA at room temperature. The solar cell performance for **FcS1** cell (V_{oc} = 578 mV, J_{sc} = 1.4 mA/cm^2, *FF* = 0.71, PCE = 0.6%) significantly decreased in the presence of CDCA compared with the result from the solution without CDCA. The IPCE spectrum of **FcS1** cell with CDCA exhibited a sharp peak, which is similar to the absorption spectrum of **FcS1** in solution. The co-adsorption with CDCA reduces the adsorption density of **FcS1** on the TiO_2 surface, thus the adsorbed **FcS1** works as a single isolated sensitizer. The red-shift of Q band and tailing of the absorption in the *J*-aggregates

of **FcS1** without CDCA on the TiO_2 surface covers a broad light-harvesting area in Vis/NIR region. The controlling organized structure of dyes on the TiO_2 could infer an important advantage to convert near-IR region of solar spectrum.

4.3. Conclusion

In conclusion, the author demonstrated the ring-expansion of an asymmetric zinc phthalocyanine sensitizer that can absorb in the near-IR region. The fusion of fluorene rings with porphyrazine ring provides the suitable HOMO and LUMO energy levels for efficient operation of DSSCs. The attachment of hexylphenyl units at the C9 position of fluorene rings enables the formation of *J*-aggregates having a tilted orientation of adsorbed dyes on the TiO_2 surface. When used as a light-harvesting dye in DSSC, the asymmetric **FcS1** gave a PCE value of 3.2 % without co-adsorbant under one sun condition. The light-harvesting area of **FcS1** cell extends close to 900 nm by the formation of *J*-aggregates on the TiO_2 surface as well as the extension of the π system of macrocyclic ligand. The conversion efficiency could improve by adjusting the electron densities of fluorene rings to create directionality in the excited state of the sensitizer.

References

[1] S. Günes, H. Neugebauer, N. S. Sariciftci, *Chem. Rev.* **2007**, 107, 1324-1338.

[2] Y.-J. Cheng, S.-H. Yang, C.-S. Hsu, *Chem. Rev*. **2009**, 109, 5868-5923.

[3] C. J. Brabec, S. Gowrisanker, J. J. M. Halls, D. Laird, S. Jia, S. P. Willams, *Adv. Mater*. **2010**, 22, 3839-3856.

[4] S. E. Shaheen, C. J. Brabec, N. S. Sariciftci, F. Padingger, T. Dromherz, J. C. Hummelen, *Appl. Phys. Lett*. **2001**, 78, 841.

[5] T. M. Clarke, J. R. Durrant, *Chem. Rev.* **2010**, 110, 6736-6767.

[6] J. Rivnay, S. C. B. Mannsfeld, C. E. Miller, A. Salleo, M. F. Toney, *Chem. Rev*. **2012**, 112, 5488-5519.

[7] P. Schilinsky, C. Waldauf, C. J. Brabec, *Appl. Phys. Lett.* **2002**, 81, 3885.

[8] M. Reyes-Reyes, K. Kim, D. L. Carroll, *Appl. Phys. Lett*. **2005**, 87, No. 083506.

[9] G. Li, V. Shrotriya, J. Huang, Y. Yao, T. Moriarty, K. Emery, Y. Yan, *Nat. Mater*., **2006**, 5, 197-203.

[10] C. N. Hoth, S. A. Choulis, P. Schilinsky, C. J. Brabec, *Adv. Mater.*, **2007**, 19, 3973-3978.

[11] J. M. Lobez, T. L. Andrew, V. Bulović, T. M. Swager, *ACS Nano*, **2012**, 6, 3044-3056.

[12] H. Neugebauer, M. A. Loi, C. Winder, N. S. Sariciftci, G. Cerullo, A. Gouloumis, P Vázquez, T. Torres, *Sol. Energy Mater. Sol. Cells,* **2004**, 83, 201-209.

[13] E. M. J. Johonsson, A. yartsev, H. Resmo, V. Sundström, *J. Phys. Chem. C*, **2009**, 113, 3014-3020.

[14] J. Peet, A. B. Tamayo, X.-D. Dang, J. H. Seo, T.-O. Nguyen, *Appl. Phys. Lett.*, **2008**, 93, 163306.

[15] P. Suresh, P. Balraju, G. D. Sharma, J. A. Milroyannidis, M. M. Stylianakis, *ACS Appl. Mater. Interface*, **2009**, 1, 1370-1374.

[16] S. S. Sharma, G. D. Sharma, J. A. Mikroyannidis, *Sol. Energy Mater. Sol. Cells* **2011**, 95, 1219-1223.

[17] G. de la Torre, C. G. Claessensm T. Torres, *Chem. Commun.*, **2007**, 2000-2015.

[18] S. Honda, T. Nogami, H. Ohkita, H. Benten, S. Ito, *ACS Appl. Mater. Interface*, **2009**, 1, 804-810.

[19] S. Honda, H. Ohkita, H. Benten, S. Ito, *Chem. Commun*., **2010**, 46,

6596-6598.

[20] S. Honda, H. Ohkita, H. Benten, S. Ito, *Adv. Energy Mater*., **2011**, 1, 588-598.

[21] T. Hori, T. Masuda, N. Fukuoka, T. Hayashi, Y. Miyake, T. Kamikado, H. Yoshida, A. Fujii, Y. Shimizu, M. Ozaki, *Org. Electron*., **2012**, 13, 335-340.

[22] J. U. Lee, Y. D. Kim, J. W. Jo, J. P. Kim, W. H. Jo, *J. Mater. Chem*., **2011**, 21, 17209-17218.

[23] J. Mack, N. Kobayashi, *Chem. Rev.*, **2011**, 111, 281-321.

[24] N. Kobayashi, T. Furuyama, K. Satoh, *J. Am. Chem. Soc.*, **2011**, 133, 19642-19645.

[25] A. Muranaka, M. Yonehara, M. Uchiyama, *J. Am. Chem. Soc.*, **2010**, 132, 7844−7845.

[26] C. Li, M. Liu, N. G. Pschierer, M. Baumgarten, K. Müllen, *Chem. Rev*., **2010**, 110, 6817−6855.

[27] S. Kajigaeshi, T. Kakinami, H. Tokiyama, T. Hirakawa, T. Okamoto, *Chem. Lett*., **1987**, 627−630.

[28] V. Diemer, F. R. Leroux, F. Colobert, *Eur. J. Org. Chem.*, **2011**, 327−340.

[29] I. Hussain, M. A. Yawer, M. Lau, T. Pundt, C. Fischer, L. P. Görls, *Eur. J. Org. Chem.*, **2008**, 503−518.

[30] K.-T. Wong, Z.-J. Wang, Y.-Y. Chien, C.-L. Wang, *Org. Lett.,* **2001**, 3, 2285−2288.

[31] M. J. Stillman, T. Nyokong, *Phthalocyanines Properties and Applications*, Vol. 1; Leznoff, C. C., Lever, A. B. P., Eds.; VCH: New York, **1989**; Chapter 3, pp 139−247.

[32] A. B. P. Lever, E.R. Milaeva, G. Speier, *Phthalocyanines Properties and Applications*, Vol. 3; Leznoff, C. C., Lever, A. B. P., Eds.; VCH: New York, **1993**; Chapter 1, pp 1−70.

[33] R. Grisorio, G. Allegretta, G. P. Suranna, P. Mastrorilli, A. Loiudice, A. Rizzo, M. Mazzeo, G. Gigli, *J. Mater. Chem.,* **2012**, 22, 19752−19760.

[34] S. Samitsu, T. Shimomura, S. Heike, T. Hashizume, K. Ito, *Macromolecules,* **2008**, 41, 8000−8010.

[35] F. Padinger, R. S. Rittberger, N. S. Sariciftci, *Adv. Funct. Mater.*, **2003**, 13, 85−88.

[36] A. J. Moulé, S. Allard, N. M. Kronenberg, A. Tsami, U. Scherf, K. Meerholz, *J. Phys. Chem. C,* **2008**, 112, 12583−12589.

[37] W. Ma, C. Yang, X. Gong, K. Lee, A. Heeger, *J. Adv. Funct. Mater.*, **2005**, 15, 1617−1622.

[38] A. Hayakawa, O. Yoshiokawa, T. Fujieda, K. Uehara, S. Yoshikawa, *Appl. Phys. Lett.*, **2007**, 90, No. 163517.

[39] A. J. Mozer, N. S. Sariciftci, L. Lutsen, D. Vanderzande, R. Österbacka, M. Westerling, G. Juška, *Appl. Phys. Lett.*, **2005**, 86, No.112104.

[40] B. T. De Villers, C. J. Tassone, S. H. Tolbert, B. J. Schwartz, *J. Phys. Chem. C,* **2009**, 113, 18978−18982.

Chapter 5

A novel covalently linked Zn phthalocyanine - Zn porphyrin dyad for dye-sensitized solar cells

Summary: A novel Zn phthalocyanine – Zn Porphyrin (ZnPc-ZnPor) dyad (**1**), in which a zinc porphyrin moiety is linked covalently with an ABAB-type zinc phthalocyanine moiety, has been designed and synthesized. The ZnPc-ZnPor dyad **1** can absorb over a wide spectral range of visible light. The fluorescence spectrum of dyad **1** revealed an intramolecular efficient energy transfer form Zn porphyrin to Zn phthalocyanine. When dyad **1** was used as a light-harvesting sensitizer for dye-sensitized solar cells, the cell sensitized by dyad 1 provided a power conversion efficiency of 2.7 % under simulated air mass 1.5 global sunlight. The incident photon-to-current efficiency spectrum of the dyad **1** cell suggested the contribution of both components in dyad **1** for the current generation.

5.1. Introduction

Natural photosynthesis, which converts solar energy to chemical energy, is one of the most important photochemical events. It is initiated by the absorption of visible light in antenna units containing dye arrays, followed by funneling of the excitation energy within the antenna assembly to a reaction center.[1] A variety of molecular arrays have been designed and synthesized to mimic photochemical events in natural photosynthesis.[2] The molecular components in the array are correctly oriented with respect to one another and interact in a well-defined intercomponent relationship. Phthalocyanines and porphyrins are considered as important molecular components in the molecular arrays due to their complementary absorption regions in visible light.[3] Moreover, intramolecular energy transfer from the porphyrin to the phthalocyanine occurs very efficiently in most phthalocyanine-porphyrin dyads because the Q band absorption of phthalocyanine almost overlaps the fluorescence wavelength of porphyrin.[4] While various phthalocyanine-porphyrin dyads have been synthesized, and their photophysical properties have been investigated, there have been few attempts to apply the dyads to organic-based optoelectronic devices.[5]

Dye-sensitized solar cells (DSSCs) have been regarded as being among the most promising candidates among alternative photovoltaic devices.[6] Continual efforts to structurally optimize of sensitizing dyes have enhanced their solar-to-electric power-conversion efficiency (PCE).[7] The PCE of DSSCs using a single sensitizer has reached a limit because currently available dyes cannot absorb all of the photons of solar radiation.[8] To further enhance the PCE of DSSCs, the expansion of the light-harvesting range is a key issue.[9] A simple way to expand the

light-harvesting range is to implement a co-sensitization strategy using two sensitizers that have different light-harvesting ranges.[10] Co-adsorption of two dyes on a TiO_2 surface usually result in a decrease of efficiency, which is mainly due to the decreased injection efficiency caused by intermolecular interactions between the two dyes on the TiO_2 surface.[11] Furthermore, each dye-adsorbing amount in the co-sensitized DSSCs decrease because the number of sites on the TiO_2 surface are limited. To avoid the unfavorable intermolecular interactions and the limitation of dye loading on the TiO_2 surface, the use of energy transfer from energy-donor molecules to the sensitizing dye has been proposed.[12] Siegers *et al*. demonstrated the improvement of DSSC performance by using intramolecular energy transfer from energy-donor moieties to the sensitizing dye in a bichromophoric dyad, in which the energy-donor moieties were covalently linked with a ruthenium sensitizer.[13] Hardin *et al.* succeeded in enhancing of photocurrent response by using Förster resonant energy transfer from the energy relay dye in electrolytes to the sensitizing dye.[14] In this study, the author designed a new phthalocyanine-porphyrin dyad **1** composed of zinc phthalocyanine (ZnPc) and zinc porphyrin (ZnPor) moieties as a photosensitizer for DSSCs. In this dyad, high-energy photons can be absorbed by the red-colored ZnPor moiety and the harvest energy undergoes energy transfer to the green-colored ZnPc moiety. The present work describes the synthesis, characterizations, and solar cell performance of the ZnPc-ZnPor dyad **1**, in which the ZnPor is linked covalently with the ZnPc having a carboxyl acid anchoring group. The DSSC cells sensitized by **1** showed a PCE of 2.7 % under simulated air mass 1.5 global sunlight, and incident photon-to-current efficiency (IPCE) measurement revealed the contribution of both components in **1** for the current generation in solar cells.

5.2. Experimental section

Syntheses of Dyad1

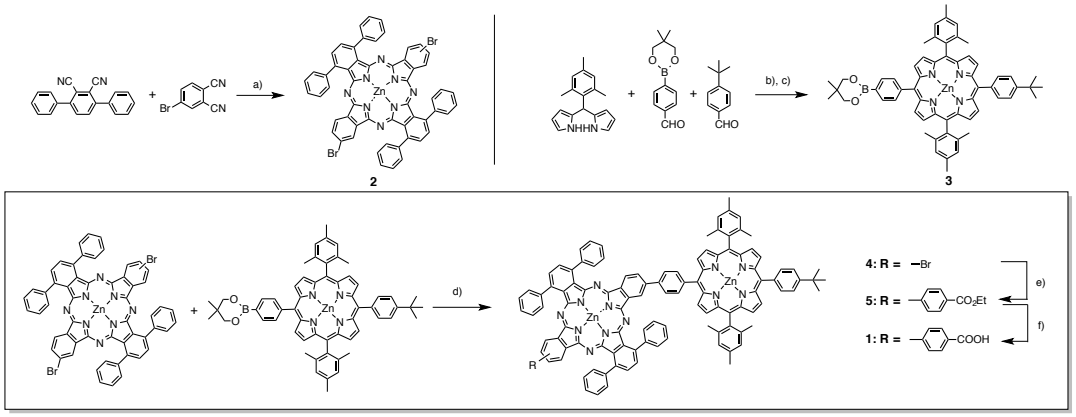

Scheme 5-1: a) $Zn(AcO)_2$, DMAE; b) TFA, CH_2Cl_2, DDQ; c) $Zn(AcO)_2$•$2H_2O$, MeOH, ; d) $Pd(PPh_3)_4$, DME, 1M K_2CO_3 aq.; e) $Pd(PPh_3)_4$, 4-(ethoxylcalbonyl)pheneylboronic acid, DME, 1M K_2CO_3 aq. f) 3M NaOH aq., THF

2: A mixture of 3,6-diphenylphthalonitrile (200 mg, 0.71 mmol), 4-bromophthalonitrile (226 mg, 1.1 mmol), $Zn(CH_3COO)_2$ (65.5 mg, 0.36 mmol) in 8 ml *N,N*-dimethyl- aminoethanol was heated at 150 °C with stirring for overnight. After the reaction mixture was cooled, the solvent was removed under vacuum and washed with methanol several times to remove excess Zn ion. The residue was purified by column chromatography on activated alumina by eluting with CH_2Cl_2 to give **2**. (38 mg, 10 %). ^{1}H NMR (400.13 MHz, DMSO-d_6): δ (ppm) = 8.24 (bs, 8H, Ar*H*), 8.11 (s, 4H, Pc*H*), 7.88-7.85 (m, 6H, Pc*H* and Ar*H*), 7.67 (s, 2H, Pc*H*), 7.68-7.47 (m, 7H, Ar*H*), 7.47-7.45 (m, 4H, Ar*H*); MALDI-TOF Ms: *m/z* 1040.44 (M+H); Calcd for $C_{56}H_{30}Br_2N_8O_8Zn$: *m/z* 1038.02.

3: Trifluoroacetic acid (0.45 ml, 6.1 mmol) was added to the solution of

5-mesitydipyrromethane (1.6 g, 6.1 mmol), 4-*tert*-butylbenzaldehyde (0.49 g, 3.0 mmol) and 2-(4-formylphenyl)-5,5-dimethyl-1,3,2-diocaborinane (0.66 g, 3.0 mmol) in 600 ml CH_2Cl_2. After stirring for 30 min at room temperature under argon, 2,3-dichloro-5,6-dicyano-1,4-benzoquinone (DDQ) (1.0 g, 4.5 mmol) was added to the reaction mixture, then the mixture was stirred for 60 min at room temperature. After the solution was evaporated, the residue was purified by column chromatography on silica gel using CH_2Cl_2 to give unsymmetrical porphyrin with a boron ester (150 mg, 6 %). ^{1}H-NMR (400.13MHz, $CDCl_3$): δ (ppm) = 8.84 (d, *J* = 4.4 Hz, 2H, Por*H*), 8.75 (d, *J* = 4.4 Hz, 2H, Por*H*), 8.67 (d, *J* = 4.0 Hz, 4H, Por*H*), 8.25 (d, *J* = 8.0 Hz, 2H, Ar*H*), 8.13 (d, *J* = 8.0 Hz, 2H, Ar*H*), 8.07 (d, *J* = 8.0 Hz, 2H, Ar*H*), 7.74 (d, *J* = 8.0 Hz, 2H, Ar*H*) 7.28 (s, 4H, Ar*H*) , 3.93 (s, 4H, -CH_2-), 2.63 (s, 6H, -CH_3), 1.84 (s, 12H, -CH_3), 1.60 (s, 9H, -CH_3), 1.16 (s, 6H, -CH_3); MALDI-TOF Ms (dithranol): *m/z* 866.68 (M+H, 100%), Calcd for $C_{59}H_{59}BN_4O_2$: *m/z* 866.47. $Zn(AcO)_2 \cdot 2H_2O$ (50 mg, 0.23 mmol) in 2 ml MeOH was added to the solution of porphyrin (150 mg, 0.19 mmol) in 7.5 ml CH_2Cl_2. After stirring for 1 hour at the room temperature, the reaction mixture was poured into water, and was extracted with CH_2Cl_2. The organic layer was washed with water and dried over with $MgSO_4$. After evaporation of the solvent, the residue was purified by column chromatography on silica gel using CH_2Cl_2 to give **3** (151 mg, 93 %). ^{1}H-NMR (400.13MHz, $CDCl_3$): δ (ppm) = 8.93 (d, *J* = 4.4 Hz, 2H, Por*H*), 8.84 (d, *J* = 4.4 Hz, 2H, Por*H*), 8.76 (d, *J* = 4.0 Hz, 4H, Por*H*), 8.29 (d, *J* = 8.0 Hz, 2H, Ar*H*), 8.15 (d, *J* = 8.0 Hz, 2H, Ar*H*), 8.10 (d, *J* = 8.0 Hz, 2H, Ar*H*), 7.74 (d, *J* = 8.0 Hz, 2H, Ar*H*) 7.28 (s, 4H, Ar*H*), 3.94 (s, 4H, -CH_2-), 2.63 (s, 6H, -CH_3), 1.83 (s, 12H, -CH_3), 1.61 (s, 9H, -CH_3), 1.17 (s, 6H, -CH_3); ^{13}C-NMR (100.61MHz, $CDCl_3$): δ (ppm) = 150.7, 150.4, 150.3, 139.7, 139.6, 137.8, 135.9, 134.6, 134.4, 132.9, 132.7, 13.6, 131.1, 131.0128.0, 123.9, 119.5, 35.3, 32.5, 32.1, 30.1, 22.5, 22.0, 21.9; MALDI-TOF Ms (dithranol): *m/z* 928.06 (M+H, 100%), Calcd for $C_{59}H_{57}BN_4O_2Zn$: *m/z* 928.39; UV-Vis (THF): λ_{max} (log ε) = 598 (4.09), 558 (4.37),

426 (5.70).

1: A solution of **2** (38 mg, 37 mmol), **3** (29 mg, 37 mmol) and $Pd(PPh_3)_4$ (1.7 mg, 1.5 mmol) in 4 ml dimethoxyethane (DME) and 2 ml 1.0 M K_2CO_3 aqueous solution was stirred at 70 ^oC for 12 h under a nitrogen atmosphere. After cooling to room temperature, the reaction mixture was poured into water. The organic layer was dried over with Na_2SO_4 and the solvent was evaporated. The residue was purified by column chromatography on silica gel using CH_2Cl_2 and recycling preparative HPLC to give **4** (13 mg, 20 %). MALDI-TOF Ms: *m/z* 1776.77 (M+H, 100%), Calcd for $C_{110}H_{77}BrN_{12}Zn_2$: *m/z* 1777.42. A solution of **4** (10 mg, 5.6 mmol), 4-ethoxyphenylboronic acid (5 mg, 5.6 mmol) and $Pd(PPh_3)_4$ (1 mg, 0.87 mmol) in 2 ml DME and 1 ml 1.0 M K_2CO_3 aqueous solution was stirred at 70 °C for 12 h under a nitrogen atmosphere. After cooling to room temperature, the reaction mixture was poured into water. The organic layer was dried over with Na_2SO_4 and the solvent was evaporated. The residue was purified by column chromatography on silica gel using CH_2Cl_2 and recycling preparative HPLC to give ester-terminated dyad (10 mg, 97 %). MALDI-TOF Ms: *m/z* 1847.56 (M+H, 100%), Calcd for $C_{119}H_{86}N_{12}O_2Zn_2$: *m/z* 1845.56. Aqueous solution of 30 µl 3.0 M NaOH was added to the solution of ester-terminated dyad (10 mg, 5.4 µl) in 3 ml THF. The mixture was stirred at 70 ^oC for 24 h. The solvent was removed in vacuo and the residue was washed with water several times. The residue was dissolved in THF and neutralized with acetic acid. After evaporation and washing with water, the solid was collected by filtration and dried in vacuo. (8 mg, 82 %). ^1H NMR (400.13 MHz, $CDCl_3$): δ (ppm) = 9.02-8.93 (m, 4H, Pc*H*), 8.76-8.73 (m, 4H, Por*H*), 8.61-8.41 (m, 8H, Pc*H*+Por*H*), 8.29-7.98 (m, 12H, Pc*H*+Ar*H*), 7.82-7.68 (m, 12H, Ar*H*), 7.51-7.39 (m, 6H, Ar*H*), 7.20-7.13 (m, 8H, Ar*H*), 2.31 (s, 12H, -CH_3), 1.29 (s, 9H, -CH_3), 1.10 (s, 6H, -CH_3); MALDI-TOF Ms: *m/z* 1818.47 (M+H, 100%), Calcd for $C_{117}H_{82}N_{12}O_2Zn_2$: *m/z* 1817.53; UV-Vis (THF): λ_{max} (log ε) = 698 (5.03),

632 (4.34), 559 (4.23), 426 (5.59), 361 (4.49).

5.3. Results and Discussion

5.3.1. Synthesis of ZnPc-ZnPor dyad 1

Directional energy flow toward the final energy acceptor in the dyads requires the precise spatial arrangement of molecular components in the molecular arrays. Molecular arrays with a linear arrangement of components provide a suitable spatial separation of donor and acceptor units. D_{2h} symmetrical phthalocyanines (ABAB-type Pcs) functionalized with two substituents at the opposite sites of the Pc ring enable the creation of linear arrangement of donor and acceptor units in the dyads.[15] ABAB-type Pcs have been synthesized by the cross-condensation of two different phthalyl derivatives 1,3-diiminoisoindoline and 1,3,3-trichloroisoindolenine.[16] However, this method can be applicable when the 1,3,3-trichloroisoindolenine derivative is either functionalized with a nitro group or lacks any functional group. On the other hand, Kobayashi *et al*. reported a simple statistical condensation method for ABAB-type Pcs by using the phthalonitriles having bulky substituents at the α-positions.[17] Torres *et al*. succeeded in preparing of the unsymmetrically substituted ABAB-type phthalocyanines functionalized with two or four iodine atoms by using the same synthetic method.[18] In this study, the ABAB-type Pc having two bromides at the opposite sites of the Pc ring was synthesized by the statistical condensation reaction of 3,6-diphenylphthalonitrile with 4-bromophthalonitrile (Scheme 5-1). The other porphyrin component **3** bearing a boronic ester was synthesized by the acid-catalyzed condensation of

5-mesityldipyrromethane with two aromatic aldehyde derivatives, followed by oxidation with 2,3-dichloro-5,6-dicyano-1,4-benzoquinone (DDQ) at room temperature. The final ZnPc-ZnPor dyad **1** having a carboxyl anchoring group was prepared by stepwise palladium-catalyzed Suzuki cross-coupling reactions with the ABAB-type ZnPc **2**, and was confirmed by matrix-assisted laser desorption/ionization time-of-flight (MALDI-TOF) mass spectroscopy and NMR. According to the molecular model of **1** as shown in Figure 5-1, the phenylene-bridged ZnPc-ZnPor dyad **1** is slightly twisted and the distance between the two central metals of porphyrin and phthalocyanine moieties in **1** is estimated to be 1.5 nm.

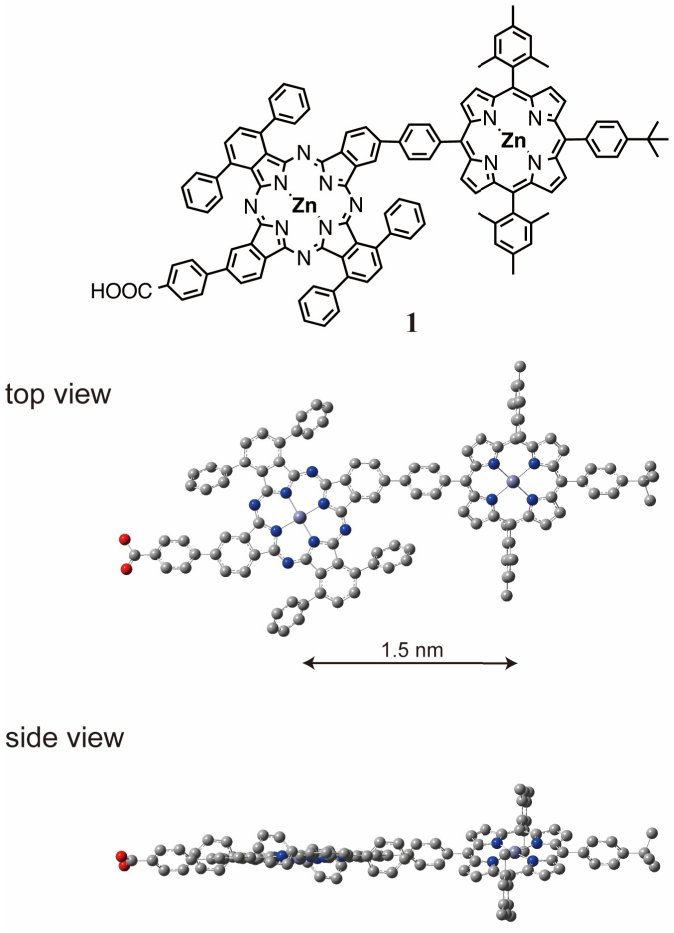

Figure 5-1: Chemical structure and computer-simulated molecular structure of optimized by Gaussian 09.

5.3.2. Optical and electrochemical property

Figure 5-2 illustrates the absorption spectra of dyad **1** and ZnPor **3** in tetrahydrofuran (THF). The absorption spectrum of **1** is the sum of the absorption spectra of ZnPc and ZnPor moieties, and showed two intense absorption bands with λ_{max} = 426 and 698 nm corresponding to the B band of ZnPor moiety and the Q band of ZnPc moiety in **1**, respectively. The dyad **1** can absorb a large part of the solar spectrum from 350 to 720 nm. The B band position of ZnPor for **1** remained unaltered as compared to that of **3**, suggesting that the electronic interaction between ZnPor and ZnPc in **1** is almost negligible. The Q band of ZnPc moiety in **1** was broadened, and the onset of the Q band was extended to 760 nm. This broadening of the Q band was attributed to the formation of dimer or oligomeric species through the intermolecular stacking among ZnPcs.[19] The steric hindrance of phenyl groups around the ZnPc in **1** is not sufficient to diminish the stacking of ZnPcs. The fluorescence spectra of **1** and **3** in degassed THF at room temperature are shown in the inset of Figure 5-2. The optical highest occupied molecular orbital-lowest unoccupied molecular orbital (HOMO-LUMO) band-gap (E_g) of **1** was determined to be 1.75 eV from the cross point of the normalized absorption and fluorescence spectra. When excited at the Soret band, ZnPor **3** exhibited two fluorescence peaks at 603 and 655 nm. However, the emission from **1** was mostly from the ZnPc upon excitation at the Soret band of ZnPor, and the residual fluorescence from the ZnPor unit was weak. This result suggests an efficient intramolecular energy transfer from the ZnPor moiety to the ZnPc moiety in **1**. The spectral overlap between ZnPor emission and ZnPc absorption induces the Förster resonant energy transfer in **1**.

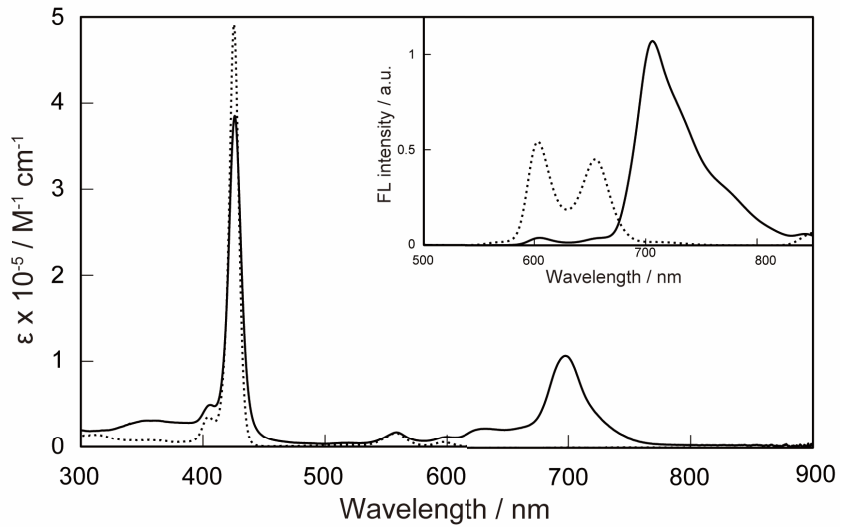

Figure 5-2: UV-Vis absorption and fluorescence (inset) spectra of **1** and **3** in THF; [**1**,**3**] = 10 μM.

The dyad **1** having a carboxyl anchoring group can adsorb onto the TiO_2 surface through the formation of ester bonds. Porous TiO_2 film on a quartz substrate was immersed into the THF solution of **1** to investigate the absorption spectrum of the dye-stained film. The absorption spectrum of **1** adsorbed on TiO_2 nanoparticles is shown in Figure 5-3. The Q band of ZnPc moiety is red shifted by 13 nm compared with that in THF. The red-shift of the Q band implies the formation of large aggregates among ZnPcs on the TiO_2 surface relative to in solution. Chenodeoxycholic acid (CDCA) has been used as a co-adsorbent to prevent dye aggregation on the TiO_2 surface. When CDCA was added to the THF solution of **1**, the Q band position of **1** adsorbed on the TiO_2 surface with CDCA was blue-shifted to 699 nm, which was similar to that in THF. The adsorption density of **1** co-adsorbed with CDCA was determined from the absorbance of **1** released from stained TiO_2 film. The adsorption density of **1** on a 4 mm TiO_2 film was 3.5 x 10^{-11} mol/cm^2, which was lower than the previous reported value for **PcS20** (8.3 x 10^{-11} mol/cm^2).[20] The co-adsorption with CDCA enabled the spatial separation of dyads on the TiO_2 surface. The molecular aggregation among ZnPcs adsorbed on the TiO_2 surface results in decrease of charge separation efficiency for

DSSCs. The DSSCs fabrication sensitized with **1** requires the co-adsorption with CDCA to improve the charge separation efficiency.

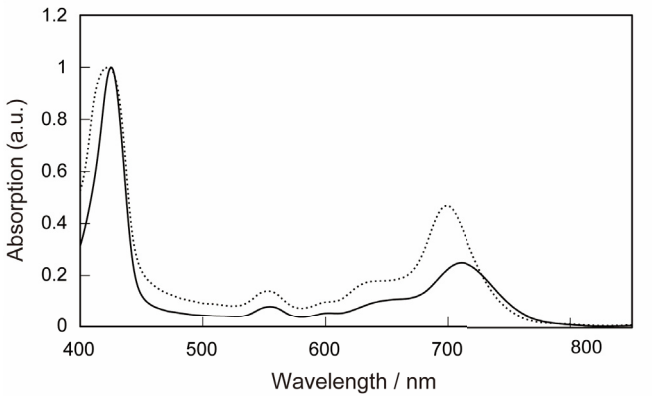

Figure 5-3: UV-Vis absorption spectra of **1** (solid line) and **1/CDCA** (dotted line) adsorbed onto 3 μm TiO_2 film.

The oxidation potential of **1** was obtained by differential pulse voltammetry (DPV) of **1**-stained TiO_2 electrodes in acetonitrile containing 0.1 M tetrabutylammonium hexaphosphate ($TBAPF_6$) as the supporting electrolyte. The first oxidation potential (E_{ox}) of **1** appeared at 0.33 V *vs.* ferrocene/ferrocenium (Fc/Fc^+), which was attributed to the phthalocyanine ring-based oxidation process. The HOMO and LUMO energy levels of **1** were evaluated from the E_{ox} and E_g values. The HOMO energy level of **1** was 0.97 V *vs.* the normal standard hydrogen electrode (NHE), which is more positive than that of the I_3^-/I^- redox couple in electrolytes for DSSCs. The LUMO energy level of **1** (-0.78 V *vs.* NHE) is sufficiently negative of the conduction-band-edge energy of TiO_2 (ca. -0.50 V *vs.* NHE). The HOMO and LUMO energy levels of **1** are thermodynamically adequate for the electron injection from the excited dye to TiO_2 and the dye regeneration of oxidized dyes by the I^-/I_3^- redox shuttle in the DSSCs.

5.3.3. Device performance

The DSSCs were fabricated using double-layered TiO_2 electrodes with electrolytes containing 0.6 M 1,2-dimethyl-3-propylimidazolium iodide (DMPImI), 0.1 M LiI, 0.05 M I_2, and 0.5 M *tert*-butylpyridine (tBP) in acetonitrile. Double layered TiO_2 electrodes were immersed in the THF solution of **1** for three hours at 25 °C. The photocurrent-voltage characteristics of the solar cells were measured under one sun condition. The cell sensitized with **1** showed short-current density (J_{sc}) of 2.0 mA/cm^2, open-circuit voltage (V_{oc}) of 0.49 V, and fill factor (*FF*) of 0.68, giving a PCE of 0.67 % under one sun condition (Figure 5-4a). As mentioned above, this low PCE value is probably due to the aggregation of ZnPc moieties on the TiO_2 surface. To diminish the aggregation of ZnPc moieties on the TiO_2 surface, TiO_2 electrodes were immersed in mixed THF solution of **1** and co-adsorbent CDCA ([**1**] = 5 mM; [CDCA] = 25 mM) for six hours. The **1** cell co-adsorbed with CDCA provided a higher PCE of 2.7 % (V_{oc} = 0.57 V, J_{sc} = 6.4 mA cm^{-2}, *FF* = 0.75) compared with that without CDCA. The IPCE spectrum displayed the both responses of ZnPc and ZnPor moieties in **1**, suggesting the conversion of harvested energy of the peripheral ZnPor to electricity through the energy transfer from ZnPor to ZnPc (Figure 5-4b). The dyad **1** sensitizer showed low IPCE values compared with the previously reported values of single ZnPor and ZnPc sensitizers, mainly because of the aggregation of ZnPc moiety. [20, 21, 22]

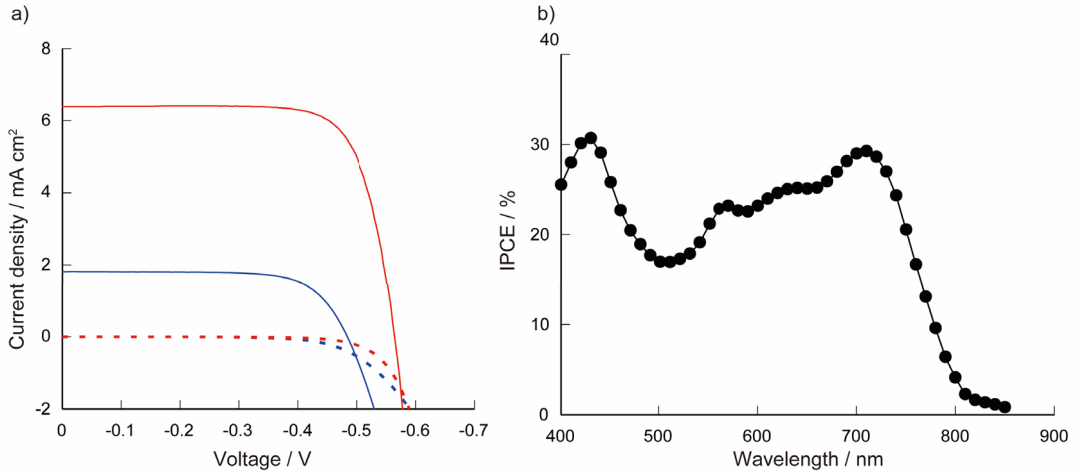

Figure 5-4: a) Photocurrent voltage curves obtained with DSSCs based on **1** (blue line) and **1/CDCA** (red line) under a standard global AM 1.5 solar condition; b) Incident photo-to-current conversion efficiency spectra of DSSCs based on **1/CDCA**.

5.4. Conclusion

The author designed and synthesized a novel ZnPc-ZnPor dyad **1** for the photosensitizer of DSSCs. The dyad **1** was synthesized by the stepwise Suzuki coupling reactions from the ABAB-type ZnPc. The peripheral ZnPor moiety in **1** was connected via a rigid phenylene linker to the carboxyl-anchored ZnPc moiety. Absorption and fluorescence spectral studies demonstrated that the energy harvested the ZnPor moiety can be efficiently transferred to the ZnPc moiety through the Förster resonant energy transfer from ZnPor to ZnPc. While **1** gave a PCE of 2.7 % with CDCA, **1** could convert the whole visible light region between 400 and 800 nm into electronic energy. The conversion efficiency could improve by the increasing of steric hindrance around the ZnPc to prevent aggregation among ZnPcs. The author will continue the molecular engineering of ZnPc-ZnPor dyads to enhance the PCE value in DSSCs.

References

[1] a) G. McDermott, S. M. Prince, A. A. Freer, A. M. Hawthornthwaite-Lawless, M. Z. Papiz, R. J. Cogdell, N. W. Isaacs, *Nature* **1995**, 374, 517; b) T. Pullerits, V. Sundström, *Acc. Chem. Res*. **1996**, 29, 381.

[2] a) D. Gust, T. A. Moore, A. L. Moore, *Acc*. *Chem*. *Res*. **2001**, *34*, 40; b) H. Imahori, *J*. *Phys*. *Chem*. *B* **2004**, 108, 6130-6143; c) I. M. Dixon, J.-P. Collin, J.-P. Sauvage, L. Flamigni, *Inorg. Chem*. **2001**,40, 5507-5517;

[3] a) J. P. C. Tome, A. M. V. M. Pereira, C. M. A. Alonso, M. G. P. M. S. Neves, A. C. Tome, A. M.S. Silva, J. A.S. Cavaleiro, M. V. Martinez-Diaz, T. Torres, G. M. A. Rahman, J. Ramey, D. M. Guldi, *Eur. J. Org. Chem*. **2006**, 257-267; b) M. Durmus, J. Y. Chen, Z. X. Zhao, T. Nyokong, *Spectrochimica Acta Part A*, **2008**, 70, 42-49; c) J. Li, J. R. Diers, J. Seth, S.I. Yang, D. F. Bocian, D. Holten, J. S. Lindsey, *J. Org. Chem*. **1990**, 64, 9090-9100; d) M. A. Miller, R. K. Lammi, S. Prathapan, D. Holten, J. S. Lindsey, *J. Org. Chem*. **2000**, 65, 6634-6649; e) S.I.Yang, J. Li, H. S. Cho, D. Kim, D. F. Bocian, D. Holten, J. S. Lindsey, *J. Mater. Chem.* **2000**, 10, 283-296; f) Z. Zhao, C.-T. Poon, W.-K. Wong, W.-Y. Wong, H.-L. Tam, K.-W. Cheah, T. Xie, D. Wang, Eur. J. Inorg. Chem, 2008, 119-128.

[4] A. R. M. Soares, M. V. Martínez-Díaz, A. Bruckner, A. M. V. M. Pereira, J. P. C. Tomé, C. M. A. Alonso, M. A. F. Faustio, M. G. P. Neves, A. C. Tomé, A. M. S. Silva, J. A. S. Cavaleiro, T. Torres, D. M. Guldi, *Org. Lett.* **2007**, 9, 1557-1560.

[5] C. B. KC, K. Stranius, P. D'Souza, N. Subbaiyan, H. Lemmetyinen, N. V. Tkachenko, F. D'Souza, *J. Phys. Chem. C* **2013**, 117, 763-773

[6] a) B. O'Regan, M. Grätzel, *Nature* **1991**, *353*, 737-740; b) A. Hagfeldt, G. Boschloo, L. Sun, K. Kloo, H. Pettersson, *Chem. Rev.*, **2010**, *110*, 6595-6663; c) M. Grätzel, *Acc. Chem. Res.*, **2009**, *42*, 1788-1798.

[7] a) M. Urbani, M. Gräzel, M. K. Nazeeruddin, T. Torres, *Chem. Rev.* **2014**, 114,12330-12396; b) L. Zhang, J. M. Cole, *ACS Appl. Mater. Interfaces* **2015**, 7, 3427-3455; c) L. Martin-Gomis, F. Fernández-Lázaro, Á. Sastre-Santos, *J. Mater. Chem. A* **2014**, 2, 15672-15682.

[8] J. I. Basham, G. K. Mor, C. A. Grimes, *ACS Nano* **2010**, 4, 1253-1258.

[9] S. K. Balasingam, M. Lee, M. G. Kang, Y. Jun, *Chem. Commun.* **2013**, 49, 1471-1487.

[10] a) C. Qin, Y. Numata, S. Zhang, A. Islam, X. Yang, K. Sodeyama, Y. Tateyama, L. Han, *Adv. Funct. Mater*. **2013**, 23, 3782-3789; b) J.-H. Yum, S.-R. Jang, P. Walter, T. Geiger, F. Nüesch, S. Kim, J. Ko, M. Grätzel, M. K. Nazeeruddin, *Chem. Commun*., **2007**, 4680-4682; c) J.-J. Cid, J.-H. Yum, S.-R. Jang, M. K. Naeeruddin, E. Martínz-Ferrero, E. Palomares, J. Ko, M. Grätzel, T. Torres, *Angew. Chem. Int. Ed.* **2007**, *46*, 8358-8362.

[11] a) V.P.S. Perera, P.K.D.D.P. Pitigala, M. K.I. Senevirathne, K. Tennakone, *Sol. Enegy Mater. Sol. Cells* 2005, 85, 91-98; b) K. Sayama, S. Tsukagoshi, T. Mori, K. Hara, Y. Ohga, A. Shinpou, Y. Abe, S. Suga, H. Arakawa, *Sol. Enegy Mater. Sol. Cells* 2003, 80, 47-71; c) A. Ehret, L. Stuhl, M. T. Spitler, *J. Phys. Chem. B* **2001**, 105, 9960-9965; d) C. Siegers, U. Würfel, M. Zistler, H. Gores, J. Hohl-Ebinger, A. Hinsch, R. Haag, *ChemPhysChem* **2008**, 9, 793-798.

[12] a) J. Warran, F. Buchet, Y. Pellegrin, E. Blart, F. Odobel, *Org. Lett.* **2011**, 13, 3944-3947; b) H. Choi, S. Paek, J. Ko, *J. Phys. Chem. C* **2014**, 118, 16319-16327.

[13] C. Siengers, J. Hohl-Enbinger, B. Zimmermann, U. Würfel, R. Mülhaupt, A. Hinsch, R. Haag, *ChemPhysChem* **2007**, 8, 1548-1556

[14] B. E. Hardin, E. T. Hoke, P. B. Armstrong, J.-H. Yum, P. Comte, T. Torres, J. M. J. Freshet, M. K. Nazeeruddin, M. Grätzel, M. D. McGehee, *Nature. Photonics.*, **2009**, 3, 406-411.

[15] J. Mack, N. Kobayashi, *Chem. Rev.* **2011**, 111, 281-321.

[16] a) J. G. Young, W. Onyebuagu, *J. Org. Chem.* **1990**, 55, 2155; b) S. Dabak, Ö. Bekaroglu, *New J. Chem*. **1997**, 21, 267

[17] N. Kobayashi, T. Ashida, T. Osa, *Chem. Lett*. **1992**, 2031-2034.

[18] E. Fazio, J. Jaramillo-García, G. de la Torre, T. Torres, *Org. Lett.* **2014**, 16, 4706-4709.

[19] M. J. Stillman, T. Nyokong, *Phthalocyanines Properties and Applications*; C. C. Lezonoff, A. B. P. Lever Eds., VCH, New York, 1989, Vol. 1, p135-289.

[20] T. Ikeuchi, H. Nomoto, N. Masaki, M. J. Griffith, S. Mori, M. Kimura, *Chem.*

Commun. **2014**, *50*, 1941-1943.

[21] M.-E. Ragoussi, J.-J. Cid, J.-H. Yum, G. de la Torre, D. D. Censo, M. Grätzel, M. K. Nazzeruddin, T. Torres, *Angew. Chem. Int. Ed.* **2012**, 51, 4375-4378.

[22] a) W. M. Campbell, K. W. Jolley, P. Wagner, K. Wagner, P. J. Walsh, K. C. Gordon, L. Schmidt-Mende, M. K. Nazeeruddin, Q. Wang, M. Grätzel, D. L. Officer, *J. Phys. Chem. C* **2007**, 111, 11760-11762; b) C.-Y. Lin, Y.-C. Wang, S.-J. Hsu, C.-F. Lo, E. W.-G. Diau, *J. Phys. Chem. C* **2010**, 114, 687-693.

Chapter 6

Low-symmetrical Ω-shaped zinc phthalocyanine sensitizers having a panchromatic light harvesting property for dye-sensitized solar cells

Summary: Two low-symmetrical phthalocyanines substituted with thiophene units at the non-peripheral (α) and the peripheral (β) positions have been synthesized and their optical, electronic structure, and electrochemical properties investigated. The substitution of thiophene units at the α positions of the phthalocyanine skeleton resulted in the red-shift of Q band as well as significantly modifying the molecular orbital electronic distributions just below the HOMO and just above the LUMO, distorting the typical "Gouterman" four orbital arrangement of MOs. Two amphiphilic Ω-shaped ZnPcs (**αPcS1** and **αPcS2**), in which π conjugation side chain with an adsorption site at an α position of Pc macrocycle, were synthesized as the sensitizers in dye-sensitized solar cells (DSSCs). The absorption spectra of **αPcS1** and **αPcS2** showed red-shifted Q band and a broad band from 350 to 550 nm assignable to the intramolecular charge-transfer transition from the ZnPc core to the side chains. TD-DFT calculations provide a clear interpretation of the effect of the thiophene conjugation on the typical phthalocyanine core π MOs. The **αPcS1** cell showed a panchromatic response in 400-800 nm with a PCE value of 5.5 % when used as a light-harvesting dye on a TiO_2 electrode for DSSCs under one-sun conditions.

6.1. Introduction

Phthalocyanines (Pcs) and their metal complexes (MPcs) are synthetic analogues of porphyrins and have attracted a special attention as sensitizers in solar-to-energy conversion applications because of their intense absorption bands (the Q band) in the red/NIR region, high molar extinction coefficients, and excellent stabilities.[1] The molecular engineering of MPc-based sensitizers has been widely explored to improve a photon-to-electron conversion efficiency (PCE) in organic-based solar cells.[2] The PCE values for MPc-based dye-sensitized solar cells (DSSCs) have been enhanced significantly by applying molecular design rules such as a low-symmetrical structure, steric isolation, intramolecular push-pull structure, and an optimization of the adsorption site.[3] The expansion of light-harvesting wavelength range in the NIR region is one of key issues to be solved in order to enhance the solar cell performance. To date, several attempts have been made to expand the light-harvesting wavelength range of MPc-based DSSCs by extension of the π-conjugation system and substitution of peripheral positions.[4] The author recently reported the light harvesting property in the NIR region of a ring-expanded sensitizer **NcS1**; and the DSSC cell sensitized with **NcS1** showed a photoresponse at wavelengths in 600-850 nm region.[4c] However, these MPc-based solar cells exhibited a little sensitization in the region between the B and the Q bands due to the absence of transitions in this area. Co-sensitization with different dyes, which have complementary absorption properties in the visible region, has been applied to cover whole regions from visible to NIR.[3d,5] The fabrication of co-sensitized DSSCs requires careful control of the adsorption process to optimize the ratio of the two dyes on the TiO_2 surface. Ince et al. reported a panchromatic response of hybrid MPc-based sensitizers having

peripheral π-conjugated bisthiophene substituents.[6] However, the reported PCE value of DSSCs sensitized with the hybrid sensitizers were less than 3% due to their strong tendency for intermolecular aggregation. In this paper, we have investigated the optical effects of substitution of thiophene at either the α or β positions of a ZnPc (**1** and **2**). Since α substituted ZnPc **1** showed a larger red-shift of Q band, we chose this for the design of two new hybrid chromophoric systems, **αPcS1** and **αPcS2**, in which a π conjugated side chain with an adsorption site introduced at an α position of the MPc, to act as the photosensitizers for DSSCs. The photoresponsive cell sensitized with **αPcS1** provided a PCE of 5.5 % under a simulated air mass with AM 1.5 global sunlight; **αPcS1** could convert photon energies into electronic energy over a wide wavelength range from the visible to the NIR regions of the solar spectrum into electronic energy

6.2. Experimental

Synthesis of ZnPc1 and 2

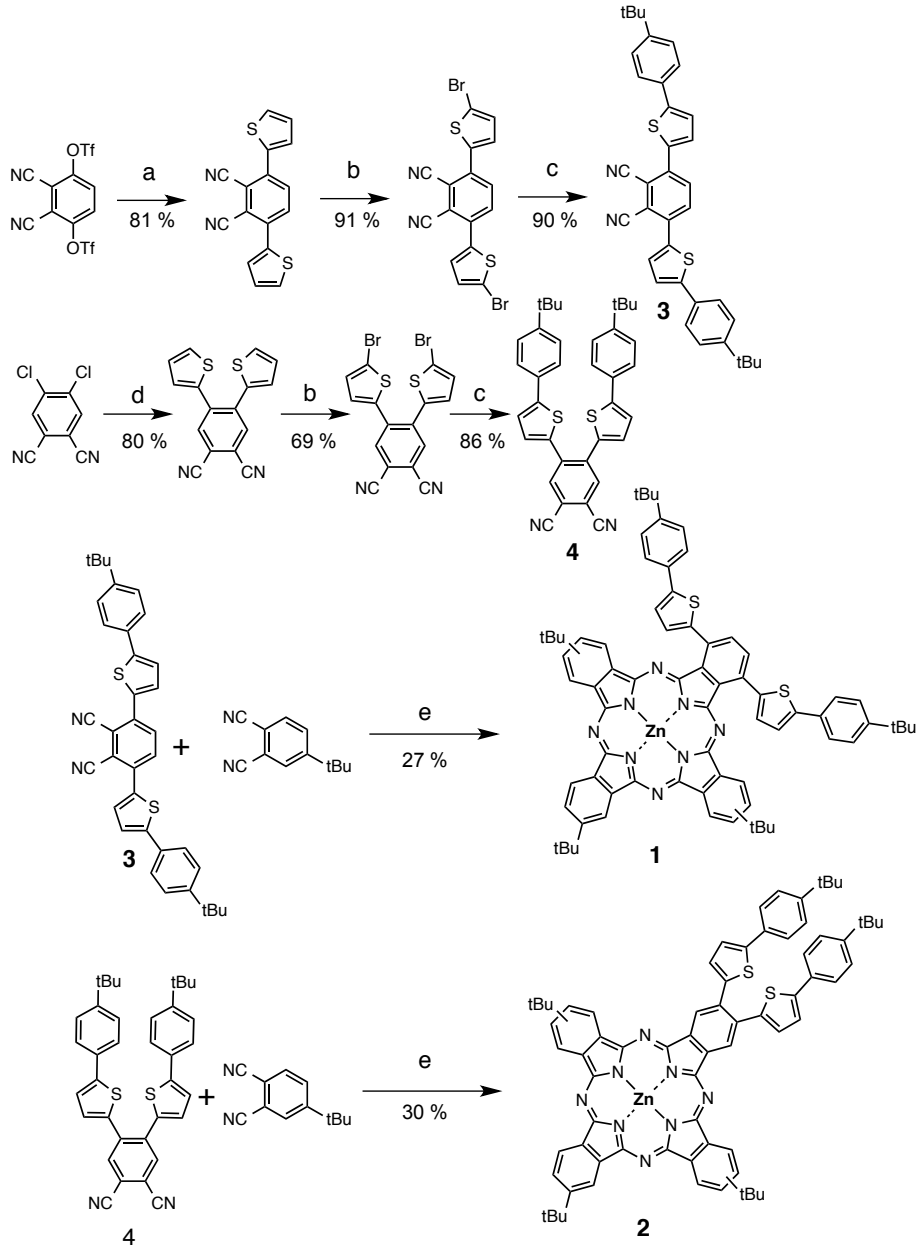

Scheme6-1: a) 2-tributylstannylthiophene, $Pd(PPh_3)_4$, LiCl, dioxane ; b) NBS, DMF; c) $Pd(PPh_3)_4$, 1M K_2CO_3 aq., DME, 4-*tert*-buthylphenylboronic acid; d) 2-thiopheneboronic acid, $Pd(AcO)_2$, Shos, K_3PO_4, toluene, e) $Zn(AcO_2)$, DMAE.

1,4-di(2-thienyl)-2,3-dicyanobenzene: $Pd(PPh_3)_4$ (54 mg, 0.47 µmol) was added to the solution of 3,6-ditrifatephthalonitrile (200 mg, 4.7 x 10^{-4} mol), 2-(tributylstannyl)thiophene (703 mg, 1.9 mmol), and lithium chloride (87 mg, 2.1 mmol) in dioxane (8 ml). The reaction mixture was stirred at 100 °C for 12 h under argon. After cooling to room temperature, the reaction mixture was poured into

water and extracted with ethyl acetate. The organic layer was washed with water and dried over Na_2SO_4. After evaporation of solvent, the residue was purified by column chromatography on silica using n-hexane/CH_2Cl_2 (1/1 v/v) to give 1,4-di(2-thienyl)-2,3-dicyanobenzene (112 mg, 81 %). ^{1}H-NMR (400.13MHz, $CDCl_3$): δ (ppm) = 7.83 (s, 2H, Ar*H*), 7.75 (dd, *J* = 0.8, 4.0 Hz, 2H, thiophene*H*), 7.53 (dd, *J* = 0.8, 5.2 Hz, 2H, thiophene*H*), 7.20 (t, *J* = 4.0, 5.2 Hz, 2H, thiophene*H*); ^{13}C-NMR (100.61 MHz, $CDCl_3$): δ (ppm) = 138.1, 137.7, 133.9, 129.3, 129.2, 129.1, 116.2, 114.83; HR-APCI-TOF MS *m/z* 292.0147 [M], Calcd for $C_{16}H_8N_2S_2$ *m/z* 292.0123.

1,2-di(2-thienyl)-4,5-dicyanobenzene : $Pd(AcO)_2$ (11 mg, 0.05 mmol) and SPhos (42mg, 0.10 mmol) were added to the solution of 4,5-dichlorophthalonitrile (200 mg, 1.0 mmol), 2-thiopheneboronic acid (320 mg, 2.5 mmol) and K_3PO_4 (850 mg, 4.0 mmol) in toluene. The reaction mixture was stirred at 80 °C for 6 hours. The reaction mixture was poured into water and extracted with CH_2Cl_2. The organic layer was washed with water and dried over Na_2SO_4. After evaporation of solvent, the residue was purified by column chromatography on silica gel using n-hexane/CH_2Cl_2 (1/1 v/v) followed by recycling preparative HPLC to give 1,2-di(2-thienyl)-4,5-dicyanobenzene as a white solid (236 mg, 80 %). ^{1}H-NMR (400.13MHz, $CDCl_3$): δ (ppm) = 7.90 (s, 2H, Ar*H*), 7.43 (dd, *J* = 2.0, 4.0 Hz, 2H, thiophene*H*), 7.04 (d, *J* = 4.0 Hz, 2H, thiophene*H*), 7.03 (d, *J* = 2.0 Hz, 2H, thiophene*H*); ^{13}C-NMR (100.61MHz, $CDCl_3$): δ (ppm) =139.4, 138.6, 136.0, 129.6, 129.3, 128.1, 115.5, 114.7; HR-APCI-TOF MS *m/z* 293.0202 [M+H], Calcd for $C_{16}H_8N_2S_2$: *m/z* 292.0123.

1,4-di(5-bromo-2-thienyl)-2,3-dicyanobenzene: N-bromosuccinimide (NBS) (280 mg, 1.6 mmol) was added to the solution of 1,4-di(2-thienyl)-2,3-dicyanobenzene (210 mg, 0.72 mmol) in *N,N*-dimethylformamide (3.6 ml). The resulting mixture was stirred overnight at 60 °C and then diluted with MeOH. The reaction mixture was poured into water and extracted with CH_2Cl_2. The organic layer was washed with water and dried over Na_2SO_4. After evaporation of solvent, the residue was purified by column

chromatography on silica using CH_2Cl_2 to give 1,4-di(5-bromo-2-thienyl)-2,3-dicyanobenzene (293 mg, 91 %). ^{1}H-NMR (400.13MHz, DMSO-*d*): δ (ppm) = 8.06 (s, 2H, Ar*H*), 7.61 (d, *J* =4.0 Hz, 2H, thiophene*H*), 7.45 (d, *J* =4.0 Hz, 2H, thiophene*H*); HR-APCI-TOF MS *m/z* 447.8334 [M], Calcd for $C_{16}H_6Br_2N_2S_2$: *m/z* 447.8334.

1,2-di(5-bromo-2-thienyl)-4,5-dicyanobenzene was synthesized from 1,2-di(2-thienyl)-4,5-dicyanobenzene according to the same procedure of 1,2-di(5-bromo-2-thienyl)-4,5-dicyanobenzene. Yield: 69 %. ^{1}H-NMR (400.13MHz, $CDCl_3$): δ (ppm) = 7.86 (s, 2H, Ar*H*), 7.04 (d, *J* =3.6 Hz, 2H, thiophene*H*), 6.90 (d, *J* =3.6 Hz, 2H, thiophene*H*); ^{13}C-NMR (100.61MHz, $CDCl_3$): δ (ppm) = 139.3, 138.1, 135.9, 135.4, 131.2, 130.2, 117.0, 115.2; HR-APCI-TOF MS *m/z* 447.8327 [M], Calcd for $C_{16}H_6N_2S_2Br_2$: *m/z* 447.8334.

1,4-di[5-(4-*tert*-butylphenyl-2-thienyl)]-2,3-dicyanobenzene (3): $Pd(PPh_3)_4$ (10 mg, 0.89 μmol) was added to the solution of 1,4-di(5-bromo-2-thienyl)-2,3-dicyanobenzene (80 mg, 0.18 mmol), and 4-*tert*-butylphenylbolonic acid (76 mg, 2.1 mmol) in DME (12 ml) and 1M K_2CO_3 aqueous solution (4 ml). The reaction mixture was stirred at 80 °C for 6 h under argon. The reaction mixture was poured into water and extracted with CH_2Cl_2. The organic layer was washed with water and dried over Na_2SO_4. After evaporation of solvent, the residue was purified by column chromatography on silica using n-hexane/CH_2Cl_2 (1/1 v/v) followed by recycling preparative HPLC to give 1,4-di[5-(4-tert-butylphenyl-2-thienyl)]-2,3-dicyanobenzene (213 mg, 90 %). ^{1}H-NMR (400.13MHz, $CDCl_3$): δ (ppm) = 7.84 (s, 2H, Ar*H*), 7.77 (d, *J* = 4.0 Hz, 2H, thiophene*H*), 7.58 (d, *J* = 8.4 Hz, 4H, Ar*H*), 7.44 (d, *J* = 8.4 Hz, 4H, Ar*H*), 7.34 (d, *J* = 4.0 Hz, 2H, thiophene*H*), 1.36 (s, 18H, -C(CH_3)$_3$); ^{13}C-NMR (100.61MHz, $CDCl_3$): δ (ppm) =152.3, 149.3, 148.5, 137.6, 136.2, 133.4, 130.9, 126.5, 126.2, 124.6, 116.5, 114.1, 35.2, 31.6; HR-APCI-TOF MS *m/z* 556.2010 [M], Calcd for $C_{36}H_{32}N_2S_2$: *m/z* 556.2007.

1,2-di[5-(4-*tert*-butylphenyl)-2-thienyl]-4,5-dicyanobenzene (4) was synthesized

from 1,2-di(5-bromo-2-thienyl)-4,5-dicyanobenzene according to the same procedure of 1,2-di[5-(4-*tert*-butylphenyl)-2-thienyl]-4,5-dicyanobenzene. Yield: 86 %. ^{1}H-NMR (400.13MHz, $CDCl_3$): δ (ppm) = 7.90 (s, 2H, Ar*H*), 7.49 (d, *J* = 8.4 Hz, 4H, Ar*H*), 7.39 (d, *J* = 8.4 Hz, 4H, Ar*H*), 7.20 (d, *J* = 3.6 Hz, 2H, thiophene*H*), 7.03 (d, *J* = 3.6 Hz, 2H, thiophene*H*), 1.31 (s, 18H, -C(CH_3)$_3$); ^{13}C-NMR (100.61MHz, $CDCl_3$): δ (ppm) = 152.1, 146.5, 139.0, 137.1, 135.9, 131.0, 130.6, 128.4, 126.3, 123.7, 115.6, 114.4, 35.1, 31.6; HR-APCI-TOF MS *m/z* 556.2007 [M], Calcd for $C_{36}H_{32}N_2S_2$: *m/z* 556.2007.

6: $Pd(PPh_3)_4$ (38 mg, 0.33 μmol) was added to the solution of 1,4-di(5-bromo-2-thienyl)-2,3-dicyanobenzene (150 mg, 0.33 mmol), and 4,4,5,5-tetramethyl-2-[5-(4,4,5,5-tetramethyl-1,3,-dioxolan-2-yl)thien-2-yl]-1,3,2-dioxaborolane (113 mg, 0.33 mmol) in dimethoxyethane (DME) (8 ml) and 1M K_2CO_3 aqueous solution (2 ml). The reaction mixture was stirred at 80 °C for 6 h under argon. After cooling the reaction mixture, the reaction mixture was poured into water and extracted with ethyl acetate. The organic layer was washed with water and dried over Na_2SO_4. After evaporation of solvent, the residue was purified by column chromatography on silica using n-hexane/CH_2Cl_2 (1/1 v/v) followed by recycling preparative HPLC to give **6** (60 mg, 31 %). ^{1}H-NMR (400.13MHz, $CDCl_3$): δ (ppm) = 7.80 (d, *J* = 8.4 Hz, 1H, Ar*H*), 7.71 (d, *J* = 8.4 Hz, 1H, Ar*H*), 7.70 (d, *J* = 4.0 Hz, 1H, thiophene*H*), 7.48 (d, *J* = 4.0 Hz, 1H, thiophene*H*), 7.22 (d, *J* = 4.0 Hz, 1H, thiophene*H*), 7.15 (d, *J* = 4.0 Hz, 1H, thiophene*H*), 7.13 (d, *J* = 4.0 Hz, 1H, thiophene*H*), 7.08 (d, *J* = 4.0 Hz, 1H, thiophene*H*), 6.16 (s, 1H, -C*H*-), 1.34 (s, 6H, -CH_3), 1.31 (s, 6H, -CH_3); ^{13}C-NMR (100.61MHz, $CDCl_3$): δ (ppm) = 144.9, 141.7, 139.0, 137.8, 137.0, 136.7, 135.8, 133.4, 131.9, 130.3, 129.7, 127.3, 125.5, 124.9, 116.6, 116.1, 115.9, 114.8, 114.2, 96.9, 83.7, 24.7, 22.5; HR-APCI-TOF MS *m/z* 579.9953 [M], Calcd for $C_{27}H_{21}BrN_2O_2S_3$: *m/z* 579.9943.

7: $Pd(PPh_3)_4$ (4.3 mg, 3.7 μmol) was added to the solution of **6** (54 mg, 92.9 μmol), and 4-*tert*-butylbenzenboronic acid (20 mg, 0.11 mmol) in DME (5 ml) and 1M K_2CO_3 aqueous solution (2.5 ml). The reaction mixture was stirred at 80 ºC for 6 h under argon. After cooling the reaction mixture, the reaction mixture was poured

into water and extracted with ethyl acetate. The organic layer was washed with water and dried over Na_2SO_4. After evaporation of solvent, the residue was purified by column chromatography on silica using n-hexane/CH_2Cl_2 (1/1 v/v) followed by recycling preparative HPLC to give **7** (50 mg, 84 %). ^{1}H-NMR (400.13MHz, $CDCl_3$): δ (ppm) = 7.80 (d, *J* = 10.4 Hz, 2H, Ar*H*), 7.76 (d, *J* = 4.0 Hz, 1H, thiophene*H*), 7.69 (d, *J* = 4.0 Hz, 1H, thiophene*H*), 7.57 (d, *J* = 8.4 Hz, 2H, Ar*H*), 7.43 (d, *J* = 8.4 Hz, 2H, Ar*H*), 7.33 (d, *J* = 4.0 Hz, 1H, thiophene*H*), 7.21 (d, *J* = 4.0 Hz, 1H, thiophene*H*), 7.12 (d, *J* = 4.0 Hz, 1H, thiophene*H*), 7.08 (d, *J* = 4.0 Hz, 1H, thiophene*H*), 6.16 (s, 1H, -C*H*-), 1.35 (s, 9H, -CH_3), 1.34 (s, 6H, -CH_3), 1.31 (s,6H, -CH_3); ^{13}C-NMR (100.61MHz, $CDCl_3$): δ (ppm) = 152.3, 148.6, 144.7, 141.3, 137.7, 137.1, 136.2, 136.1, 133.4, 133.3, 130.9, 130.3, 130.1, 127.3, 126.5, 126.2, 125.4, 125.4, 124.8, 124.6, 116.4, 114.1, 96.9, 83.7, 35.2, 31.6, 24.7, 22.5; HR-APCI-TOF MS *m/z* 634.1788 [M], Calcd for $C_{37}H_{34}N_2O_2S_3$: *m/z* 634.1782.

Synthesis of 1 and 2

3: A mixture of **3** (19 mg, 0.22 μmol), 4-*tert*-butylphthalonitrile (12 mg, 0.66 μmol), $Zn(AcO)_2$ (4 mg, 0.22 μmol) in 3 ml DMAE was heated at 160 °C with stirring for overnight. After the reaction mixture was cooled, and then diluted with MeOH. A precept formed which was filtered, washed with MeOH several times to remove excess Zn ion. The residue was purified by column chromatography on activated alumina by eluting with CH_2Cl_2 followed by recycling preparative HPLC to give **3** (14 mg, 27 %). ^{1}H-NMR (400.13MHz, $CDCl_3$): δ (ppm) = 8.11-7.77 (m, 11H, Pc*H*), 7.61-7.50 (m, 8H, Ar*H*), 7.48-7.38 (m, 4H, thiophene*H*), 1.53 (brs, 18H, -C(CH_3)$_3$), 1.47 (brs, 27H, -C(CH_3)$_3$); HR-APCI-TOF MS *m/z* 1172.4262, Calcd for $C_{72}H_{68}N_8S_2Zn$: *m/z* 1172.4294; UV-Vis (THF): λ_{max} (log ε) = 694 (4.84), 678 (4.83), 347 (4.84).

2 was synthesized from **4** according to the same procedure of **1**. Yield: 30 %. ^{1}H-NMR (400.13MHz, $CDCl_3$): δ (ppm) = 8.15-7.73 (m, 11H, Pc*H*), 7.61-7.39 (m, 12H, Ar*H*+ thiophene*H*), 1.66 (brs, 18H, -C(CH_3)$_3$), 1.43 (brs, 27H, -CH_3); HR-APCI-TOF MS *m/z* 1172.4254, Calcd for $C_{72}H_{68}N_8S_2Zn$: *m/z* 1172.4294;

UV-Vis (THF): λ_{max} (log ε) = 690 (5.19), 675 (5.05), 350 (4.91).

Synthesis of αPcS1

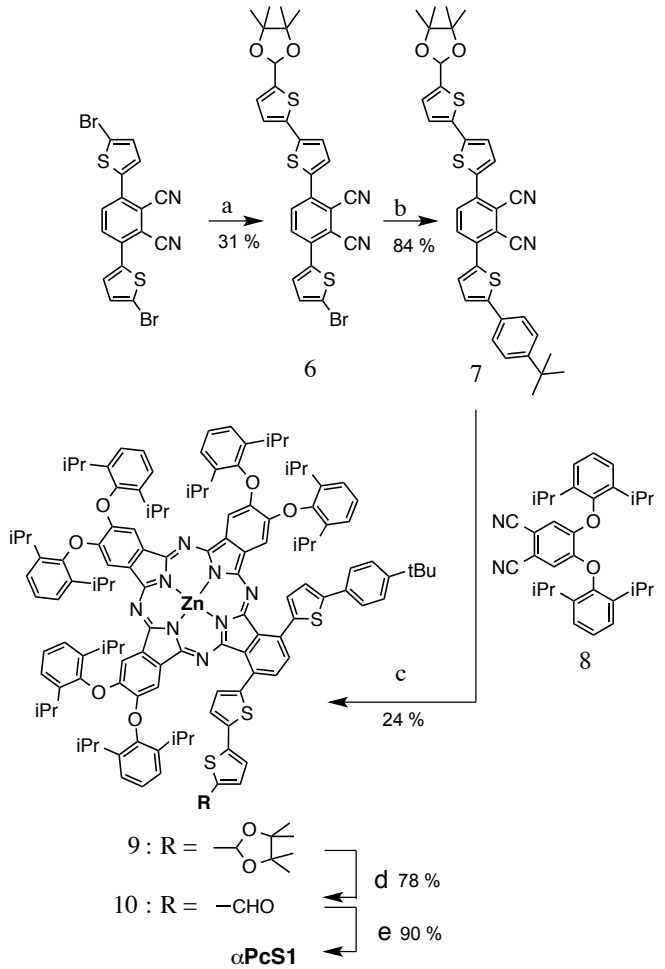

Scheme 6-2: a)4,4,5,5,-tetramethyl-2-[5-(4,4,5,5-tetrametyl-1,3-dioxolan-2-yl)-thien-2-yl]-1,3,2-dioxanrolane, $Pd(PPh_3)_4$, DME, 1M K_2CO_3 aq.; b) 4-*tert*-butyl-phenylboronic acid, $Pd(PPh_3)_4$, DME, 1M K_2CO_3 aq.; c) $Zn(AcO)_2$, DMEA, *o*-DCB; d) 10 % HCl aq., THF; e) piperidine, cyanoacetic acid, $CHCl_3$

αPcS1: A mixture of **7** (34 mg, 0.54 μmol), **8** (78 mg, 0.16 mmol), $Zn(CH_3COO)_2$ (9.8 mg, 0.54 μmol) in 6 ml DMAE and 3ml *o*-dichlorobenzene was heated at 160 °C with stirring for overnight. After the reaction mixture was cooled, it was diluted with MeOH. A precipitate formed which was filtered, washed with MeOH several times to remove excess Zn ion. The residue was purified by column chromatography on activated alumina by eluting with CH_2Cl_2, followed by

recycling preparative HPLC to give **9** (27 mg, 24 %). ^{1}H-NMR (400.13MHz, $CDCl_3$): δ (ppm) = 8.93 (d, *J* = 4.0 Hz, 1H, thiophene*H*), 8.78 (d, *J* = 4.0 Hz, 1H, thiophene*H*), 8.34 (s, 1H, Pc*H*), 8.32 (s, 1H, Pc*H*), 8.21 (s, 1H, Pc*H*), 8.12 (s, 1H, Pc*H*), 8.15 (s, 2H, Pc*H*), 8.14 (s, 2H, Pc*H*), 7.64-7.54 (m, 10H, Ar*H*), 7.49-7.42 (m, 12H, Ar*H*), 7.19 (d, *J* = 3.6 Hz, 1H, thiophene*H*), 7.15 (d, *J* = 3.6 Hz, 1H, thiophene*H*), 6.41 (d, *J* = 4.0 Hz, 1H, thiophene*H*), 6.34 (d, *J* = 4.0 Hz, 1H, thiophene*H*), 6.28 (s, 1H, -C*H*-), 3.49-3.34 (m, 12H, -C*H*-), 1.47 (s, 9H, -C(CH_3)$_3$), 1.44 (s, 6H, -CH_3), 1.36 (s, 6H, -CH_3), 1.22 (brs, 72H, -CH_3); MALDI-TOF Ms (dithranol): *m/z* 2140.35 (M, 100%), Calcd for $C_{133}H_{142}N_8O_8S_3Zn$: *m/z* 2139.94. **9** (27 mg, 0.13 µmol) was dissolved in 1.2 mol/L HCl aqueous solution (3 ml) and THF (6 ml). The mixture was heated at 50 °C for 3 h and then poured into water. Ethyl acetate was added, and the organic layer was washed with water until neural pH, dried over anhydrous Na_2SO_4 and the solvent was evaporated. The residue was purified by column chromatography on activated alumina using CH_2Cl_2 to give **10** (20 mg, yield 78 %). ^{1}H-NMR (400.13MHz, $CDCl_3$): δ (ppm) = 9.71 (s, 1H, -CHO), 8.84 (d, *J* = 4.0 Hz, 2H, thiophene*H*), 8.34 (s, 1H, Pc*H*), 8.27 (s, 1H, Pc*H*), 8.21 (s, 2H, Pc*H*), 8.15 (s, 4H, Pc*H*), 7.74 (d, *J* = 4.0 Hz, 1H, thiophene*H*), 7.64-7.54 (m, 10H, Ar*H*), 7.49-7.44 (m, 8H, Ar*H*), 7.38 (s, 4H, Ar*H*), 7.33 (d, *J* = 4.0 Hz, 1H, thiophene*H*), 6.54 (d, *J* = 4.0 Hz, 1H, thiophene*H*), 6.42 (d, *J* = 4.0 Hz, 1H, thiophene*H*), 3.48-3.34 (m, 12H, -C*H*-), 1.47 (s, 9H, -C(CH_3)$_3$), 1.26 (s, 72H, -CH_3); MALDI-TOF Ms (dithranol): *m/z* 2037.9 (M, 100%), Calcd for $C_{127}H_{130}N_8O_7S_3Zn$: *m/z* 2038.9; IR (ATR): 1666.50 (-CHO) cm^{-1}. Cyanoacetic acid (8.3 mg, 9.8 µmol) and a catalytic amount of piperidine were added to the solution of **10** (20 mg, 9.8 µmol) in $CHCl_3$ (3 ml). After stirred for overnight at 65 °C, water (50 ml) was poured into the reaction mixture. The mixture was stirred till precipitate is formed. Isolation of the precipitate by vacuum filtration afforded the pure product, **αPcS1**, as dark-green solid (18 mg, 90 %). ^{1}H-NMR (400.13MHz, $CDCl_3$): δ (ppm) = 8.82 (brs, 1H, -C*H*=), 8.35-8.30 (m, 4H, thiophene*H*), 8.23-8.05 (m, 8H, Pc*H*), 7.60-7.54 (m, 10H, Ar*H*), 7.49-7.45 (m, 12H, Ar*H*), 6.51-6.49 (m, 2H, thiophene*H*), 3.47-3.36 (m, 12H, -C*H*-), 1.60 (s, 18H, -C(CH_3)$_3$), 1.25 (brs, 72H, -CH_3); MALDI-TOF Ms (dithranol): *m/z* 2105.2 (M+H, 100%), Calcd for $C_{130}H_{131}N_9O_8S_3Zn$: *m/z* 2105.9; UV-Vis (THF): λ_{max} (log ε) = 702 (5.05), 687

(5.05), 359 (4.92).

αPcS2 was synthesized according to the same procedure of **αPcS1**.

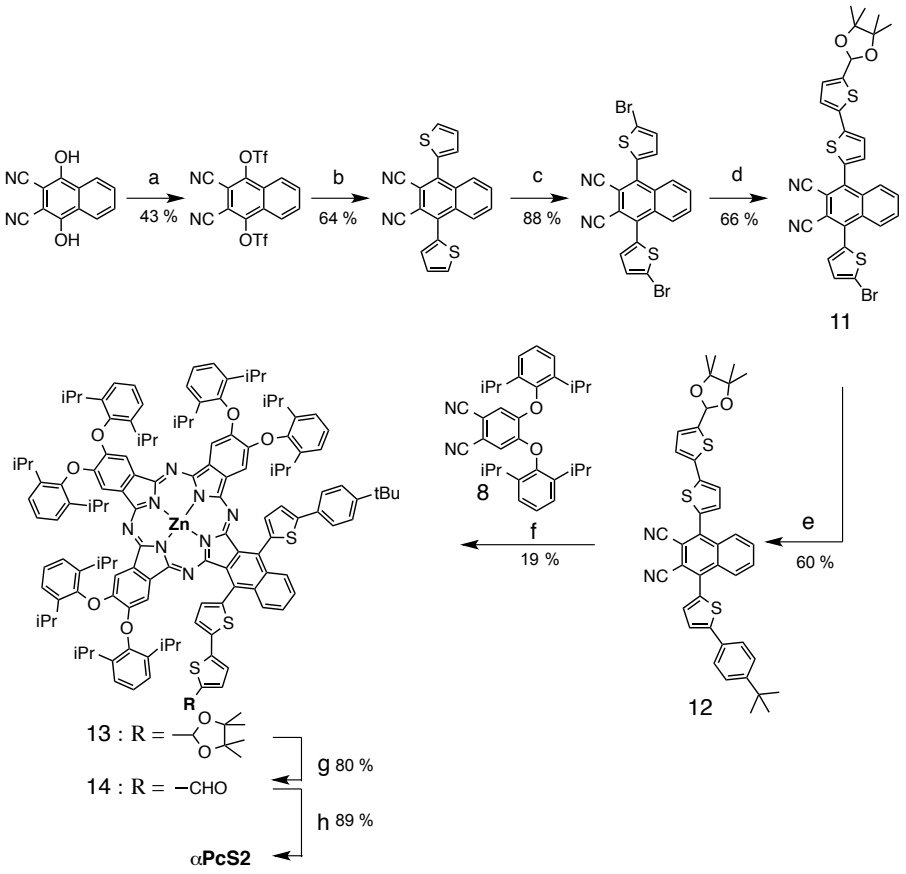

Scheme 6-3: a) trifluoromethansulfonic anhydride, pyridine, CH_2Cl_2; b) 2-tributylstannylthiophene, $Pd(PPh_3)_4$, LiCl, dioxane; c) NBS, DMF; d) 4,4,5,5,-tetramethyl-2-[5-(4,4,5,5-tetrametyl-1,3-dioxolan-2-yl)-thien-2-yl]-1,3,2-dioxanrolane, $Pd(PPh_3)_4$, DME, 1M K_2CO_3 aq.; e) 4-*tert*-butylphenylboronic acid, $Pd(PPh_3)_4$, DME, 1M K_2CO_3 aq.; f) $Zn(AcO)_2$, DMEA,*o*-DCB; g) 10 % HCl aq.,THF; h) piperidine, cyanoacetic acid, $CHCl_3$

12 was synthesized from 1,4-dihydroxy-2,3-dicyanonaphthalene through Stille cross coupling reaction, bromination, and Suzuki coupling reaction according to the same procedure of **7**.

1,4-ditrifate-2,3-dicyanonaphthalene: Yield: 43 %. ^{1}H-NMR (400.13MHz, $CDCl_3$): δ (ppm) = 8.38 (dd, *J* = 3.2, 6.4 Hz, 2H, Ar*H*), 8.11 (dd, *J* = 3.2, 6.4 Hz, 2H, Ar*H*); ^{13}C-NMR (100.61 MHz, $CDCl_3$): δ (ppm) = 147.7, 134.1, 129.9, 124.2, 123.7, 110.9, 106.4; HR-APCI-TOF MS *m/z* 474.9498 [M+H], Calcd for

$C_{14}H_4N_2O_6S_2F_6$: *m/z* 473.9415.

1,4-di(2-thienyl)-2,3-dicyanonaphthalene: Yield: 64 %. ^{1}H-NMR (400.13MHz, $CDCl_3$): δ (ppm) = 8.04 (dd, *J* = 3.2, 6.4 Hz, 2H, Ar*H*), 7.73 (dd, *J* = 3.2, 6.4 Hz, 2H, Ar*H*), 7.65 (d, *J* = 5.2 Hz, 2H, thiophene*H*), 7.35 (d, *J* = 3.6 Hz, 2H, thiophene*H*), 7.30 (d, *J* = 4.8 Hz, 2H, thiophene*H*); ^{13}C-NMR (100.61 MHz, $CDCl_3$): δ (ppm) =134.7, 134.4, 131.0, 129.3, 128.3, 128.2, 112.7; HR-APCI-TOF MS *m/z* 343.0359 [M+H] , Calcd for $C_{20}H_{10}N_2S_2$: *m/z* 343.0358.

1,4-di(5-bromo-2-thienyl)-2,3-dicyanonaphthalene: Yield: 88 %. ^{1}H-NMR (400.13MHz, $CDCl_3$): δ (ppm) = 8.08 (dd, *J* = 3.2, 6.4 Hz, 2H, Ar*H*), 7.77 (dd, *J* = 3.2, 6.4 Hz, 2H, Ar*H*), 7.26 (d, *J* = 4.0 Hz, 2H, thiophene*H*), 7.12 (d, *J* = 4.0 Hz, 2H, thiophene*H*); HR-APCI-TOF MS *m/z* 497.8569 [M], Calcd for $C_{20}H_8Br_2N_2S_2$: *m/z* 497.8490.

11: Yield: 66 %. ^{1}H-NMR (400.13MHz, $CDCl_3$): δ (ppm) = 8.17-8.20 (m, 1H, Ar*H*), 8.08-8.05 (m, 1H, Ar*H*), 7.75-7.77 (m, 2H, Ar*H*), 7.32 (d, *J* = 3.6 Hz, 1H, thiophene*H*), 7.25 (d, *J* = 3.6 Hz, 1H, thiophene*H*), 7.13 (d, *J* = 3.6 Hz, 1H, thiophene*H*), 7.09 (d, *J* = 3.6 Hz, 1H, thiophene*H*), 7.02 (d, *J* = 3.6 Hz, 1H, thiophene*H*), 7.00 (d, *J* = 3.6 Hz, 1H, thiophene*H*), 6.18 (s, 1H, -C*H*-), 1.35 (s, 6H, -CH_3), 1.32 (s, 6H, -CH_3); ^{13}C-NMR (100.61 MHz, $CDCl_3$): δ (ppm) =146.0, 144.6, 143.2, 141.9, 141.3, 140.1, 138.6, 136.2, 134.2, 133.1, 132.1, 131.5, 131.4, 131.1, 128.4, 128.0, 127.2, 124.8, 124.6, 123.7, 116.4, 115.6, 112.4, 97.0, 83.9, 24.7, 22.5; HR-APCI-TOF MS *m/z* 630.0157 [M], Calcd for $C_{31}H_{23}BrN_2S_3O_2$: *m/z* 630.0100.

12: Yield: 60 %. ^{1}H-NMR (400.13MHz, $CDCl_3$): δ (ppm) = 8.17-8.22 (m, 2H, Ar*H*), 7.74-7.77 (m, 2H, Ar*H*), 7.61 (d, *J* = 8.9 Hz, 2H, Ar*H*), 7.45 (d, *J* = 8.9 Hz, 2H, Ar*H*), 7.43 (d, *J* = 3.6 Hz, 1H, thiophene*H*), 7.32 (d, *J* = 3.6 Hz, 2H, thiophene*H*), 7.26 (d, *J* = 3.6 Hz, 1H, thiophene*H*), 7.14 (d, *J* = 3.6 Hz, 1H, thiophene*H*), 7.08 (d, *J* = 3.6 Hz, 1H, thiophene*H*), 6.18 (s, 1H, -C*H*-), 1.36 (s, 9H, -CH_3), 1.35 (s, 6H, -CH_3), 1.32 (s, 6H, -CH_3); ^{13}C-NMR (100.61 MHz, $CDCl_3$): δ

(ppm) = 152.1, 148.9, 144.5, 141.7, 141.5, 140.7, 137.1, 134.3, 134.3, 133.3, 134.2, 132.2, 132.0, 131.2, 131.1, 131.0, 128.3, 127.2, 126.4, 126.3, 116.0, 115.9, 112.6, 112.5, 97.0, 88.7, 53.9, 35.1, 24.7, 22.5; HR-APCI-TOF MS *m/z* 684.1976 [M], Calcd for $C_{41}H_{36}N_2S_3O_2$: *m/z* 684.1933.

13: Yield: 19 %. ^{1}H-NMR (400.13MHz, $CDCl_3$): δ (ppm) = 8.33 (dd, *J* = 3.2, 6.0 Hz, 2H, Pc*H*), 8.10-8.08 (m, 6H, Pc*H*), 7.74 (d, *J* = 3.2 Hz, 2H, thiophene*H*), 7.68-7.66 (m, 2H, Pc*H*), 7.63-7.52 (m, 10H, Ar*H*), 7.46-7.41 (m, 12H, Ar*H*), 7.07 (d, *J* = 3.6 Hz, 1H, thiophene*H*), 6.99 (d, *J* = 3.6 Hz, 1H, thiophene*H*), 6.68 (d, *J* = 3.6 Hz, 1H, Thiophene*H*), 6.56 (d, *J* = 3.6 Hz, 1H, thiophene*H*), 6.21 (s, 1H, -C*H*-), 3.47-3.31 (m, 12H, -C*H*-), 1.39 (s, 9H, -C(CH_3)$_3$), 1.38 (s, 6H, -CH_3), 1.33 (s, 6H, -CH_3), 1.20 (brs, 72H, -CH_3); MALDI-TOF Ms (dithranol): *m/z* 2189.4 (M, 100%), Calcd for $C_{137}H_{144}N_8O_8S_3Zn$: *m/z* 2188.96.

14: Yield: 80 %. ^{1}H-NMR (400.13MHz, $CDCl_3$): δ (ppm) = 9.11 (s, 1H, -CHO), 8.36-8.22 (m, 2H, Pc*H*), 8.12-8.07 (m, 6H, Pc*H*), 7.96 (d, *J* = 3.6 Hz, 1H, thiophene*H*), 7.74 (d, *J* = 3.2 Hz, 2H, thiophene*H*), 7.69-7.65 (m, 2H, Pc*H*), 7.64-7.45 (m, 10H, Ar*H*), 7.44-7.41 (m, 12H, Ar*H*), 7.10 (d, *J* = 3.6 Hz, 1H, thiophene*H*), 6.74 (d, *J* = 3.6 Hz, 1H, thiophene*H*), 6.68 (d, *J* = 3.6 Hz, 1H, thiophene*H*), 3.45-3.26 (m, 12H, -C*H*-), 1.38 (s, 9H, -C(CH_3)$_3$), 1.26 (s, 72H, -CH_3); MALDI-TOF Ms (dithranol): *m/z* 2088.9 (M, 100%), Calcd for $C_{131}H_{132}N_8O_7S_3Zn$: *m/z* 2088.87; IR (ATR): *ν* 1672.28 (-CHO) cm^{-1}.

αPcS2: Yield: 89 %. ^{1}H-NMR (400.13MHz, $CDCl_3$): ***δ*** (ppm) = 8.33 (brs, 1H, -C*H*=), 8.13-8.08 (m, 8H, Pc*H*), 8.02-7.95 (m, 4H, thiophene*H*), 7.78-7.75 (m, 2H, Pc*H*), 7.69-7.50 (m, 10H, Ar*H*), 7.47-7.06 (m, 12H, Ar*H*), 6.63 (m, 2H, thiophene*H*), 3.41-3.26 (m, 12H, -C*H*-), 1.40 (s, 9H, -C(CH_3)$_3$), 1.26 (brs, 72H, -CH_3); MALDI-TOF Ms (dithranol): *m/z* 2156.3 (M, 100%), Calcd for $C_{134}H_{133}N_9O_8S_3Zn$: *m/z* 2155.87; UV-Vis (THF): λ_{max} (log ε) = 707 (5.35), 357 (4.99).

6.3. Results and Discussion

6.3.1. Effect of thiophene substitution positions on the optical and electrochemical properties

The effect of substituents on the position and intensity of the Q bands has been systematically investigated.[7] Peripheral substitution with electron-donating groups such as alkoxyl and alkylthio groups at the α positions of the MPc skeleton shifts the Q band to longer wavelength than when β-substituted, and these effects can be reasonably explained by considering the magnitude of the atomic orbital coefficients of the carbon atoms derived from molecular orbital calculations.[7b] However, the effect of the introduction of thiophene units at the α and β positions of MPc skeleton on the optical and electrochemical properties has not been examined. The author synthesized two structural isomers **1** and **2** having two thiophenes at either the α or β positions on one side of the macrocycle and investigated their optical and electrochemical differences.

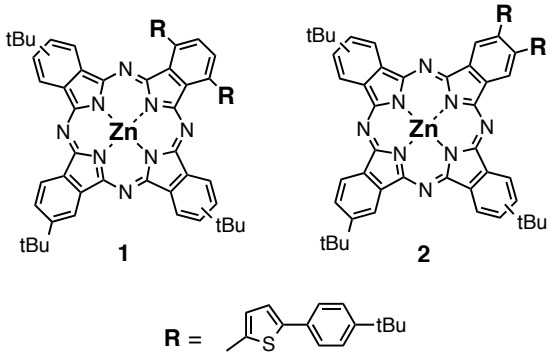

Figure 6-1: Substitution patterns in the $ZnPc(tBu)_4$ core of compounds **1** and **2**.

Two phthalonitriles, **3** and **4,** bearing two thiophene rings at different positions

on the phthalonitrile were synthesized from 3,6-dihydroxyphthalonitrile and 4,5-dichlorophthalonitrile, respectively, as starting materials via palladium-catalyzed coupling reactions (Scheme 6-1). The phthalonitrile having thiophenes at the 3 and 6 positions was synthesized by the Migita-Kosugi-Stille cross coupling reaction between 3,6-bis(trifluoromethanesulfonyloxy)phthalonitrile and 2-(tributylstannyl)thiophene in 81% yield.[8,9] The other, the 4,5-dithiophenephthalonitrile, was synthesized by the Suzuki-Miyaura cross coupling reaction of 4,5-dichlorophthalonitrile with 2-thiopheneboronic acid using 2-dicyclohexylphosphino-2',6'-methoxybiphenyl (SPhos) as a ligand in 88% yield.[10] After treatment with *N*-bromosuccinimide (NBS), bromides were reacted with 4-*tert*-butylphenylboronic acid using $Pd(PPh_3)_4$ to produce **3** and **4** in 90 and 86% yields, respectively. The peripherally-substituted, low-symmetry ZnPcs, **1** and **2,** were prepared by mixed condensation reaction between 4-*tert*-butylphthalonitrile and **3** or **4** in 3:1 molar ratio in *N,N*-dimethylaminoethanol (DMAE) in the presence of $Zn(AcO)_2$, and were isolated by column chromatography and preparative HPLC.[11]

Figure 6-2a shows absorption spectra of the α-substituted **1** and β-substituted **2** in tetrahydrofuran (THF). While the absorption spectrum of $ZnPc(tBu)_4$ lacking thiophene rings showed the expected sharp and strong Q band at 672 nm, the low-symmetry **1** and **2** displayed broader, split Q bands red-shifted by ca. 20 nm relative to that of $ZnPc(tBu)_4$. Furthermore, the molar extinction (ε) at the Q band for **1** was significantly lower than that of **2** (Table 6-1). Splitting of the Q band was not observed in the previously reported zinc α-octaphenylphthalocyanine complexes.[13] Thus, the introduction of the thiophene units at both the α and β positions on MPc skeleton strongly affects the electronic properties of the MPc π-system. The emission maxima of **1** is red-shifted by 14 nm relative to that of **2**, suggesting that **1** has a narrower band gap than **2** (Figure 6-2a). The magnetic

circular dichroism (MCD) spectrum of **1** showed a Faraday *A*-term like curve with a peak at 672 nm and trough at 697 nm (Figure 6-2b). This is probably assigned as a pseudo-Faraday *A*-term produced by superimposition of closely lying Faraday *B* terms of opposite sign because of the approximate C_{2v} symmetry.[14] This suggests that there is splitting of the lowest unoccupied molecular orbitals (LUMO and LUMO+1 energy levels) of the low-symmetrical complexes. The highest occupied molecular orbital (HOMO) energy levels of **1** and **2** were also determined by using a differential pulse voltammetric (DPV) technique (Figure 6-3). The first oxidation potentials of **1** (+0.02 V *vs*. Fc^+/Fc) and **2** (+0.04 V *vs*. Fc^+/Fc) are negatively shifted as compared to $ZnPc(tBu)_4$ (+0.09 V *vs*. Fc^+/Fc). The higher HOMO level of **1** compared with that of **2** indicates the effective destabilization of the HOMO levels by the substitution at a positions.

Table 6-1: Optical and electrochemical data for **1** and **2**

Dye	Absorption[a] / nm (ε x 10^{-5} /M^{-1} cm^{-1})	Emission[b] / nm (ϕ_f)[c]	E_{HOMO}[d] / V *vs*. Fc^+/Fc	$E_{0\text{-}0}$[e] / eV	E_{LUMO}[f] / V *vs*. Fc^+/Fc
1	694 (0.68), 678 (0.69), 347 (0.72)	713 (0.1)	+0.02	1.76	-1.74
2	690 (1.56), 675 (1.1), 350 (0.82)	698 (0.2)	+0.04	1.79	-1.75

[a] In THF; [b] In THF by exciting at the peak position of the B band; [c] Fluorescence quantum yield (ϕ_f) was determined with $ZnPc(tBu)_4$ as a standard in THF, ϕ_f = 0.3[12]; [d] E_{HOMO} was determined from the first oxidation potential of dye in *o*-DCB solution; [e] Optical band gap ($E_{0\text{-}0}$) was determined from the intercept of the normalized absorption and emission spectra; [f] E_{LUMO} was calculated from HOMO and band gap.

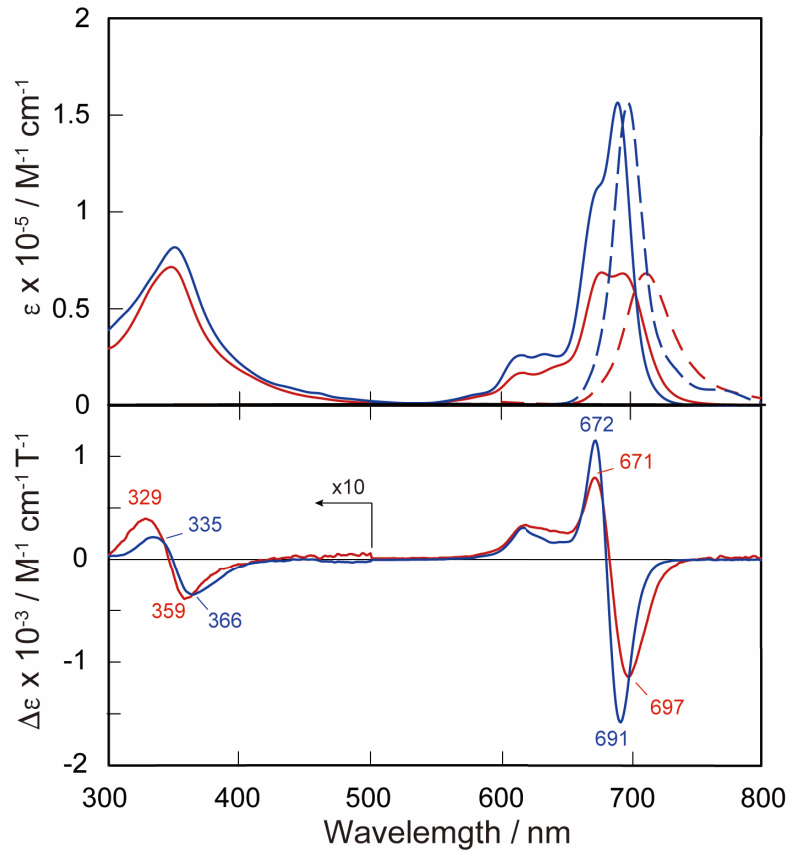

Figure 6-2: a) Absorption (solid line) and emission (dashed line) spectra of **1** (red) and **2** (blue) in the THF; b) MCD spectra of **1** (red) and **2** (blue) in THF.

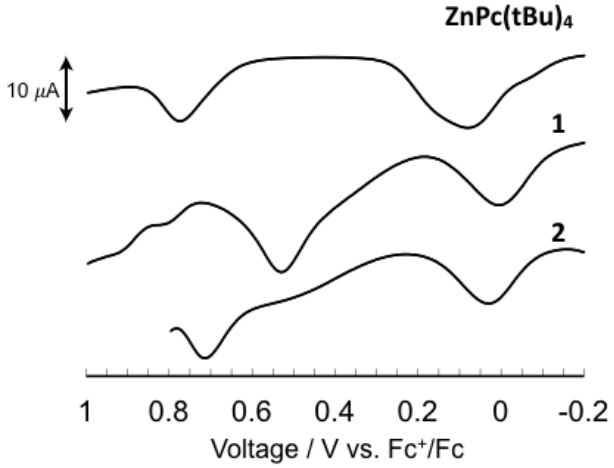

Figure6-3: Differential plus voltammetry of $ZnPc(tBu)_4$, **1**, and **2** in *o*-DCB containing 0.1 M $TBAPF_6$ as a supporting electrolyte.

Density functional theory (DFT) calculations at the CAM-B3LYP/6-31G* level[15] (Gaussian 09) were carried out for ZnPc, **1** and **2** to enhance our understanding of the spectroscopic and electrochemical data. Figure 6-4 shows energy level diagrams of **1**, **2** and the core ZnPc, and calculated electronic absorption spectra of **1** and **2**. Whereas the estimated LUMO and LUMO+1 levels of unsubstituted ZnPc are degenerate, the degeneracy of LUMO and LUMO+1 levels for **1** and **2** were broken by the substitution with thiophene units. The appearance of thiophene-related orbitals between the HOMO and the typical, Gouterman HOMO-1 orbital[16] that are identified by the nodal patterns for the +/-4 angular momentum of the core porphyrazine ring is an important aspect of the use of the thiophene. While the HOMO-1 for the phthalocyanines is always lower in energy by a significant amount (here over 2 eV) for peripheral substitution that does not interact with the conjugation, there are no orbitals introduced between the HOMO and its paired 4-node-orbitals (nominally e_u in symmetry). The energy splitting correlates well with the Q band intensity.[17] Time-dependent (TD) DFT calculations reproduced the spectral differences between **1** and **2** (Figure 6-3b) very well. The split Q bands can be assigned to the HOMO→LUMO and HOMO→LUMO+1 transitions of the Pc ligand. The lowest-lying electronic transition of **1** was red-shifted by 13 nm compared with that of **2** due to the narrowing of the HOMO-LUMO band gap through the destabilization of HOMO level and the stabilization of LUMO level. For isolated MOs like those in ZnPc, the HOMO-LUMO gap can closely predict the Q band energy.[17] These results reveal that substitution of thiophene units at the α positions of the Pc skeleton leads to expansion of the light-harvesting region in the NIR region by the red-shifting of Q band as well as tuning of the HOMO and LUMO energy levels to optimize photoinduced electron transfer reaction for the DSSC system. Thus, the α-substituted ZnPc sensitizers were used to form **αPcS1** and **αPcS2** by adding an adsorption site that was designed and synthesized to improve the enhancement of

DSSC performance.

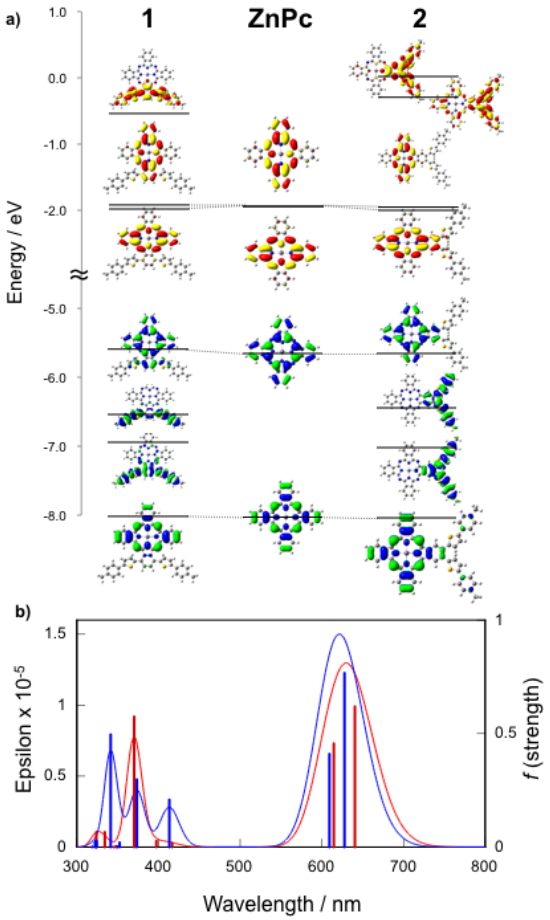

Figure 6-4: a) Calculated energy levels of **1** (left), ZnPc (middle), and **2** (right); b) Calculated absorption spectra of **1** (red) and **2** (blue) derived frin CAM-B3LYP/6-31G(d) DFT calculations. LUMO and LUMO+1 at about -2 eV are degenerate for ZnPc, and slightly split for **1** and **2**.

6.3.2. Optical data for αPcS1 and αPcS2

The author designed and synthesized two ZnPc-based dyes based on **1**, **αPcS1** and **αPcS2**, in which cyanocarbonic acid was attached at one terminal of the conjugated thiophene side chain on the Pc ring (Figure 6-5). Since the ring expansion of Pc leads to more red-shifting of the Q band,[18] the ring-expanded dye

αPcS2 was synthesized from 1,4-dihydroxy-2,3-dicyanonaphthalene, with the expectation of further enhancement of light-harvesting area for DSSC. For both dyes, six bulky 2,6-diisopropylphenoxy substituents were added to the peripheral positions of the ZnPc core to prevent the formation of intermolecular aggregates.[3f,19] Phthalonitriles **7** and **12** possessing a protected aldehyde terminal group were synthesized by the stepwise coupling reactions as shown in Scheme 6-2 and Scheme 6-3. Low-symmetry AB_3-type ZnPcs were synthesized by the statistical tetramerization of the bulky 4,5-bis(2,6-diisopropyl)phenoxy phthalonitrile **8** and **7** or **12**. After the deprotection of pinacol-protected aldehyde group, the aldehyde terminal group was allowed to react with excess cyanoacetic acid in the presence of piperidine to afford **αPcS1** and **αPcS2**. We also synthesized a symmetrical ZnPc **5** prepared using phthalonitrile **8** as a reference compound.[19]

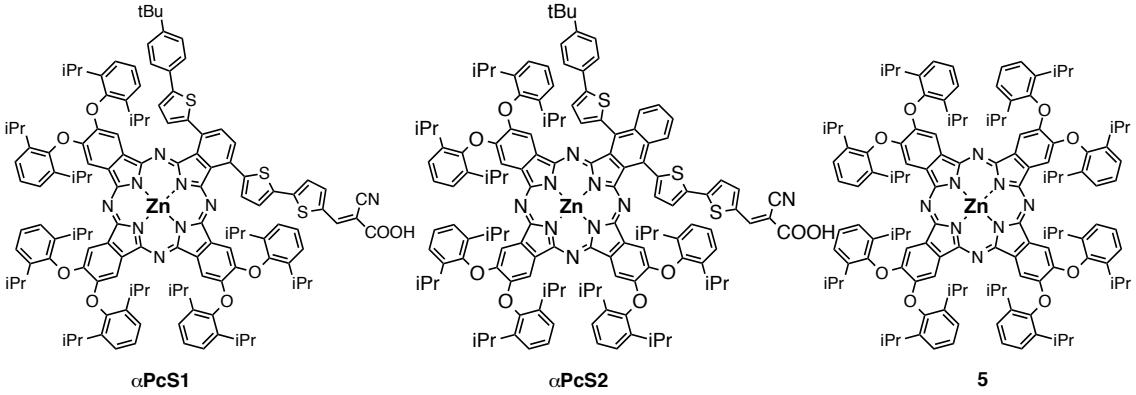

Figure6-5: Chemical structures of **αPcS1** and **αPcS2** and **5**[19]

Figure 6-5 shows the absorption and MCD spectra of **αPcS1** and **αPcS2** in THF. The attachment of thiophene side chains at the a positions on one side of the Pc macrocycle resulted in the red-shift and the splitting of the Q band as compared to the symmetrical ZnPc **5**. The Q MCD bands of **αPcS1** and **αPcS2** appeared at longer wavelengths and their bandwidths were wider than that of **5** (particularly, the Q band for **αPcS1**), indicating that the Q band MCD can be interpreted as

pseudo-Faraday *A*-terms. The ring-expanded **αPcS2** displays a sharp Q band at 708 nm, which is slightly red-shifted as compared with that of **αPcS1**. The split width of Q bands for **αPcS2** predicted by the TD-DFT calculation (15.0 nm) was narrower than that of **αPcS1** (29.2 nm). This narrow split width of **αPcS2** results in the increase of sharpness of the Q MCD pseudo Faraday *A*-term as well as absorption coefficient of the Q band. The first oxidation potential of **αPcS2** measured by DPV in *o*-DCB was +0.02 V vs. Fc^{+}/Fc, which is negative than **αPcS1** by 50 mV (Figure 6-7). The TD-DFT calculation also suggested destabilization of the HOMO energy level for **αPcS2** by the annulation with benzene unit. Therefore, we can conclude that the HOMO-LUMO gap of **αPcS2** decreased because of the destabilization of HOMO level through the annulation with benzene ring.

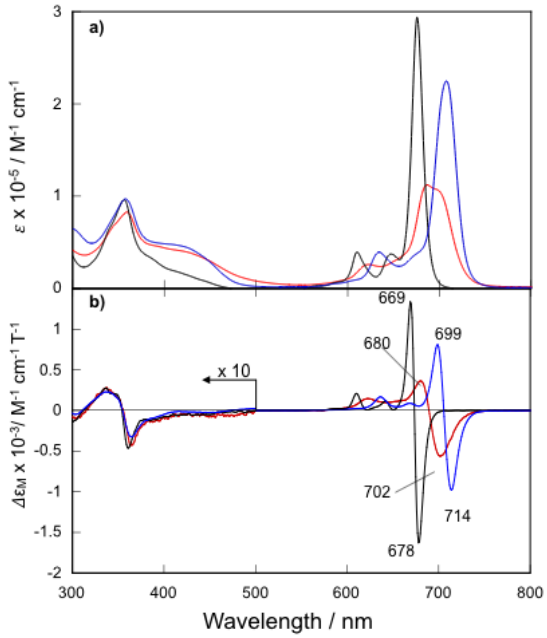

Figure 6-6: a) Absorption and b) MCD spectra of **αPcS1** (red), and **αPcS2** (blue) and **5** (black) in THF solution.

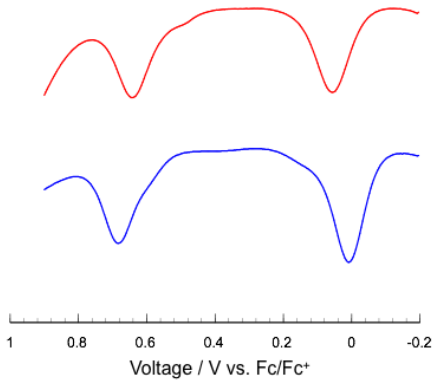

Figure 6-7: Differential plus voltammetry of **αPcS1** (red) and **αPcS2** (blue) in o-DCB containing 0.1 M $TBAPF_6$ as a supporting electrolyte.

Table 6-2. Optical and electrochemical data for **αPcS1** and **αPcS2**

Dye	Absorption[a] /nm (ε x 10^{-5} /M^{-1} cm^{-1})	Emission / nm (ϕ_f)[b]	Absorption[c] / nm	E_{HOMO} / V *vs.* NHE	$E_{0\text{-}0}$ [e]/ eV	E_{LUMO} [f]/ V *vs.* NHE
αPcS1	702 (1.0), 687 (1.1), 359 (0.83)	713 (0.1)	692	+0.70[d]	1.76	-1.06
αPcS2	708 (2.2), 357(0.97)	715 (0.02)	708	+0.65 [d]	1.74	-1.09

[a] In THF; [b] Fluorescence quantum yields (ϕ_f) were determined with $ZnPc(tBu)_4$ as a standard in THF (Fig. S6); [c] On TiO_2 electrode; [d] E_{HOMO} was determined from the first oxidation potential of dye in *o*-DCB solution; [e] Optical band gap ($E_{0\text{-}0}$) was estimated from the cross point of the normalized absorption and emission spectra; [f] E_{LUMO} was calculated as $E_{HOMO} - E_{0\text{-}0}$.

6.3.3. Identification of a thiophene-specific charge-transfer band from the MCD spectra and TDDFT calculations

A new broad band appeared in the 380-480 nm region in the absorption spectrum of **αPcS1** and **αPcS2**, that is not seen for **3, 4** or **5**. The MCD spectra in the 380-480 nm regions are surprisingly very similar for **αPcS1, αPcS2** and **5**. The lack of significant MCD intensity under the broad absorption band in 380-480 nm region implies there is negligible angular momentum involved in these electronic transitions,[20] and this is consistent with the TD-DFT calculation result for **αPcS1** and **αPcS2**. Namely, the transition estimated between the B and Q band for **αPcS1** at 467 nm (f = 0.69) is assigned to HOMO→LUMO+2 transition (Table 6-3). The transition for **αPcS1** showed a negative solvatochromism with increasing solvent

polarity, indicating that there was a change of the energy level in this excited state following the interaction between the dye and the solvent molecules.[16b,21] The introduction of the electron accepting cyanocarbonic acid on one end of the conjugated side chains is considered to create this intramolecular charge-transfer (ICT) transition from the electron-rich Pc core to the side chain. Because of the close connection to the Pc core, this broad absorption band will contribute to the improvement in the light-harvesting efficiency in the wavelength region between the Q and the B bands in DSSCs.

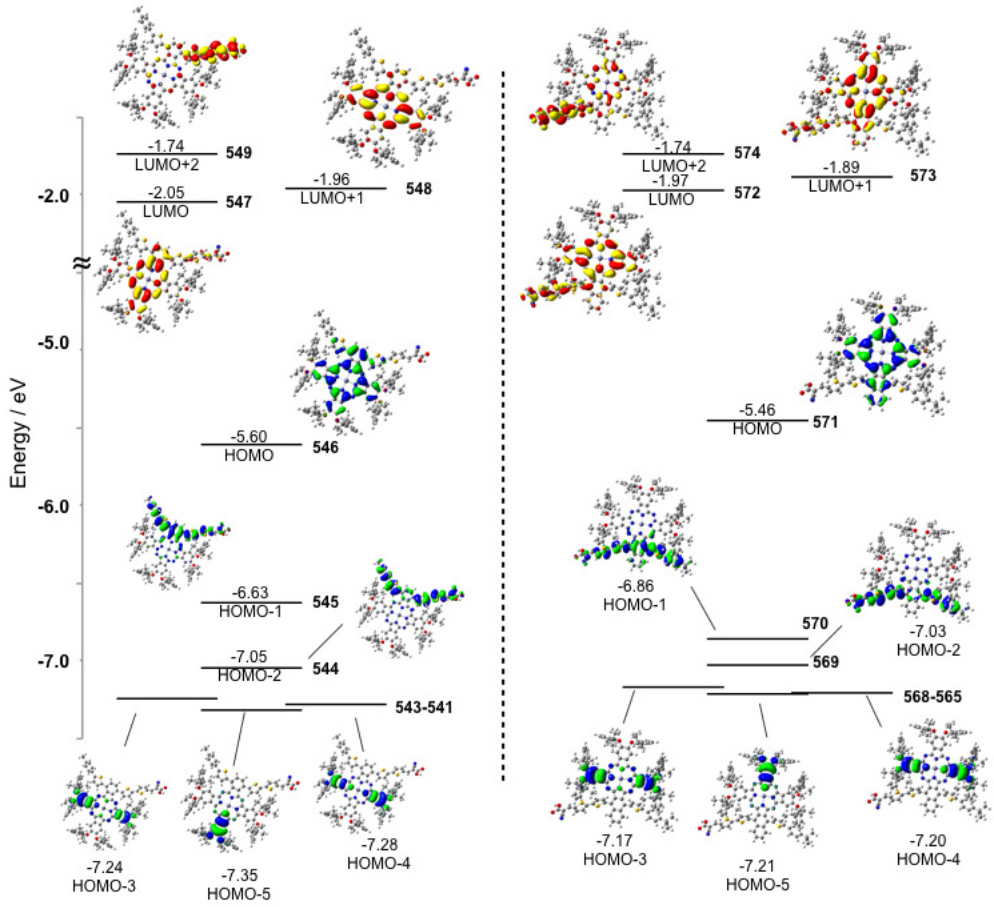

Figure 6-8: DFT-calculated energy level diagrams and molecular orbital surfaces of **αPcS1** (left) and **αPcS2** (right) (The HOMO is #546 in **αPcS1** and #571 in **αPcS2**).

Table 6-3 Calculated transition energies, oscillator strengths *f*, and configurations.

Dye	Energy / eV (nm)	*f*	Configurations (Main percentage contributions)
αPcS1	1.87 (661.50)	0.69	546(H)→547 (L) (90%)
	1.96 (632.22)	0.62	546→547 (3%), 546→548 (89%)
	2.65 (467.27)	0.69	545→549 (9%), 546→549 (62%), 546→550 (8%)
	3.04 (408.40)	0.19	545→547 (73%)
	3.14 (395.40)	0.08	545→548 (37%), 545→549 (20%)
	3.25 (382.10)	0.52	542→548 (21%), 545→548 (26%), 545→549 (17%)
	3.27 (379.10)	0.19	541→547 (73%)
	3.29 (376.47)	0.04	542→548 (50%), 545→548 (19%)
	3.34 (371.17)	0.08	543→548 (66%)
	3.44 (360.45)	0.11	546→550 (65%)
αPcS2	1.84 (672.50)	0.66	571(H)→572 (L) (82%), 571→573 (4%), 571→574 (8%)
	1.89 (657.54)	0.67	571→573 (84%), 571→574 (9%)
	2.59 (477.96)	0.18	571→572 (9%), 571→574 (66%), 571→575 (12%)
	3.07 (403.38)	0.82	565→574 (2%), 569→572 (11%), 569→574 (15%), 570→572 (19%), 570→574 (9%), 571→574 (11%), 571→575 (13%)
	3.12 (397.76)	0.27	569→574 (7%), 571→575 (65%)
	3.23 (383.90)	0.01	557→572 (62%)
	3.30 (376.28)	0.12	568→572 (60%)
	3.36 (368.73)	0.05	566→572 (11%), 566→573 (47%), 566→574 (14%)
	3.37 (367.42)	0.06	566→573 (14%), 570→573 (40%)
	3.46 (358.47)	0.04	570→572 (41%), 570→574 (15%)

6.3.4. Performance of αPcS1- and αPcS2-based DSSCs

Mesoporous TiO_2 electrodes were immersed in THF solutions of **αPcS1** or **αPcS2** (5 x 10^{-5} M) at room temperature to give dye-stained TiO_2 electrodes through the formation of an ester linkage between the carboxylic anchoring group in dyes and the TiO_2 surface. In general, the adsorption of dyes on the TiO_2 surface resulted in the absorption spectral and electrochemical changes because of either the deprotonation of anchoring group[22] or the electronic interaction between the LUMO of dyes and the conduction band of TiO_2.[23] Whereas the Q band positions of **αPcS1** and **αPcS2** were almost the same as those in solution, the red-shifts of Q band onsets and positive shifts of the HOMO levels from the electrochemical measurements were observed (Figure 6-7, Table 2).

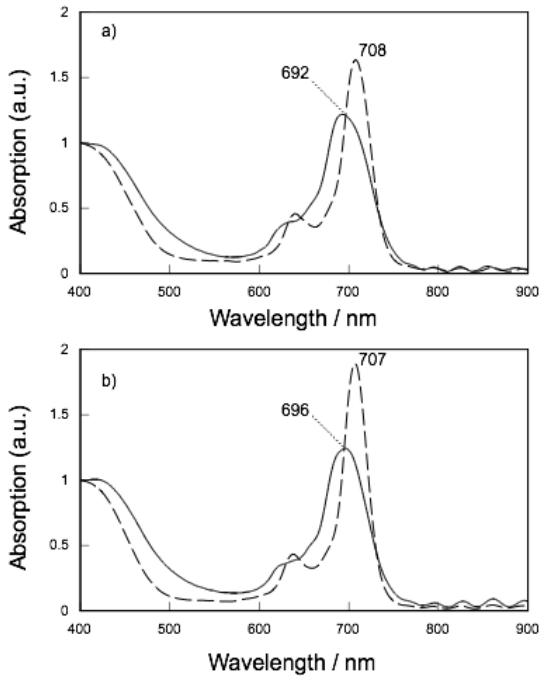

Figure 6-9: Absorption spectra of **αPcS1** (a, solid line), **αPcS2** (a, dashed line), **αPcS1+CDCA** (b, solid line), and **αPcS2+CDCA** (b, dashed line) on 6 μm TiO_2 transparent films.

The adsorption densities of **αPcS1** and **αPcS2** on the TiO_2 surface were determined from the absorbance of the ZnPcs released from the dye-stained TiO_2 electrodes. The adsorption densities of **αPcS1** and **αPcS2** are lower than those of the previously reported value for **PcS18** (1.4×10^{-4} mol cm^{-3}).[4c] The occupied areas of **αPcS1** and **αPcS2** on the TiO_2 surface were estimated to be 3.0 nm^2 by using their optimized molecular models (Figure 6-10). These estimated areas are about 1.6 times of that of **PcS18**. The enlargement of the molecular size by the attachment of the conjugated side chain to the ZnPc core reduced the packing density of the dyes within the self-assembled dye monolayer on the TiO_2 surface.

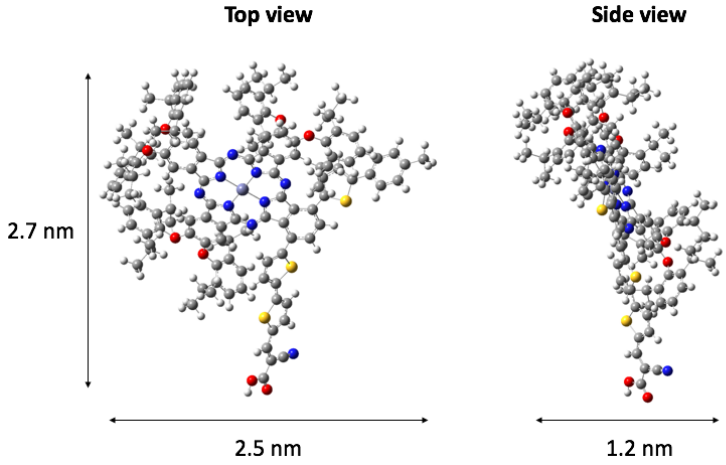

Figure 6-10: Simulated molecular dimension of **αPcS1** optimized by Gaussian09.

The photovoltaic performances of the **αPcS1** and **αPcS2** cells were evaluated using liquid electrolyte containing 0.6 M 1,2-dimethyl-3-propylimidazolium iodide, 0.1 M LiI, 0.05 M I_2, and 0.5 M *tert*-butylpyridine in acetonitrile. Figure 6-11a shows the *J-V* curves measured under the simulated AM 1.5 G full sunlight illumination (100 mW cm^2) solar light for cells based on the two ZnPcs. The **αPcS1** cell showed a short-current density (J_{sc}) of 10.1 mA/cm^2, an open-circuit voltage (V_{oc}) of 0.61 V, and a fill factor (FF) of 0.73, giving the overall PCE of 4.5 % (Figure 6-11 and Table 4). In contrast, the **αPcS2** cell showed a lower J_{sc}, leading to a lower PCE value of 3.2 %.

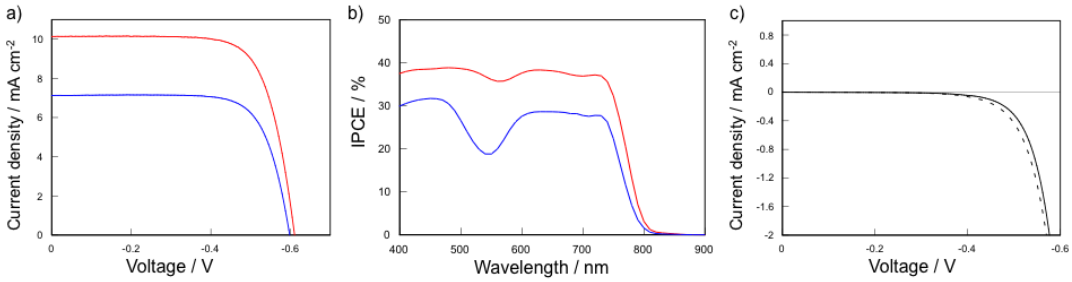

Figure 6-11: *J-V* curves (a) and IPCE spectra (b) for the DSSCs based on **αPcS1** (red) and **αPcS2** (blue) under one sunlight; (c) *J-V* curves for**αPcS1** (solid line) and **αPcS1+CDCA** (dashed line) in dark.

Chenodeoxycholic acid (CDCA) was used as a co-adsorbent in the DSSCs to prevent the dye aggregation on the TiO_2 surface.[24] The half widths of Q band of **αPcS1** decreased from 63 nm to 56 nm following the addition of CDCA (Figure 6-9), suggesting that the aggregates on the TiO_2 surface were dissociated by the co-adsorption with CDCA. The **αPcS1** cell co-adsorbed with CDCA provided a higher PCE of 5.5 % compared with the cell without CDCA (Figure 6-12a). The onset of voltage in dark current was improved by the co-adsorption with CDCA, implying the enhanced blocking effect of I_3^-.[24b] Since the enlarged dyes make a space within the dye layer on the TiO_2 surface, electrons in the TiO_2 lose by the contact with I_3^- in electrolyte passing through the loose packing layer of dyes. The dissociation of aggregates and the enhancing of blocking of I_3^- by co-adsorption with CDCA could improve the performance of **αPcS1** and **αPcS2** cells. The incident photon-to-current (IPCE) spectrum of **αPcS1** cell followed the absorption feature of **αPcS1** adsorbed onto TiO_2 electrode, and showed a panchromatic response from visible to NIR light regions (Figure 6-12b). The **αPcS1** cell showed a photoresponse in the wavelength of 400-600 nm corresponding to the broad ICT band. The substitution of oligothiophene units with the adsorption site at the α positions of Pc skeleton leads to filling of the absorption valley of ZnPcs as well as the expansion of the light harvesting range by 50 nm compared to that of **PcS18**. However, the maximum IPCE value at the Q band of **αPcS1** was 47 %, which is lower than that of **PcS18** (ca. 80 %). This implies a lower electron injection efficiency from the excited ZnPc to the conduction band of TiO_2 electrode than that of **PcS18**. This is probably caused by a poor electronic coupling between the ZnPc core and the adsorption site at the LUMO and LUMO+1 levels as shown in Figure 6-8. The further improvement of IPCE values can be achieved by the structural optimization of p-conjugated linker between the ZnPc core and the adsorption site.

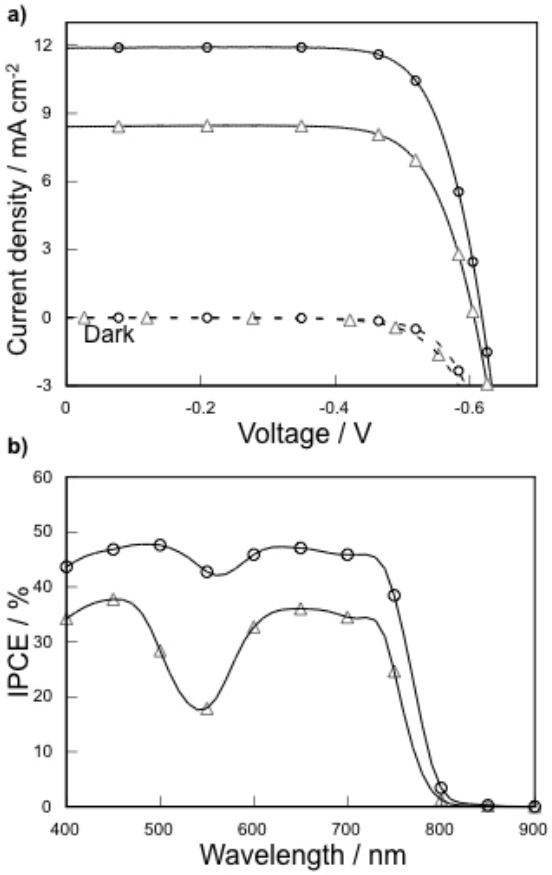

Figure 6-12: a) *J-V* curves for DSSCs based on **αPcS1**+CDCA (○) and **αPcS2+CDCA** (△) under AM 1.5g simulated solar light; b) IPCE spectra of DSSCs based on **αPcS1+CDCA** and **αPcS2+CDCA**.

Table 6-4. Cell performance of ZnPc-sensitized DSSCs

Dye[a]	[CDCA]/ mM	V_{oc} / V	J_{sc} / mA cm^{-2}	FF	PCE / %	Absorption density/ x 10^{-5} mol cm^{-3}
αPcS1	0	0.61	10.1	0.73	4.5	6.8
	0.5	0.62	11.9	0.75	5.5	4.1
αPcS2	0	0.60	7.1	0.74	3.2	5.2
	0.5	0.63	7.8	0.77	3.8	2.8

[a] [dye] = 0.05 mM in THF

6.4. Conclusion

In summary, the author demonstrated the expansion of the light-harvesting wavelength range for ZnPc-based DSSCs by hybridization with p-conjugated side chains. The effect of the α position substitution in low-symmetrical ZnPc on the optical and electrochemical properties was investigated. The author found that the substitution of thiophene units at the α positions resulted in the red-shifting of the Q band into the NIR region as well as tuning of the HOMO and LUMO energy levels. Two ZnPc-based photosensitizers **αPcS1** and **αPcS2**, in which the π conjugation side chain with an adsorption site was attached at the α positions of Pc ring, were synthesized by the stepwise coupling reactions. The presence of the non-peripheral thiophene groups resulted in insertion of thiophene-located MOs between the HOMO and the typical, 4-node, "a_{2u} HOMO-1" of the Gouterman model. Similarly, there were new thiophene-related MOs just above the LUMO and LUMO+1. The absorption spectra of **αPcS1** and **αPcS2** showed a broad band from ca. 380 to 480 nm, which was assigned to an intramolecular charge-transfer transition from the ZnPc core to the side chain based on the lack of significant MCD signal intensity and the predicted spectral bands from TD-DFT calculations. While the previous reported ZnPc-based sensitizers for DSSCs have not harvested in green light region, the **αPcS1** cell showed a panchromatic response in 400-800 nm with a PCE value of 5.5 % when used as a light-harvesting dye on a TiO_2 electrode for DSSCs under one-sun conditions. The hybridization of chromophores is a one way for designing the panchromatic ZnPc-based sensitizers with high energy conversion efficiencies.

References

[1] A. Hagfeldt, G. Boschloo, L. Sun, L. Kloo and H. Pettersson, *Chem. Rev.,* **2010**, *110*, 6595-6663.

[2] a) M. V. Martínez-Díaz, G. de la Torre, T. Torres, *Chem. Commun.* **2010**, *46*, 7090-7108; b) L. Martín-Gomis, F. Fernández-Lázaro and Á. Sastre-Santos, *J. Mater. Chem. A*, **2014**, *2*, 15672–15682.

[3] a) J.-J. Cid, J.-H. Yum, S.-R. Jang, M. K. Nazeeruddin, E. Martínez-Ferrero, E. Palomares, J. Ko, M. Grätzel and T. Torres, *Angew. Chem. Int. Ed*., **2007**, *46*, 8358-8362; b) P. Y. Reddy, L. Giribabu, C. Lyness, H. J. Snaith, C. Vijaykumar, M. Chandrasekharam, M. Lakshmikantam, J.-H. Yum, K. Kalyanasundaram, M. Grätzel and M. K. Nazeeruddin, *Angew. Chem. Int. Ed.,* **2007**, *46*, 373-376; c) S. Mori, M. Nagata, Y. Nakahata, K. Yasuta, R. Goto, M. Kimura and M. Taya, *J. Am. Chem. Soc*., **2010**, *132*, 4054-4055; d) M. Kimura, H. Nomoto, N. Masaki and S. Mori, *Angew. Chem. Int. Ed.,* **2012**, *51*, 4371-4374, e) M.-E. Ragoussi, J.-J. Cid, J.-H. Yum, G. de la Torre, D. D. Censo, M. Grätzel, M. K. Nazeeruddin, T. Torres, *Angew. Chem. Int. Ed.,* **2012**, *51*, 4375-4378; f) M. Kimura, H. Nomoto, H. Suzuki, T. Ikeuchi, H. Matsuzaki, T. N. Murakami, A. Furube, N. Masaki, M. J. Griffith and S. Mori, *Chem. Eur. J*., **2013**, *19*, 7496-7502; g) T. Ikeuchi, H. Nomoto, N. Masaki, M. J. Griffith, S. Mori and M. Kimura, *Chem. Commun*., **2014**, *50*, 1941-1943.

[4] a) L. Yu, X. Zhou, Y. Yin, Y. Liu, R. Li and T. Peng, *ChemPlusChem*, **2012**, *77*, 1022-1027; b) B. Lim, G. Y. Margulis, J.-H. Yum, E. L. Unger, B. E. Hardin, M. Grätzel, M. D. McGehee and A. Sellinger, *Org. Lett*., **2013**, *15*, 784-787; c) T. Ikeuchi, S. Mori, N. Kobayashi and M. Kimura, *Inorg. Chem.,* **2016**, *55*, 5014-5018.

[5] a) C. Qin, Y. Numata, S. Zhang, A. Islam, X. Yang, K. Sodeyama, Y. Tateyama and L. Han, *Adv. Funct. Mater*., **2013**, *23*, 3782-3789; b) J.-H. Yum, S.-R. Jang, P. Walter, T. Geiger, F. Nüesch, S. Kim, J. Ko, M. Grätzel and M.

K. Nazeeruddin, *Chem. Commun*., **2007**, *44*, 4680-4682.

[6] M. Ince, F. Cardinali, J.-H. Yum, M. V. Martínez-Díaz, M. K. Nazeeruddin, M. Grätzel and T. Torres, *Chem. Eur. J.*, **2012**, *18*, 6343-6348.

[7] a) N. Kobayashi, N. Sasaki, Y. Higashi and T. Osa, *Inorg. Chem.*, **1995**, *34*, 1636-1637; b) N. Kobayashi, H. Ogata, N. Nonaka, E. A. Luk'yanets, *Chem. Eur. J.*, **2003**, *9*, 5123-5134.

[8] K. Sakamoto, E. Ohno-Okumura, T. Kato and H. Soga, *J. Porphyrins Phthalocyanines,* **2010**, *14*, 47-54

[9] S. Y. Al-Raqa, *J. Porphyrins Phthalocyanines,* **2006**, *10*, 55-62

[10] S. Eu. T. Katoh, T. Umeyama, Y. Matano and H. Imahori, *Dalton Trans*., **2008**, *40*, 5476-5483

[11] J. Mack and N. Kobayashi, *Chem. Rev*., **2011**, *111*, 281-321.

[12] D. M. Guldi, I. Zilbermann, A. Gouloumis, P. Vázquez and T. Torres, *J. Phys. Chem. B*, **2004**, *108*, 18485-18494.

[13] T. Fukuda, S. Homma and N. Kobayashi, *Chem. Eur. J*., **2005**, *11*, 5205-5216.

[14] J. Mack, M. J. Stillman and N. Kobayashi, *Coord. Chem. Rev.*, **2007**, *251*, 429-453.

[15] a) J. Mack, J. Stone and T. Nyokong, *J. Porphyrins Phthalocyanines,* **2014**, *18*, 630-641; b) S.-H. Chou, C.-H Tsai, C.-C. Wu, D. Kumar and K.-T. Wong, *Chem. Eur. J.* 2014, **20**, 16574-16582.

[16] J. Mack and M. J. Stillman, in *The Porphyrin Handbook*, Eds.: K. M. Kadish, K. M. Smith, R. Guilard, Academic press, New York, 2002, Chapter103, pp. 43-116.

[17] J. Mack, Y. Asano, N. Kobayashi, M. J. Stillman, *J. Am. Chem. Soc*., **2005**, *127*, 17697-17711.

[18] N. Kobayashi, J. Mack, K. Ishii and M. J. Stillman, *Inorg. Chem*., **2002**, *41*, 5350.

[19] N. B. McKeown, S. Makhseed, K. J. Msayib, L.-L. Ooi, M. Helliwell and J. E.

Warren, *Angew. Chem. Int. Ed.*, **2005**, *44*, 7546-7549.

[20] S. Omomo, Y. Maruyama. K. Furukawa, T. Furuyama, H. Nakano, N. Kobayashi and Y. Matano, *Chem. Eur. J.*, **2015**, *21*, 2003-2010.

[21] J. T. Lin, P.-C. Chen, Y.-S. Yen, Y.-C. Hsu, H.-H. Chou and M.-C. P. Yeh, *Org. Lett.*, **2009**, *11*, 97-100.

[22] a) Z.-S. Wang, Y. Cui, Y. Dan-oh, C. Kasada, A. Shinpo and K. Hara, *J. Phys. Chem. C*, **2007**, *111*, 7224-7230; b) X.-H. Zhang, Z.-S. Wang, Y. Cui, N. Koumura, A. Furube and K. Hara, *J. Phys. Chem. C*, **2009**, *113*, 13409-13415.

[23] C. Kim, H. Choi, S. Kim, C. Baik, K. Song, M.-S. Kang, S. O. Kang and J. Ko, *J. Org. Chem*., **2008**, *73*, 7072-7079.

[24] a) S. Zhang, X. Yang, C. Qin, Y. Numata and L. Han, *J. Mater. Chem. A*, **2014**, *2*, 5167-5177, b) J. Li, W. Wu, J. Yang, J. Tang, Y. Long and J. Hua, *Sci. China: Chem*, **2011**, *54*, 699-706.

[25] M. J. Frisch, G. W. Trucks, H. B. Schlegel, G. E. Scuseria, M. A. Robb, J. R. Cheeseman, G. Scalmani, V. Barone, B. Mennucci, G. A. Petersson, H. Nakatsuji, M. Caricato, X. Li, H. P. Hratchian, A. F. Izmaylov, J. Bloino, G. Zheng, J. L. Sonnenberg, M. Hada, M. Ehara, K. Toyota, R. Fukuda, J. Hasegawa, M. Ishida, T. Nakajima, Y. Honda, O. Kitao, H. Nakai, T. Vreven, J. Montgomery, J. A., J. E. Peralta, F. Ogliaro, M. Bearpark, J. J. Heyd, E. Brothers, K. N. Kudin, V. N. Staroverov, R. Kobayashi, J. Normand, K. Raghavachari, A. Rendell, J. C. Burant, S. S. Iyengar, J. Tomasi, M. Cossi, N. Rega, N. J. Millam, M. Klene, J. E. Knox, J. B. Cross, V. Bakken, C. Adamo, J. Jaramillo, R. Gomperts, R. E. Stratmann, O. Yazyev, A. J. Austin, R. Cammi, C. Pomelli, J. W. Ochterski, R. L. Martin, K. Morokuma, V. G. Zakrzewski, G. A. Voth, P. Salvador, J. J. Dannenberg, S. Dapprich, A. D. Daniels, Ö. Farkas, J. B. Foresman, J. V. Ortiz, J. Cioslowski, D. J. Fox, Revision A.1 ed., Gaussian, Inc., Wallingford CT, 2009.

Chapter 7

Conclusion

7.1. Conclusions and Summary

The main aim of the present thesis was to develop novel phthalocyanines to extend the light-harvesting range of organic photovoltaic devices. In this thesis, three approaches have been tested to shift the Q band of Pcs to longer wavelength, namely changing the size and symmetry of the Pc macrocycle (**Chapters 3** and **4**), the formation of a dyad system (**Chapter 5**), and the introduction of the peripheral substitutes (**Chapter 6**). The optical and electrochemical properties of synthesized novel zinc phthalocyanines were investigated using UV-Vis, fluorescence, MCD spectroscopy, cyclic voltammetry, and differential pulse voltammetry techniques, and DFT calculations. These studies are summarized in the relevant sections as follows:

Chapter 3 describes the design, syntheses, and characterization of novel ring-expanded phthalocyanines. Fusing fluorene rings with the porphyrazine core resulted in a narrower band gap and the tuning of both the HOMO and LUMO energy levels compared with unsubstituted ZnPcs. The synthesized ring-expanded phthalocyanines **1-3** were incorporated into bulk-heterojunction solar cells based on P3HT and PCBM. The addition of **3** decorated with eight alkyl chains resulted in improved device performance with a 16 % enhancement of the short circuit current compared to a reference cell without **3**.

Chapter 4 investigates the potential of the novel ring-expanded phthalocyanines as a photosensitizer in dye-sensitized solar cells (DSSCs) because of their suitable HOMO levels and the red-shifted Q band. In this chapter, a ring-expanded near-IR absorbing sensitizer **4**, in which three fluorene rings are

fused with a porphyrazine core, was synthesized from 9,9-diarylfluorene precursor and 3,4-dicyanobenzoate. The fusion of fluorene rings with a porphyrazine ring provides suitable HOMO and LUMO energy levels for efficient operation of DSSCs. Furthermore, the attachment of hexlphenyl groups at the C9 position of the fluorene rings enables the formation of suitable packing that has a tilted orientation of adsorbed dyes on the TiO_2 surface. When used as a light-harvesting sensitizer in DSSCs, **FcS1** based cells gave a PCE value of 3.2 %. The light-harvesting region of the **FcS1** extends close to 900 nm though the formation of suitable packing on the TiO_2 surface.

In **Chapter 5**, a novel covalently linked zinc phthalocyanine - zinc porphyrin dyad is reported. The phthalocyanines and porphyrins are considered to be important molecular components in molecular arrays due to their complementary absorption regions in visible light. Moreover, intramolecular energy transfer from the porphyrin to phthalocyanine occurs very efficiently in most phthalocyanine-porphyrin dyads because the Q band absorption of phthalocyanine almost overlaps the fluorescence wavelength of porphyrin. Thus, a new phthalocyanine – porphyrin dyad was designed and synthesized for the photosensitizer of DSSCs. UV-Vis absorption and fluorescence spectral studies demonstrated that the energy harvested from the zinc porphyrin moiety can be efficiently transferred to the zinc phthalocyanine unit through the Förster resonance energy transfer. While the dyad gave an energy conversion efficiency of 2.7 %, the dyad could convert the entire visible light region between 300 to 800 nm into electronic energy.

Chapter 6 investigates the optical effect of the substitution of thiophene at the α or β position. Since α-substituted ZnPc showed a larger red shift of the Q band, the two new hybrid chromophoric systems (**αPcS1** and **αPcS2**) were designed and

synthesized, in which a π-conjugated side chain with an adsorption site was introduced at an α position of the MPc to act as the photosensitizer in DSSCs. UV-Vis absorption spectra of **αPcS1** and **αPcS2** showed a red-shift of Q band as well as a broad absorption at around 450 nm, which is assigned to an ICT transition from the ZnPc core to the accepter unit. The **αPcS1** cell showed a panchromatic response in the range of 300-800 nm with a PCE of 5.5 %.

7.2. Concluding remarks

The design and development of near-IR sensitizing dyes to expand the light-harvesting region of organic photovoltaic devices remains a challenging task in the field of material chemistry as well as organic synthetic chemistry. To solve this problem, the author focused on phthalocyanine complexes. In this thesis, the author found that the ring-expansion approach could be useful for expansion of the light-harvesting region not only for OPVs but also for DSSCs. In particular, the asymmetric near-IR sensitizing dye (**FcS1**) fused with fluorene units expands the light-harvesting region to approximately 900 nm by forming an aggregation on TiO_2. In addition, the panchromatic chromophore is ideal as a photovoltaic device because the solar photon flux extends from the visible region to the near-IR region. In this regard, this thesis provides a new panchromatic sensitizer (**αPcS1**) with a broad light-harvesting area. The author revealed that substitution at the α position of the phthalocyanine core leads to a red shift of the Q band and results in an ICT transition. As a result, the author found that **αPcS1** exhibits photo-to-electron conversion over a wide wavelength range of 300 - 800 nm.

As a final remark, this thesis has focused on the design of panchromatic sensitizers of phthalocyanine complexes with improved optical properties aiming at

applications in the photovoltaic field.

7.3. Recommendations for future work

A range of organic semiconductors has been developed to improve the conversion efficiency of organic solar cells. Two strategies are typically considered to improve the PCE of the organic-based solar cell: (i) improving the light-harvesting efficiency to increase the number of photo-generated carriers, and (ii) promoting the charge collection which is determined by two competing processes – the transport and recombination of the photo-generated carriers. The aim of this thesis was to design and synthesize photosensitizers that enhance the photo-conversion efficiency in the near-IR region. This goal was successfully achieved because the work provided some novel metallophthalocyanines which could contribute to photovoltaic generation in the near-IR region where other dyes cannot convert photons to electrons. However, further detailed studies are needed to improve the conversion efficiency.

- Further investigations, such as like open-circuit photovoltage decay (OCVD) and electrochemical impedance spectroscopic (EIS) mesurements of **FcS1** (**Chapter 4**), which succeeded in expanding the light-harvesting region, and **αPcS1** (**Chapter 6**) showing panchromatic response, are necessary. In particular, since **αPcS1** shows a wide range of light trapping regions, the PCE can be expected to be improved by performing structural optimization based on the obtained results.

- In the fabrication of DSSCs in this thesis, because of the purpose of designing the photosensitizer, the device structure such as titanium oxide, electrolyte, and platinum were all the same. In order to improve the conversion efficiency, it is necessary to optimize the device suitable for the photosensitizer.

- An interesting potential application example of the near-IR sensitizing dye, is as a transparent solar cell. This is a very interesting possibilty, since it could be used as a window if solar cells that transmit visible light and generate power with near-IR light can be developed.

Acknowledgements

Firstly, I would like to thank Prof. Mutsumi Kimura for his limitless patience, understanding and honest support. Without his guidance and persistent help this dissertation would not have been possible. I am also very thankful to Prof. Nagao Kobayashi and Prof. Martin J. Stillman for their kindness supports and advices.

I would like to express great appreciation to Prof. Shogo Mori, Dr. Pawel Wagner and Prof. Atilla J. Mozer for giving me a chance to study in Australia.

I would like to extend my special thanks to Prof. Masanobu Uchiyama of Tokyo University, Prof. Kazuchika Ohta, Prof. Naoki Asao, and Prof. Yoshinori Nishii for reviewing my thesis.

I would like to thank Ms. Eri Amasawa for her kindness advices and discussions. I am particularly grateful for the assistance given by Ms. Seiko Uda, Ms. Junko Yakizawa, Dr. Yoshie Shinohara, Mr. Tadashi Fukawa. Thanks to all my colleagues and friends in Kimura Lab, who are still here or left including Dr. Keisuke Takemoto, Dr. Hiroyuki Suzuki, Hiroki Yamagiwa, Junya Masuo, Hirotaka Nomoto, Eriko Sasaki, Naoki Sasazawa, Nobuhiro Yoshii, Rei Tamura, Sixiao Ren, Teruaki Oshima, Kazuma Yokota, Saki Takahashi, Takeshi Shii, Kengo Kuribayashi, and Takahiro Kawata who made my Ph.D. journey much more enjoyable.

Finally, I am greatly indebted to my parents Masa-aki and Kimiyo Yamamoto for their moral supports and warm encouragements.

March 2017

Satoshi Yamamoto